ISBN 978-82-326-4690-6 (printed version)
ISBN 978-82-326-4691-3 (electronic version)
ISSN 1503-8181

Doctoral Thesis
Christine Marie Lykken

Doctoral theses at NTNU, 2020:171

Christine Marie Lykken

The contribution of grid field firing rates to hippocampal remapping

NTNU
Norwegian University of
Science and Technology
Faculty of Medicine and Health Sciences
Department of Neuromedicine and Movement Sciences

NTNU
Norwegian University of
Science and Technology

Doctoral theses at NTNU, 2020:171
NTNU

NTNU
Norwegian University of
Science and Technology

Christine Marie Lykken

The contribution of grid field firing rates to hippocampal remapping

Thesis for the degree of Philosophiae Doctor

Trondheim, May 2020

Norwegian University of Science and Technology
Faculty of Medicine and Health Sciences
Department of Neuromedicine and Movement Sciences

NTNU
Norwegian University of
Science and Technology

NTNU
Norwegian University of Science and Technology

Thesis for the degree of Philosophiae Doctor

Faculty of Medicine and Health Sciences
Department of Neuromedicine and Movement Sciences

ISBN 978-82-326-4690-6 (printed version)
ISBN 978-82-326-4691-3 (electronic version)
ISSN 1503-8181

Doctoral theses at NTNU, 2020:171

Printed by Skipnes Kommunikasjon as

NORSK SAMMENDRAG

Bidrag fra gittercellenes (felt)fyringsfrekvens til remapping i hippocampus

Hippocampus er avgjørende for navigering og for episodisk minne, eller vår evne til å huske funksjonene "hva", "når" og "hvor" i en hendelse. Stedceller i hippocampus er aktive på bestemte lokasjoner i miljøet, referert til som cellens stedsfelt. Siden hver stedcelle er aktiv i en litt ulik lokasjon, dekker aktiviteten til en liten populasjon av celler hele miljøet, og danner dermed et "kart" over det miljøet. Flere typer celler i den mediale entorhinale cortex (MEC), en viktig input til hippocampus, bidrar også til den nevrale representasjonen av rommet ved å representere avstand, retning eller lokale grenser. Aktivitetsmønstrene til disse nevronene er, på samme måte som stedcellene, generelt stabile over tid.

Som svar på endringer i miljøet viser stedceller store endringer i deres lokasjon og / eller fyringsfrekvens, et fenomen som kalles "remapping". Remapping gjør at hippocampus kan lagre flere, uavhengige kart for ulike miljøer, og til og med for forskjellige opplevelser i samme miljø. I motsetning til stedceller, som ser ut til å endre seg uforutsigbart fra det ene miljøet til det neste, endres aktiviteten til MEC-nevroner samstemt under disse forholdene. Gitterceller skifter og / eller roterer sine sekskantede fyringsmønstre mellom miljøer, men de gjør det på en måte som opprettholder det romlige forholdet mellom cellene. Det er derfor fortsatt uklart hvordan samstemte endringer i MEC-nevroner kan føre til uforutsigbare endringer i stedceller.

For å undersøke dette forholdet manipulerte vi aktiviteten til MEC-nevroner ved å bruke Designer Receptors Exclusiveively Activated by Designer Drug (DREADDs). Ved å uttrykke hM3Dq eller hM4Di DREADDs i transgene mus, var vi i stand til å øke eller redusere aktiviteten til en undergruppe av celler i lag II av MEC (MEC LII) ved å administrere et designer legemiddel.

I artikkel 1 demonstrerte vi at å øke aktiviteten til MEC LII-nevroner fremkalte en større omorganisering av CA1-stedcelleaktivitet og svekket romlig hukommelse. Når vi i motstning reduserte aktiviteten til den samme undergruppen av MEC LII nevroner, resulterte det hverken i svekket i romlig hukommelse eller remapping av stedceller. Disse resultatene gir sterke bevis for rollen stedceller har i spatialt minne: forstyrrelse av stedcellekartet i et miljø forstyrret også den romlig hukommelsen. Videre demonstrerte vi nøyaktig hvilke endringer i MEC-aktivitet som var assosiert med remapping av stedceller. Til vår overraskelse endret ikke økende aktivitet i MEC LII plasseringen av fyringsfeltene i MEC (som tidligere har blitt

observert når stedceller remapper). I stedet produserte denne manipulasjonen uavhengige endringer i fyringsfrekvensen til individuelle gitterfelter, og modifiserte den romlige informasjonen som ble formidlet av hver gittercelle uten å endre plasseringen av gitterfeltet. Vi foreslo dermed at endringer i fyringsfrekvensen til gitterfelter gir et kontekstuelt signal som er i stand til å utløse remapping i hippocampus.

I artikkel 2 demonstrerte vi at remappingen av stedceller som følge av en økning i MEC LII-aktivitet er svært forutsigbar: for mange av stedcellene vi registrerte, kunne vi forutsi hvor de ville dukke opp ganske enkelt ved å undersøke aktivitetsmønstret deres før starten av manipulasjonen. Ved å innlemme resultatene i en datamodel av celle-til-sted-celletransformasjon, demonstrerte vi at endringer i fyringsfrekvensen til gitterfeltene alene er tilstrekkelige til å produsere den samme typen sterk, men likevel forutsigbar, remapping i hippocampus som vi observerte i våre eksperimenter. Lignende endringer i fyringsraten til gitterfeltene (gjort ved å gjenta manipulasjonen vår eller ved å justere datamodellen) ga veldig like, forutsigbare endringer i stedcelle lokasjon. I motsetning til tidligere antakelser, er dermed ikke rempping av stedceller alltid tilfeldig og uforutsigbar. I stedet kan stedceller, ved forhold som får individuelle gitterfelter til å endre sine fyringsfrekvenser, være i stand til å vise heterogene, men forutsigbare, endringer i plasseringen av stedsfeltene. Over tid var stabiliteten til den nylig remappede stedcellelokasjonen tett korrelert med stabiliteten av fyringsfrekvensen til gitterfeltene. Dermed indikerer resultatene våre at endringer i gitterfeltenes fyringsfrekvens påvirker plasseringen og stabiliteten til stedsfelt i hippocampus.

Selv om CA3 og CA1-underregionene til hippocampus er direkte sammenkoblet, antas de å støtte ulike aspekter av hukommelsen, og at disse funksjonsforskjellene kan oppstå fra den unike anatomiske konnektiviten i hvert område. I artkkel 3 undersøkte vi derfor om økning av MEC LII-aktivitet med forskjellige mengder ville påvirke stedceller i CA3 og CA1 på ulike måter. Etter en stor endring i MEC LII-aktivitet, svarte stedceller i de to regionene på lignende måte, og utviste betydelige endringer i fyringsfrekvens, stedsfeltstørrelse og stedsfelt lokasjon. Responsen i CA3, men ikke CA1, var like sterk etter en liten endring i MEC LII-aktivitet, noe som indikerer at responsene fra CA1-stedceller ikke bare arves fra CA3. Selv om den nøyaktige mekanismen som ligger til grunn for denne forskjellen fremdeles ikke er klar, gir dette arbeidet en viktig demonstrasjon av at å endre MEC LII-aktivitet alene kan gi distinkte remappinger i CA1 og CA3.

Navn kandidat: Christine Marie Lykken
Institutt: Kavli Institute for Systems Neuroscience / Centre for Neural Computation
Veileder(e): Clifford G. Kentros og May-Britt Moser
Finansieringskilde: NIH Grant R01MH097130-05, Kavli Foundation, the Centre of Excellence scheme of the Research Council of Norway – Centre for Biology of Memory and Centre for Neural Computation, The Egil and Pauline Braathen and Fred Kavli Centre for Cortical Microcircuits, and the National Infrastructure scheme of the Research Council of Norway – NORBRAIN

Ovennevnte avhandling er funnet verdig til å forsvares offentlig
for graden PhD I neurovitenskap.
Disputas finner sted i auditoriet Kunnskapsenteret
Onsdag 20. mai 2020, kl 12.15

SUMMARY

The contribution of grid field firing rates to hippocampal remapping

The hippocampus is essential for navigation and for episodic memory, or our ability to recall the “what”, “when”, and “where” features of an event. Place cells in the hippocampus are active in specific locations of the environment, referred to as the cell’s place field. Since each place cell is active at a slightly different position, the activity of a small population of cells covers the entire environment, thus forming a “map” of that environment. Several types of cells in the medial entorhinal cortex (MEC), a major input to the hippocampus, also contribute to the neural representation of space by representing distance, direction, or local boundaries. The activity patterns of these neurons are generally stable over time, as they are in place cells.

In response to changes in the environment, place cells exhibit large changes in their location and/or rate of firing, a phenomenon referred to as “remapping”. Remapping allows the hippocampus to store multiple, independent maps for distinct environments, and even for different experiences within the same environment. Unlike place cells, which seem to change unpredictably from one environment to the next, the activity of MEC neurons changes coherently under these conditions. Grid cells, for example, shift and/or rotate their hexagonal firing patterns between environments, but they do so in a manner that maintains the spatial relationship among the cells. It is therefore still unclear how coherent changes in MEC neurons can lead to unpredictable changes in place cells.

To investigate this relationship, we manipulated the activity of MEC neurons using Designer Receptors Exclusively Activated by Designer Drug (DREADDs). By expressing hM3Dq or hM4Di DREADDs in transgenic mice, we were able to increase or decrease the activity of a subset of cells in layer II of MEC (MEC LII) by administering a designer drug.

In Paper 1, we demonstrated that increasing the activity of MEC LII neurons elicited a major reorganization of CA1 place cell activity and impaired spatial memory. In contrast, there was no impairment in spatial memory and no place cell remapping when we decreased the activity of the same subset of MEC LII neurons. These results provide strong evidence for the role of place cells in spatial memory: disrupting the place cell map of an environment also disrupted spatial memory. Next, we demonstrated precisely which changes in MEC activity were associated with place cell remapping. To our surprise, increasing activity in MEC LII did not alter the location of firing fields in MEC (as has been observed previously

when place cells remap). Instead, this manipulation produced independent changes in the firing rates of individual grid fields, modifying the spatial information conveyed by each grid cell without changing the location of its fields. Thus, we proposed that grid field rate changes provide a contextual signal capable of triggering hippocampal remapping.

In Paper 2, we demonstrated that the place cell remapping that results from an increase in MEC LII activity is highly predictable: for many of the place cells we recorded, we could predict where they would remap simply by examining their activity patterns before the onset of our manipulation. By incorporating our results into a computational model of the grid cell-to-place cell transformation, we demonstrated that grid field rate changes alone are sufficient to produce the same kind of strong, yet predictable, hippocampal remapping we observed in our experiments. Similar changes in grid field rates (made by repeating our manipulation or by adjusting our computational model) produced very similar, predictable changes in place field locations. Thus, contrary to previous assumptions, place cell remapping is not always random and unpredictable. Instead, place cells may be able to exhibit heterogeneous, but predictable, changes in the location of their fields under any conditions that cause individual grid fields to change their rates. Over time, the stability of the newly remapped place cell representation was tightly correlated with the stability of grid field rates. Thus, our results indicate that grid field rate changes influence the location and stability of hippocampal place fields.

Even though the CA3 and CA1 subregions of the hippocampus are directly connected, they are thought to support different aspects of memory function, and these functional differences may arise from the unique anatomical connectivity of each area. Therefore, in Paper 3, we investigated whether increasing MEC LII activity by different amounts would affect place cells in CA3 and CA1 in different ways. Following a large change in MEC LII activity, place cells in the two regions responded similarly, exhibiting substantial changes in firing rate, place field size, and place field location. The response in CA3, but not CA1, was just as strong after a small change in MEC LII activity, indicating that the responses of CA1 place cells are not simply inherited from CA3. Although the exact mechanism that underlies this difference is still not clear, this work provides an important demonstration that altering MEC LII activity alone can produce distinct remappings in CA1 and CA3.

DEDICATION

For our daughter Lottie, born 06 April 2019:

“Everything great that ever happened in this world happened first in somebody’s imagination.”

-Astrid Lindgren

ACKNOWLEDGMENTS

The work contained in this thesis was carried out at The Kavli Institute for Systems Neuroscience, Centre for Neural Computation, NTNU, and the University of Oregon Department of Biology, Institute of Neuroscience. I would like to extend my thanks to both institutes for providing such incredible facilities, resources, and technical support.

I would like to thank my fellow lab members and peers for their insight, encouragement, and friendship. It is incredibly inspiring to work with such passionate and talented scientists. I thank my co-supervisor May-Britt Moser and Edvard Moser for offering valuable insight on our research projects. Finally, I thank my supervisor Clifford Kentros for the opportunity to pursue such interesting research projects and for financial support.

Thank you to our dear friends both in Norway and abroad in the United States. Over the years, we have shared so many delightful meals, game nights, relaxing hikes, and coffee dates. You have always made us feel at home, wherever that home may be.

I would also like to thank Rick Kanter, Karen Kanter, Jared Elster, Jessica Elster, and Blair Elster for welcoming me into their family. I am so grateful for your love and support.

Thank you to my dear friend and sister Jenny, who I have always admired. When we were kids, I tried to be just like you: a natural leader, an excellent student, and avid list-maker. As an adult, I continue to follow in your example, which means being fiercely independent and committed to pursuing my passions.

I extend my love and gratitude to my parents, Warren and Debby, for a lifetime of support and guidance. Since I was small, you have nurtured my love of reading and learning, which has benefited me immensely throughout my life. You have always encouraged me to pursue my goals and you have unending faith that I can achieve them. It means so much to me to make you both proud.

Thank you to my beautiful daughter Charlotte, who provides an immeasurable amount of joy and lightness to my life. And finally, my deepest thanks to my husband Ben: it would not have been possible to do this without you. Thank you for always keeping a smile on my face and for inspiring me to be very best version of myself. I love you both so much.

LIST OF PAPERS

Paper 1

A novel mechanism for the grid-to-place cell transformation revealed by transgenic depolarization of medial entorhinal cortex layer II.

Benjamin R. Kanter [1,2], **Christine M. Lykken** [1,2], Daniel Avesar [2], Aldis Weible [2], Jasmine Dickinson [2], Benjamin Dunn [1], Nils Z. Borgesius [1], Yasser Roudi [1], and Clifford G. Kentros [1,2]

[1] Kavli Institute for Systems Neuroscience and Centre for Neural Computation, Norwegian University of Science and Technology, Olav Kyrres gate 9, 7030 Trondheim, Norway

[2] Institute of Neuroscience, University of Oregon, 1254 University of Oregon, Eugene, OR 97403, USA

2017. *Neuron* 93(6): 1480-1492.

Paper 2

Grid field firing rate changes control the predictability and stability of hippocampal remapping.

Christine M. Lykken [1,2], Benjamin R. Kanter [1,2], Jasmine Dickinson [2], Oscar M.T. Chadney [1], Kadjita Asumbisa [1], and Clifford G. Kentros [1,2]

[1] Kavli Institute for Systems Neuroscience and Centre for Neural Computation, Norwegian University of Science and Technology, Olav Kyrres gate 9, 7030 Trondheim, Norway

[2] Institute of Neuroscience, University of Oregon, 1254 University of Oregon, Eugene, OR 97403, USA

In preparation for submission to *Neuron*

Paper 3

Distinct remappings in CA3 and CA1 elicited by depolarization of medial entorhinal cortex layer II.

Benjamin R. Kanter [1,2], **Christine M. Lykken** [1,2], Kadjita Asumbisa [1], Thanh-Tin P. Nguyen [2], and Clifford G. Kentros [1,2]

[1] Kavli Institute for Systems Neuroscience and Centre for Neural Computation, Norwegian University of Science and Technology, Olav Kyrres gate 9, 7030 Trondheim, Norway

[2] Institute of Neuroscience, University of Oregon, 1254 University of Oregon, Eugene, OR 97403, USA

In preparation for submission to *Journal of Neuroscience*

ABBREVIATIONS

BL	Baseline session
BOLD	Blood-oxygen-level-dependent
CA	Cornu ammonis
cAMP	Cyclic adenosine 3',5'-cyclic monophosphate (AMP)
CNO	Clozapine-N-oxide
Con	Control mice
DG	Dentate gyrus
DREADD	Designer Receptor Exclusively Activated by a Designer Drug
EC	Entorhinal cortex
fMRI	Functional magnetic resonance imaging
GIRK	G-protein inwardly-rectifying potassium
GPCR	G-protein-coupled receptor
hM3	hM3Dq-expressing mice
hM4	hM4Dq-expressing mice
IP	Intraperitoneal
LEC	Lateral entorhinal cortex
LTP	Long-term potentiation
MAPK	Mitogen-activated protein kinase
MEC	Medial entorhinal cortex
MEC LII	Medial entorhinal cortex layer II
MEC LIII	Medial entorhinal cortex layer III
MTL	Medial temporal lobe
NMDAR	N-Methyl-D-aspartate receptor
PLC	Phospholipase C
PV	Parvalbumin-positive
tetO	Tet operator
TRE	Tetracycline-response element
tTA	Tetracycline transactivator
Vm	Membrane potential

TABLE OF CONTENTS

INTRODUCTION

Hippocampus & memory

How are memory functions organized in the brain? Franz Joseph Gall was the first to propose that mental functions could be localized to specific areas of the brain, and he attempted to do so by examining the surface of the skull through an approach later referred to as phrenology (Gall and Spurzheim, 1810-1819). His ideas contrasted sharply with those of other scientists, such as Pierre Flourens, who believed that all regions of the brain participate in every mental function. Over 50 years later, Paul Broca's clinical discovery of an area in the brain dedicated to speech provided strong support for Gall's concept of localized brain function (Broca, 1861). However, the debate between localizationist and equipotential views continued. For over 20 years, the neuropsychologist Karl Lashley attempted to pinpoint where memories are localized in the brain by systematically removing different cortical areas of the rodent brain (Lashley, 1929; Lashley, 1950). Despite his efforts, he repeatedly failed to identify any particular area that was necessary for memory storage, ultimately concluding that memories are widely distributed throughout the cortex.

A fundamental role for the hippocampus and associated structures in the medial temporal lobe (MTL) in long-term memory first became evident from studies of the now-famous patient Henry Molaison, formerly known as H.M., who suffered from frequent generalized epileptic seizures (Scoville and Milner, 1957). Since the available treatments were ineffective, he underwent a bilateral MTL resection, involving the removal of portions of the hippocampal formation and amygdala. After the resection, he exhibited profound anterograde amnesia, meaning he could no longer create new memories. Despite this devastating impairment, H.M. retained his intelligence, personality, and perceptual abilities, in addition to his early childhood memories. Extensive studies of H.M. and his pattern of impairments contributed several fundamental principles to our modern-day understanding of memory. First, it became clear that memory is indeed separable from other cognitive abilities, such as intelligence and perceptual functions, which were generally undisturbed after damage to the MTL. Second, H.M. was able to keep perceptual information, such as a number or a visual image, in memory for approximately 30-40 seconds, indicating that MTL structures are not essential for immediate memory. Third, H.M. retained his early childhood memories, suggesting that structures in the MTL are not the final storage site for memories. Finally, the demonstration that H.M. was able to learn new motor skills, such as drawing in a mirror (Milner, 1962), led to the proposal that there are multiple memory systems in the brain that operate in parallel (**Figure 1**). Continued studies of H.M. and other amnesic patients with MTL damage

revealed that their impairment was limited to just one type of memory, declarative memory (i.e., our conscious recollection of facts and events), while their capacity for other types of memory, including motor skill learning, was spared. Given these insights, declarative memory was distinguished from a collection of unconscious, non-declarative forms of memory, including skill or habit learning, priming, classical conditioning, and non-associative learning. Eventually, case studies of human patients, animal models of human memory impairment (Mishkin, 1978), and neuroanatomical work pinpointed the hippocampus and surrounding entorhinal, perirhinal, and parahippocampal cortices, as the specific structures in the MTL critical for supporting declarative memory (Squire and Zola-Morgan, 1991).

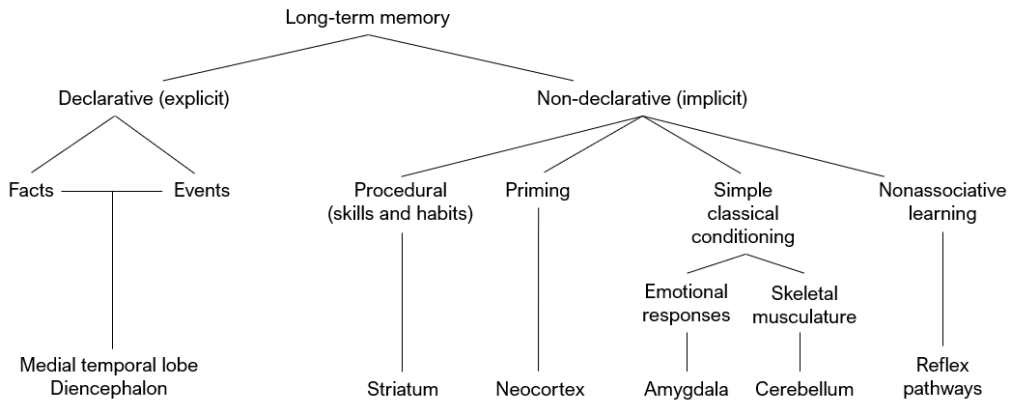

Figure 1 | Multiple memory systems in the mammalian brain. Memories can be classified as declarative or nondeclarative. Declarative memory refers to the conscious recollection of facts and events and depends on the integrity of the medial temporal lobe and diencephalon. Non-declarative memory refers to a collection of abilities that are independent of the medial temporal lobe and can be dissociated based on the structures involved. Adapted from Milner et al., 1998.

Declarative memory can be further sub-categorized into memories for facts (i.e., semantic memory) and events (i.e., episodic memory). More specifically, episodic memory refers to our ability to consciously recall and mentally re-experience events that occurred at a particular time and place. Episodic memories therefore incorporate information about the content of the event itself (i.e., "*what*") with information regarding the context in which the event occurred (i.e., "*when"* and "*where"*) (Tulving, 1983). This rich recollection of spatiotemporal context distinguishes episodic memories from generic, context-free semantic memories. While there is some debate as to whether the ability to form new semantic memories is impacted following MTL damage (Zola and Squire, 2001), episodic memory impairment is a hallmark symptom observed in amnesic patients such as H.M., who was

unable to recall any events from his daily life after his surgery (Corkin, 2002). Today, there is a general consensus that the hippocampus in humans is involved in episodic memory (Eichenbaum and Cohen, 2001; Kinsbourne and Wood, 1975; O'Keefe and Nadel, 1978; Squire and Zola-Morgan, 1991; Vargha-Khadem et al., 1997).

The importance of the hippocampus in memory processing was subsequently validated by the discovery of long-term potentiation (LTP) in this area (Bliss and Lømo, 1973). Using in vitro recordings from hippocampal slices of brain tissue, Bliss and Lømo demonstrated that the repeated coactivation of excitatory synapses in the hippocampus produced a long-lasting increase in synaptic strength. This study provided the first direct evidence supporting Donald Hebb's famous postulate that coordinated activity between a presynaptic neuron and a post-synaptic neuron must strengthen the connection between them (Hebb, 1949). Due to the prolonged duration of these changes in synaptic transmission, LTP is still considered to be the cellular correlate of learning and memory.

The discovery of place cells

A growing interest in hippocampal function thus led John O'Keefe and his graduate student Johnathan Dostrovsky to begin recording the activity of hippocampal neurons in rodents freely foraging for food rewards. They discovered cells in the hippocampus that fired action potentials in specific locations of the environment (**Figure 2**; O'Keefe and Dostrovsky, 1971). These "place cells" fired at their maximal rate in the center of the cell's "place field," and their firing rates decreased as a function of the distance from the place field center. Each place cell was active in a slightly different location in the environment; therefore, even a small ensemble of place cells can represent the entire space accessible to the animal. This discovery led O'Keefe and Nadel (1978) to propose that the hippocampus provided the neural substrate for the "cognitive map" originally postulated by Edward Tolman in 1948.

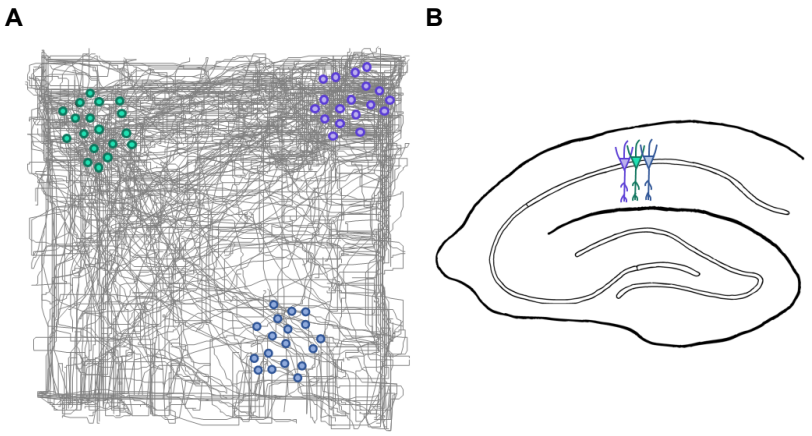

Figure 2 | Place cells in the hippocampus. (A) As an animal explores a square open field environment, individual place cells in the hippocampus fire action potentials in a specific location, referred to as their place field (indicated by colored dots). The animal's path is indicated in gray. (B) Neighboring cells in the hippocampus do not typically have neighboring place field locations. Colored cells correspond to colored place fields depicted in panel A.

In Tolman's study, rats were trained to traverse a circuitous maze (**Figure 3A**). After the rats learned to run through the maze from the starting location (point A), across a circular table and through the alley walls to the food box (point G) for a reward, the apparatus was changed. While the starting location and the circular table remained the same, a series of radial arms replaced the alley walls and the original route was blocked (**Figure 3B**). When presented with these new alternative routes, the majority of rats selected the arm that led just a few inches from the previous reward location, even though they had never physically occupied this location. Given this result, Tolman argued that the brain contains a cognitive map of the external world, enabling animals to calculate shortcuts through locations not previously experienced by the animal (Tolman, 1948). Inspired by this work, O'Keefe and Nadel (1978) proposed that the hippocampus constructs a cognitive map by representing the environment, locations within the environment, and their contents, thus providing the basis for spatial memory and flexible navigation.

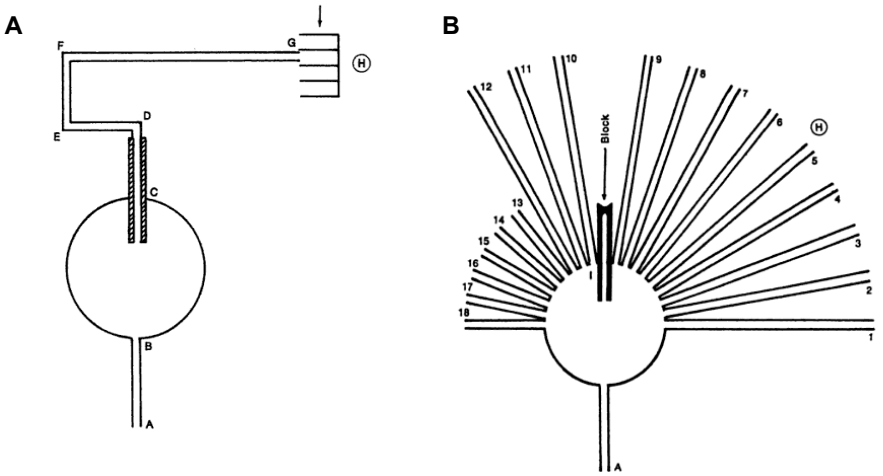

Figure 3 | Behavioral evidence for a cognitive map in rodents. (A) Apparatus used during behavioral training. Rats were trained to navigate through the environment from the starting location (point A) to a rewarded location (point G). (B) Apparatus used during behavioral testing. Rats were placed at the starting location (point A) and were allowed to enter any of the radial arms, though the original route was blocked. The majority of rats selected the arm that led near the reward location (arm 6) without prior experience of that route. Adapted from Tolman, 1948.

O'Keefe & Nadel's cognitive map theory of hippocampal function was also based on a thorough analysis of emerging evidence indicating that lesions of the hippocampus produced deficits in spatial learning and memory (O'Keefe et al., 1975; Olton et al., 1978; Jarrard, 1978). Similarly, aged rats, which were shown to have deficits in the maintenance of hippocampal LTP, exhibited impairments on spatial tasks (Barnes, 1979). Most notably, hippocampal lesions in rodents resulted in profound and lasting impairments in performance of the newly developed Morris Water Maze task (Morris, 1981; Morris et al., 1982). In this task, animals are placed in a random start location, and they must learn to navigate to a hidden goal location using only distal sensory cues. Together, these studies demonstrated that spatial information is encoded by neurons in the same brain area that is necessary for spatial memory, supporting the notion that the hippocampus is specialized for mapping space (O'Keefe and Nadel, 1978).

Place cells, remapping, & memory

Following the discovery of place cells, many attempts were made to understand exactly what causes these cells to fire where they do. O'Keefe and Conway (1978) were the first to report that polymodal sensory cues can exert control over place cell firing. They showed that

rotating a set of distal cues resulted in equal rotations of the cells' place fields. Subsequently, Muller and Kubie (1987) demonstrated that in a cue-controlled environment, a single visual cue can impact place field location, as the rotation of a salient cue card produced equal rotations of place fields (**Figure 4B**). Despite the dominant influence of visual stimuli, the location-specific activity of place fields persists in the absence of visual cues (Muller and Kubie, 1987), in total darkness (Quirk et al., 1990), and even in blind rats (Save et al., 1998), indicating that auditory, olfactory, tactile, or self-motion information can support spatial firing when visual information is absent. These studies (and many others) provided an important demonstration that place cell activity is not simply determined by the conjunction of stimuli available at a specific location. Rather, it seems that place cell activity is defined relative to the collective features (i.e., a gestalt view) of an environment, and that place cells as a population encode an animal's current position within that specific environment. In fact, it has been shown that an accurate estimate of the animal's position (i.e. within 1 cm) can be decoded from the activity of as few as 130 place cells (Wilson and McNaughton, 1993).

Subsequent studies have shown that place cell activity not only represents an animal's current position, but also represents past and future locations and/or trajectories (Skaggs and McNaughton, 1996; Pfeiffer and Foster, 2013; Frank et al., 2000; Wood et al., 2000; Ferbinteanu and Shapiro, 2003), goal locations and distance to a goal (Sarel et al., 2017; Danielson et al., 2016), and the position of other animals or objects (Omer et al., 2018; Danjo et al., 2018). Additionally, place cells are capable of representing a variety of nonspatial information, including odors (Eichenbaum et al., 1987; Wood et al., 1999; Igarashi et al., 2014), tactile inputs (Young et al., 1994), and elapsed time (Pastalkova et al., 2008; MacDonald et al., 2011), suggesting that the role of place cells is not limited to spatial navigation. This ability to represent not only location, but also information about events that took place in a specific location at a specific time, indicates that place cells are involved in episodic memory.

Rather than forming a unique hippocampal representation upon each exposure to an environment, place cell activity is generally stable within a single recording session as well as between sessions separated by hours, weeks, or even months (**Figure 4A**; Muller et al., 1987; Thompson and Best, 1990; but see Mau et al., 2018). In contrast, when an animal is exposed to a distinct recording environment, the hippocampal representation undergoes a drastic reorganization (Muller and Kubie, 1987), a phenomenon later referred to as "remapping" (Bostock et al., 1991; Kubie and Muller, 1991). Some place cells shift the location of their fields between environments, while others turn on or turn off (**Figure 4C**). It

is important to note that remapping is characterized by two fundamental features (Kubie and Muller, 1991). First, the hippocampal representation of an individual environment uses a relatively small proportion of cells (i.e., the “active subset”), which represent a random sample from the total population of hippocampal cells. In fact, the overlap between the active subset in two distinct environments is not larger than expected by chance (Leutgeb et al., 2004; Alme et al., 2014). Second, for the subset of place cells active in both environments, the location of firing shifts unpredictably, such that there is no discernible relationship between the place field of a single cell and its neighbors between environments (O'Keefe and Conway, 1978; Kubie and Ranck, 1983; Muller and Kubie, 1987). Thus, the hippocampal representations of distinct environments are thought to be completely uncorrelated (Leutgeb et al., 2005). These experiments (and many that followed) have provided an important demonstration that place cells can participate in multiple spatial maps, allowing the hippocampus to generate a vast number of orthogonal representations with a limited number of cells. This orthogonalization process is critical if hippocampal representations are indeed expressions of individual memories, as it is capable of minimizing interference between similar memories while maximizing the number of memories stored within the same network.

Subsequent experiments revealed that there are two essentially independent forms of remapping that may signify different levels of environmental change (Leutgeb et al., 2005). Between distinct environments, when the degree of environmental change is highest, place cells exhibit large changes in their location and/or rate of firing, resulting in hippocampal representations that are completely uncorrelated (**Figure 4C**; Leutgeb et al., 2005). This phenomenon is referred to as “global remapping,” and it is similar to the “complete remapping” originally described by Muller et al. (1987). As outlined above, the orthogonalization of representations through global remapping ensures that memories for distinct environments are encoded as separate spatial maps. In response to more subtle changes in the color or shape of the recording environment, however, place cells typically exhibit large changes in firing rate while maintaining stable place field locations (**Figure 4D**). During this “rate remapping,” the active subset of neurons and the location of their fields is unchanged. Therefore, rate remapping may enable the hippocampus to represent nonspatial information on top of a stable place code via changes in firing rate alone.

If remapping is a neural mechanism for creating distinct memories, then alterations in the place cell map should be correlated with predictable changes in behavior during spatial learning tasks. In other words, disrupting the place cell map of a familiar environment should

disrupt spatial memory performance in that environment. In support of this idea, several studies have demonstrated a clear link between remapping and spatial memory performance (O'Keefe & Speakman 1987; Lenck-Santini et al., 2001; Lenck-Santini et al., 2002; Barnes et al., 1997; Bahar et al., 2011; Lee et al., 2018; but see Jeffery et al., 2003).

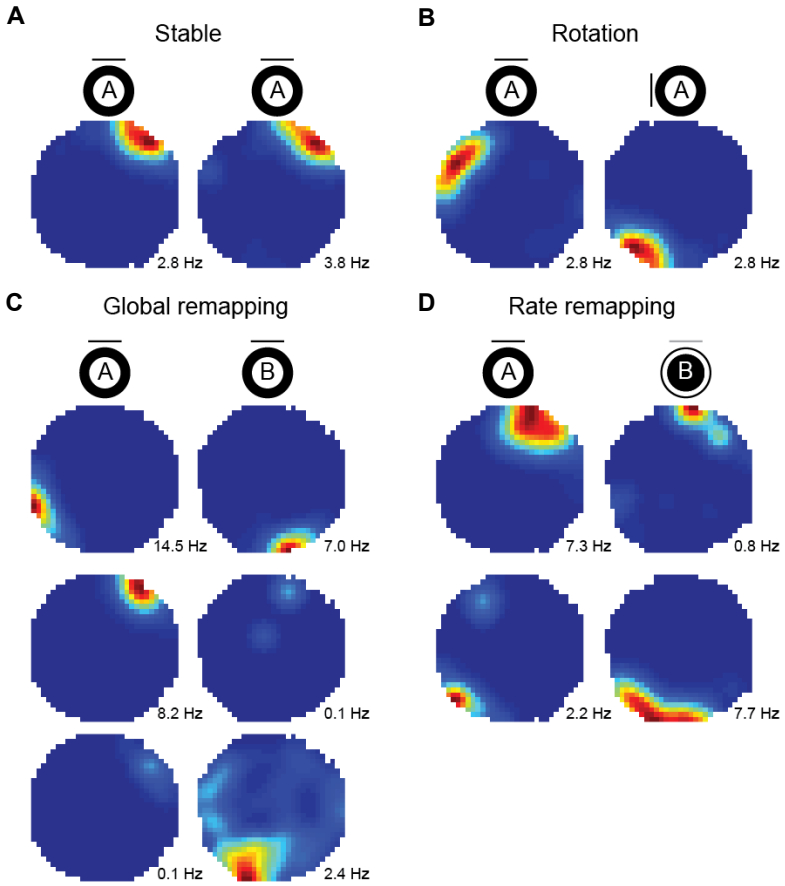

Figure 4 | In response to changes in context, hippocampal place cells remap. (A) Place cells are generally stable between repeated exposures to the same environment. (B) Place cells rotate the location of their fields in conjunction with the rotation of a single polarizing cue card. (C) Place cells globally remap when rodents are moved between identical environments in distinct physical locations. Simultaneously recorded cells can change their location and/or rate of firing (top row), turn off (middle row), or turn on (bottom row). (D) Place cells rate remap in response to subtle changes in the environment, such as a change in the color of the walls. Simultaneously recorded cells can decrease (top row) or increase (bottom row) their firing rates while maintaining a constant place field location. (A-D) Activity is color coded from blue to red. Peak firing rate is indicated at the bottom right of each rate map. Panels A through D are unpublished data from C. Lykken.

Anatomy of the hippocampal formation

Due to its relatively simple yet elegant anatomical organization and integral function in the brain, our understanding of the neuroanatomy of the hippocampus is highly sophisticated. This structure has been the focus of neuroanatomical studies for over four hundred years. The term hippocampus is derived from the Greek word for sea horse because the shape of the human hippocampus is said to be reminiscent of this sea creature (Arantius, 1587).

The hippocampus consists of two main parts: the hippocampus proper and the dentate gyrus (DG). The DG has a characteristic V- or U-shaped organization, and its name is derived from the Latin word “dentate,” meaning “jagged” or “toothed,” due to its serrated appearance. The hippocampus proper is divided into three subregions: cornu ammonis 1 (CA1), cornu ammonis 2 (CA2), and cornu ammonis (CA3). Together, the shape of the cornu ammonis (CA), or “Ammon’s horn,” regions of the hippocampus are similar in shape to a ram’s horn. Although the basic architecture of the hippocampus is generally similar across a range of mammals (**Figure 5**), the hippocampus proper is more elongated in rodents, with its characteristic C-shaped structure extending from the midline of the brain into the temporal lobe. The hippocampus has a distinctive three-layered appearance with a single dense layer of pyramidal neurons surrounded by fiber-rich plexiform layers. The larger hippocampal formation encompasses several associated structures, including the subiculum, presubiculum, parasubiculum, and entorhinal cortex (EC).

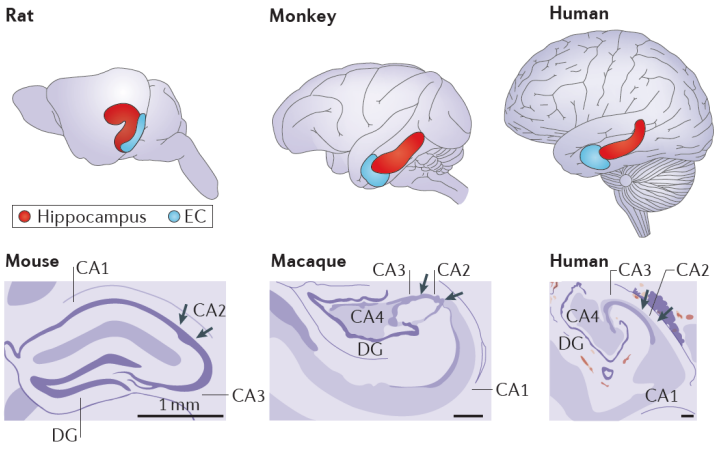

Figure 5 | The basic architecture of the hippocampal formation is similar across species. Panels in the top row depict the location of the hippocampus (red) and entorhinal cortex (EC, blue) in rats, monkeys, and humans. Panels in the bottom row are drawings of Nissl cross-sections of the

hippocampus in mice, macaques, and humans. DG, dentate gyrus. Adapted from Strange et al., 2014.

The primary input to the hippocampus comes from layer II of the EC via the perforant pathway (**Figure 6**). The DG is organized into three layers: the molecular layer, the granule cell layer, and the polymorphic layer. The granule cell layer is the principal cell layer in the DG, containing densely packed granule cells with dendrites extending toward the superficial portion of the molecular layer. Granule cell axons, called mossy fibers, branch extensively and form collaterals in the polymorphic layer before exiting the DG. The principal cellular layer of the hippocampal CA regions is the pyramidal cell layer, which contains tightly packed, glutamatergic pyramidal neurons. The proximal apical dendrites of pyramidal cells in the CA3 subregion of the hippocampus receive glutamatergic innervation from the mossy fibers. CA3 pyramidal neurons are heavily innervated by recurrent collaterals of their own axons as well as by contralateral CA3 neurons. In addition to these associational and commissural hippocampal projections, CA3 pyramidal cells also receive direct input onto their distal dendrites from layer II of the EC via the perforant path. The Schaffer collateral projections from CA3 target the dendrites of pyramidal neurons in CA1, which also receive a direct projection from layer III of the EC via the temporoammonic pathway. Cells in CA1 and the subiculum then give rise to extrinsic projections to the deep layers (V and VI) of the EC. Layer V entorhinal neurons project not only to widespread cortical and subcortical targets, but also to more superficial layers (II and III), connecting the hippocampus and EC in a loop.

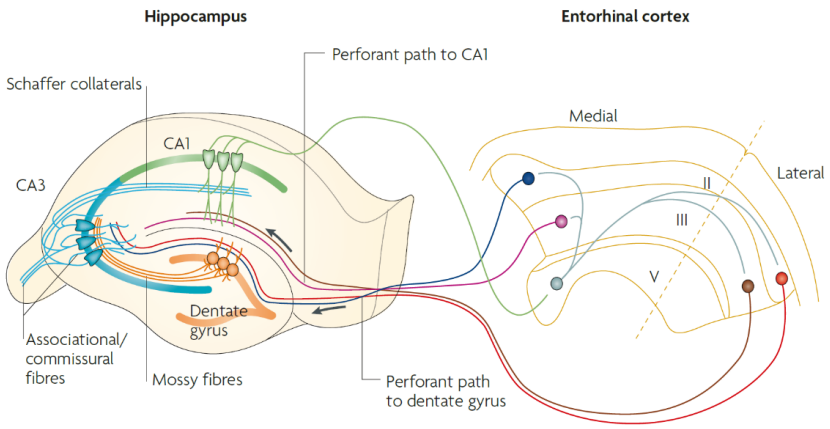

Figure 6 | Anatomy of the entorhinal-hippocampal circuit. Perforant path input to the dentate gyrus originates in layer II of the medial and lateral entorhinal cortices. Granule cells in the dentate gyrus project to CA3 pyramidal cells through the mossy fibers. CA3 pyramidal neurons are also innervated by direct input from layer II of the EC and by dense recurrent collaterals from other CA3 neurons. CA3

pyramidal neurons project to CA1 pyramidal neurons via the Schaffer collaterals. CA1 pyramidal neurons also receive direct input from layer III of the EC. CA1 pyramidal neurons provide output to layer V of the EC, which in turn projects superficially to layers II and III. Adapted from Neves et al., 2008.

Functional cell types in the medial entorhinal cortex

Given this pattern of anatomical connectivity, empirical studies sought to determine whether the spatial selectivity of hippocampal place cells was generated locally in the hippocampus, or upstream in the EC. To that end, Brun et al. (2002) severed the connections between areas CA3 and CA1, thus isolating CA1 from its intra-hippocampal inputs, leaving only direct connections from layer III of the EC intact. Following the disconnection, CA1 neurons still expressed place fields, providing crucial evidence that the source of the spatial signal is likely extrinsic to the hippocampus. Early recordings in the deeper, more ventral portions of the EC had reported only weak spatial modulation in that area (Quirk et al., 1992; Barnes et al., 1990; Frank et al., 2000). Upon consideration of the anatomical projections between these two regions, subsequent recording studies focused on the dorsal part of the medial entorhinal cortex (MEC), which projects directly to the dorsal hippocampus (Kjelstrup et al., 2008), where canonical place cells had first been reported. Only then it became clear that cells in MEC are also strongly modulated by position, like place cells, but express multiple firing fields in a single environment (Fyhn et al., 2004). Subsequent recordings made while animals explored a larger enclosure finally revealed the striking regularity of the spatial firing pattern of cells in this region (Hafting et al., 2005). These “grid cells” exhibit a regularly repeating hexagonal pattern that tiles the entire space available to the animal (**Figure 7A**).

Grid cells are characterized by three main properties: phase, scale, and orientation (**Figure 7B**). Grid phase refers to the spatial location of grid fields, and neighboring grid cells exhibit slightly offset phases (Hafting et al., 2005). Grid scale, or the distance between grid fields, is similar among co-localized grid cells, but increases along the dorsoventral axis of MEC (**Figure 7C**; Hafting et al., 2005). Rather than progressing continuously, recent evidence indicates that grid spacing has a discrete organization (**Figure 7D**; Barry et al., 2007; Stensola et al., 2012). Similarly, grid orientation, which denotes how much the axes through the grid fields is tilted relative to an external reference frame, is discretized in the same manner as grid spacing (Stensola et al., 2012). Thus, grid cells cluster into modules of cells with similar spacing and orientation, but different phases (Stensola et al., 2012).

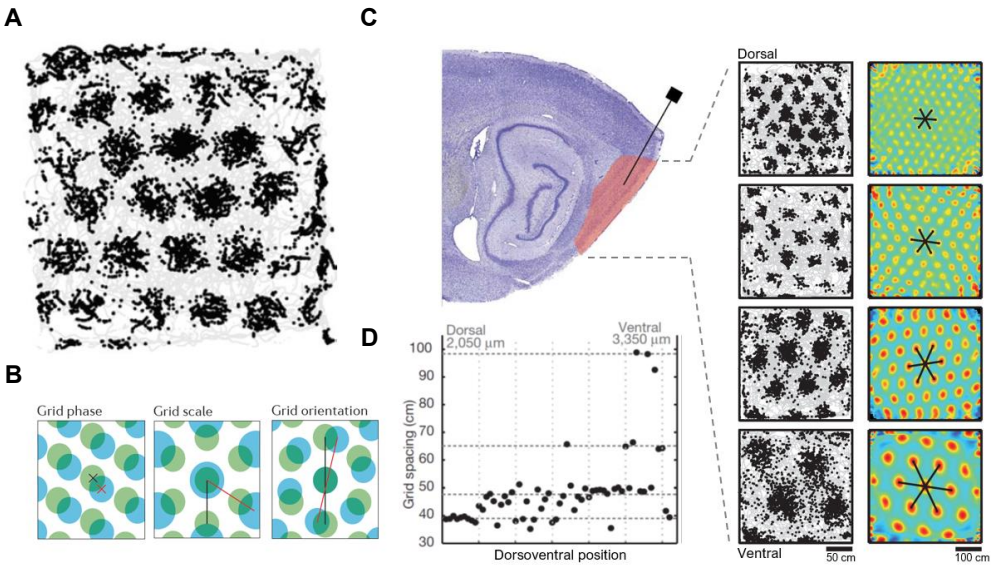

Figure 7 | Basic properties of grid cells. (A) Hexagonal firing pattern of a grid cell recorded in MEC. Gray lines indicate the trajectory of the animal, black dots indicate the location of action potentials for this cell. (B) Grid cells are characterized by their phase, scale, and orientation. Green and blue dots indicate the vertices of two grid cells differing in phase (*xy* location of grid vertices), scale (distance between grid peaks), or orientation (rotation of grid axes). (C) Grid scale increases along the dorsoventral axis of MEC. (D) Grid cells are organized into modules with distinct grid spacing that increases in a stepwise manner along the dorsoventral axis. Black dots indicate the spacing of individual grid cells recorded in a single rat. Panels A and B adapted from Moser et al., 2014. Panels C and D adapted from Stensola et al., 2012.

Since their discovery, it has become clear that grid cells are part of a wider network of functional cell types in MEC that each may contribute to the location-specific coding observed in the hippocampus. Head direction cells, which were first reported in the adjacent presubiculum (Ranck, 1985; Taube et al., 1990a; Taube et al., 1990b), were found in layers III through VI of MEC (**Figure 8A**; Sargolini et al., 2006). These cells encode the head direction of the animal regardless of its location in the environment. In the same study, grid cells with head direction tuning (i.e., conjunctive cells; **Figure 8B**) were discovered in layers III through VI, whereas pure grid cells are most abundant in layer II (Sargolini et al., 2006). Border cells, which fire along salient environmental boundaries, such as the walls of an enclosure or the edge of a platform, were also found in MEC, although they are relatively sparse, making up less than 10% of the local cell population (**Figure 8C**; Solstad et al., 2008; Savelli et al., 2008). More recently, speed cells (**Figure 8D**; Kropff et al., 2015), spatial non-grid cells (**Figure 8E**; Sargolini et al., 2006; Krupic et al., 2012; Diehl et al., 2017), and

object vector cells (**Figure 8F**; Høydal et al., 2019) were also characterized in MEC. Together, the activity of the different functional cell types found in MEC is thought to form the basis of the brain's navigation system (Moser et al., 2017).

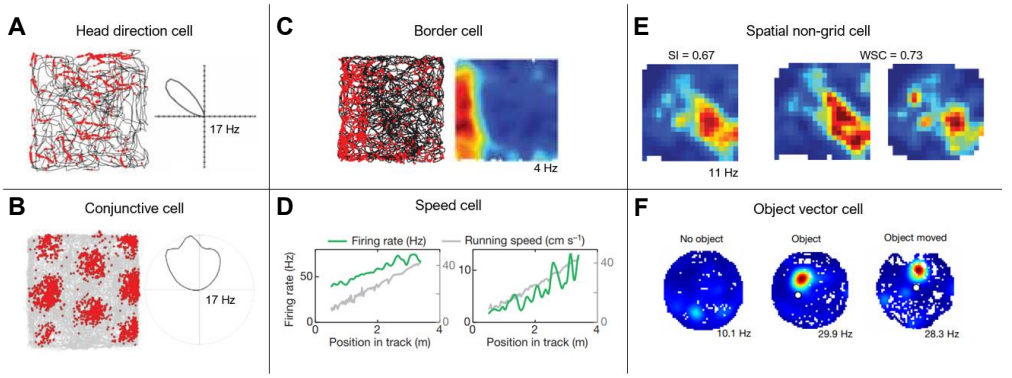

Figure 8 | Functional cell types in MEC. (A) Head direction cells are active when an animal faces a particular direction. (B) Conjunctive grid x head direction cell. (C) Border cells are active along environmental boundaries. (A-C) Black or gray lines indicate the animal's path through the environment, and red dots denote the location of action potentials. (D) Speed cell firing rates are linearly correlated with running speed. The firing rate (green) of two example speed cells increases with the running speed (gray) of a rat traversing a linear track. (E) Spatial non-grid cells exhibit high spatial information (SI) content and high within-session spatial correlation (WSC) values. (F) Object vector cells are active at a fixed distance and direction from objects in the environment. (C,E,F) Activity is color coded from blue to red. Peak firing rate is indicated at the bottom right of each rate map. Panels A and B adapted from Moser et al., 2017. Panel C adapted from Solstad et al., 2008. Panel D adapted from Kropff et al., 2015. Panel E adapted from Diehl et al., 2017. Panel E adapted from Høydal et al., 2019.

Grid-to-place cell models

Of these functional cell types, grid cells are the most numerous spatially modulated cell type in the superficial layers of MEC (Sargolini et al., 2006), and they provide the most abundant spatial input to the hippocampus (Zhang et al., 2013). Therefore, following their discovery, many computational models have focused on the role of grid cells in the generation and remapping of place cells.

It had been shown previously that hippocampal pyramidal neurons can perform linear summation of synaptic inputs (Cash and Yuste, 1998; Cash and Yuste, 1999; Gasparini and Magee, 2006). Thus, the discovery of grid cells, located just one synapse upstream from the

hippocampus, led to the proposal that place fields could be generated via linear summation of grid cell inputs, in the same way that orientation-selectivity of visual cortical neurons results from the linear summation of the receptive fields of upstream neurons (Hubel and Wiesel, 1962). Original proposals suggested that place cells could be generated using a simple summate-and-threshold mechanism (McNaughton et al., 2006; O'Keefe and Burgess, 2005). In other words, place cells could summate the inputs they receive from an arbitrary set of grid cells, and a postsynaptic thresholding mechanism could prevent activation everywhere except for the single region in which input is maximal (McNaughton et al., 2006; O'Keefe and Burgess, 2005). However, the random selection of grid inputs with unique phases generally results in high levels of synaptic excitation at multiple locations, interfering with a thresholding mechanism intended to select a single place field location (Solstad et al., 2006). This problem can be circumvented if grid inputs share a single location in which they all fire, which can be implemented using hard-wired anatomical inputs (Solstad et al., 2006). Accordingly, several models have used the weighted summation of grid cells with overlapping spatial phases but diverse spacings and orientations to generate place fields (**Figure 9A**; Solstad et al., 2006; Fuhs and Touretzky, 2006; McNaughton et al., 2006; O'Keefe and Burgess, 2005). Variations in the spacing and orientation of the summed grid patterns leads to cancellation at all locations surrounding a common central peak (Solstad et al., 2006), thus producing a spatially confined place field from a biologically plausible number of grid cells. It is important to note that these models assume hard-wired anatomical connectivity reflecting the topographical projections among the hippocampus and MEC, with dorsal and ventral place cells receiving the highest proportion of inputs from dorsal and ventral grids, respectively (Kjelstrup et al., 2008). However, anatomical hard-wiring is not necessary for the formation of place fields. Additionally, it is unclear how a subset of grid cells with overlapping vertices could be selected at a behaviorally relevant timescale. Instead, it has been shown that grid inputs with overlapping spatial phases can be selected via Hebbian learning mechanisms (Rolls et al., 2006; Savelli and Knierim, 2010; Si and Treves, 2009).

Alternative models have demonstrated that place fields can be formed via summation of randomly selected excitatory grid inputs in conjunction with a competitive winner-take-all mechanism mediated by gamma frequency feedback inhibition (**Figure 9B**; de Almeida et al., 2009a; de Almeida et al., 2009b; de Almeida et al., 2012; Lyttle et al., 2013) or by global feedback inhibition (Monaco and Abbott, 2011). Importantly, these models show that place field formation does not require any type of learning mechanism or input from grid cells with overlapping spatial phases. One of these models, by Monaco and Abbott (2011), accounted not only for the generation of place fields, but also for their remapping between distinct

environments (Monaco and Abbott, 2011). Here, the authors tested whether translation of the grid pattern, changes in grid ellipticity, or uniform rescaling of the grid would produce place cell remapping. Grid inputs were divided into modules, and changes in grid configuration were coherent within, but not between, modules. Although place fields were essentially intact following changes in grid ellipticity and rescaling of the grid pattern, dividing grid cells into a small number of modules that shifted independently was sufficient to produce complete hippocampal remapping.

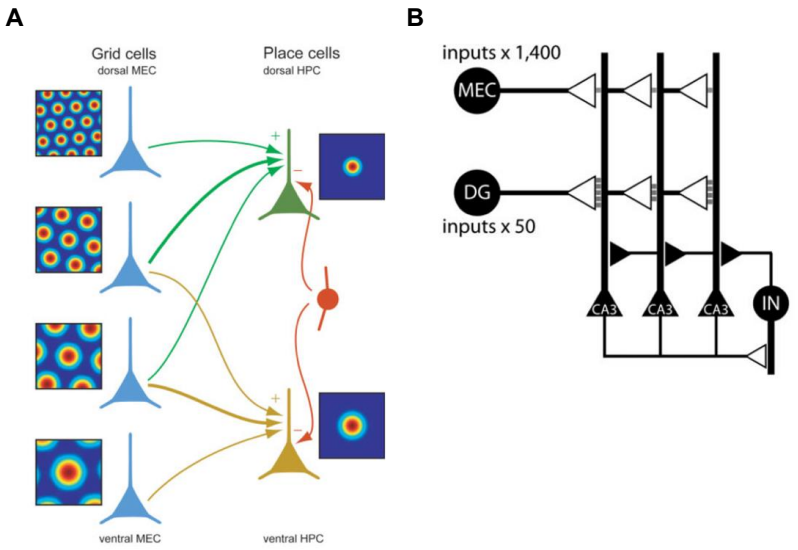

Figure 9 | Models of the grid-to-place cell transformation. (A) Linear summation of anatomically hard-wired grid inputs with overlapping spatial phases but different spacing and orientation (blue) produces single place fields. Place cells in the dorsal hippocampus (green) have smaller fields and receive stronger inputs from grid cells with smaller spacing in dorsal MEC. Place cells in the ventral hippocampus (yellow) have larger fields and receive stronger inputs from grid cells with larger spacing in ventral MEC. Interneurons provide nonspecific inhibition (red). Activity is color coded from blue to red. (B) Pyramidal cells receive spatial inputs from randomly selected excitatory cells in MEC and DG. Place cells excite an inhibitory network that provides gamma frequency feedback inhibition. Single place fields are generated as a result of linear summation of spatial inputs and a competitive winner-take-all mechanism. Panel A adapted from Solstad et al., 2006. Panel B adapted from de Almeida et al., 2012.

Remapping in MEC

Between distinct environments, place cells remap extensively, with simultaneously recorded neurons exhibiting drastic and unpredictable changes in firing rate and/or place field location. How do the firing patterns of MEC neurons change when place cells remap? Under these conditions, the hexagonal pattern of grid fields for each cell shifts and/or rotates (**Figures 10A-B**; Fyhn et al., 2007). However, grid cells with similar spacings (i.e., within a grid module) respond coherently, without changing the phase or orientation relationships between cells (Fyhn et al., 2007). Inducing hippocampal remapping by introducing the animals to a novel environment produces changes in grid spacing that are also coherent among grids cells within a module (Barry et al., 2012). Similar coherence has been observed in other functional cell types in MEC. Between environments, head direction cells rotate coherently, such that the difference in angular tuning between each pair of head direction cells is maintained (Taube et al., 1990a; Taube et al., 1990b; Taube and Burton, 1995; Yoganarasimha et al., 2006). Border cells that fire along the same wall in one environment continue firing along the same wall in a second environment (Solstad et al., 2008). This coherence is also present across functional types: if a border cell rotates its representation by 180 degrees, the orientation of simultaneously recorded grid cells and head direction cells also rotates by 180 degrees (**Figure 10C**; Solstad et al., 2008). Since these types of coherent changes are presumably incapable of producing an orthogonal hippocampal representation, it has been suggested that place cell remapping may result from the independent realignment of grid cells in different modules, which would yield new patterns of coactivity between the modules (**Figure 11**; Fyhn et al., 2007; Monaco and Abbott, 2011). Linearly summating grid inputs from differentially aligned modules would thereby activate a different subset of place cells at each location in the environment. In support of this proposal, recent empirical evidence indicates that grid modules respond independently to the rescaling of an environment (Stensola et al., 2012). When a familiar recording environment was compressed, grid cells in modules with larger spacings rescaled their firing patterns, while the firing patterns of grid cells in the module with the smallest spacing were essentially unchanged (Stensola et al., 2012). While these results clearly indicate that grid modules are capable of operating independently, it has not been shown whether grid modules realign independently under conditions that elicit hippocampal remapping. Additionally, it remains unclear whether remapping actually requires independent realignment, or if another mechanism would be sufficient to induce remapping.

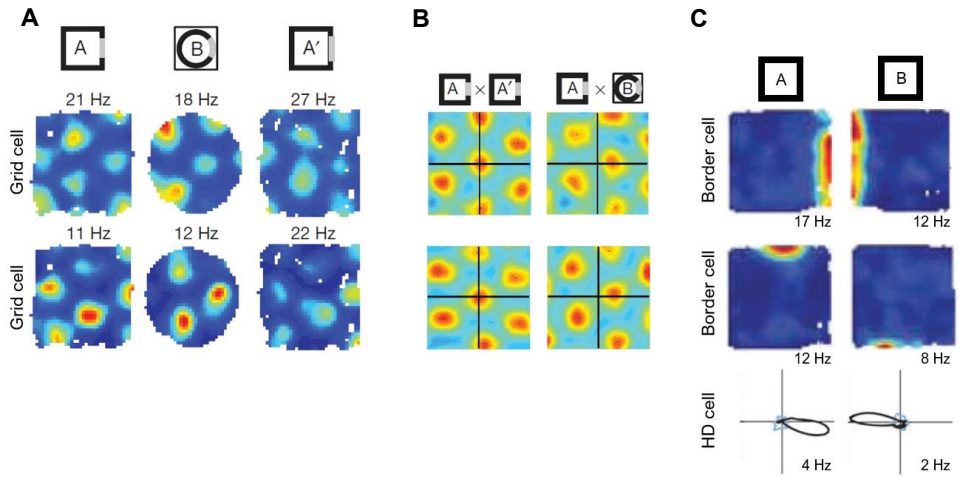

Figure 10 | Coherent changes in functional cell types in MEC under conditions that elicit place cell remapping. (A) Introducing animals to a distinct recording environment causes grid cells within a module to realign coherently. Firing rate maps for two simultaneously recorded grid cells in square and circular recording environments. Peak firing rate is indicated above each rate map. (B) Cross-correlation matrices for grid cells in panel A illustrate that grid patterns of cells within a module shift coherently between environments. The magnitude and direction of the displacement of the peak of the cross-correlogram (A x B) from the origin is similar for simultaneously recorded neurons. (C) Between separate rooms, the firing patterns of simultaneously recorded border cells (top two rows) and head direction cells (bottom row) also rotate coherently. Peak firing rate is indicated at the bottom right of each rate map. (A-C) Activity is color coded from blue to red. Panel A adapted from Fyhn et al., 2007. Panel B adapted from Solstad et al., 2008.

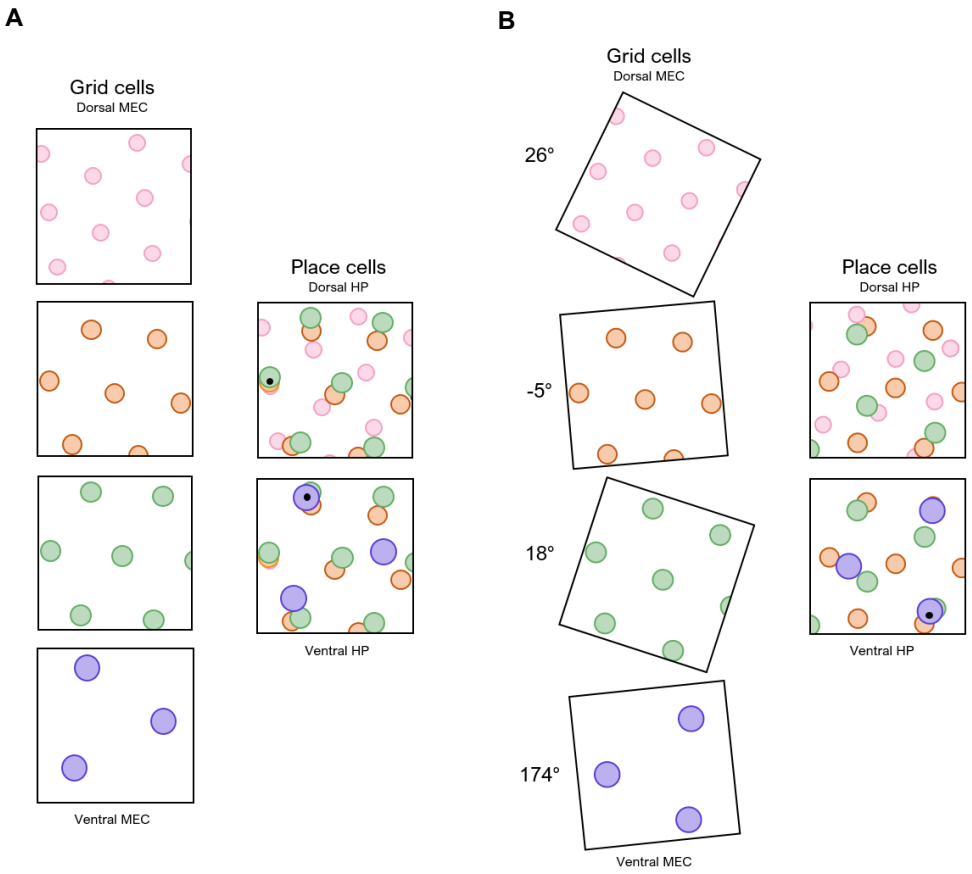

Figure 11 | Independent realignment of grid modules as a mechanism for place cell remapping. (A) Place cells linearly summate input from a subset of grid modules. Place cells in the dorsal hippocampus (HP) receive input from dorsal grid modules, while place cells in the ventral HP receive input from ventral grid modules. Place fields (indicated by black dots) are located in the position where grid fields overlap. (B) Grid cells in each module shift and/or rotate independently between distinct environments. Linear summation of grid inputs that have realigned independently results in global remapping in downstream place cells. Grid inputs no longer overlap for the place cell in the dorsal HP and the cell turns off. Grid inputs overlap in a distinct location for the place cell in the ventral HP causing the cell to shift the location of its field. Adapted from Fyhn et al., 2007.

Challenging the grid-to-place cell model

Despite these intriguing findings, several recent studies have cast doubt on the assumption that grid cells are the sole determinant of place cell firing (for review, see Bush et al., 2014). First, pharmacological inactivation of the medial septum, which reduces theta power and disrupts grid cell activity, does not have a strong impact on the stability of place fields in a

familiar environment (Koenig et al., 2011). Furthermore, this manipulation does not interfere with the development of place fields in a novel environment (Brandon et al., 2014). Second, during development, stable, adult-like place fields are present when rat pups leave the nest for the first time, several days before the emergence of stable grid firing patterns (Wills et al., 2010; Langston et al., 2010). In contrast to grid cells, both head direction and border cells exhibit adult-like firing patterns from the first visit outside the nest (Bjerknes et al., 2014). Given that all functional cell types in MEC project directly to the hippocampus (Zhang et al., 2013), it seems plausible that the spatial and directional signals conveyed by a variety of functional cell types in MEC could contribute to the generation of hippocampal place fields and their remapping.

Influence of MEC on place cells & spatial memory

To determine whether the activity of these functional cell types is required for hippocampal spatial firing, several studies have lesioned or inactivated MEC. Surprisingly, even extensive lesions of MEC do not prevent location-specific activity in the hippocampus, although the resulting place fields lack precision and stability (Miller and Best, 1980; Van Cauter et al., 2008; Brun et al., 2008; Hales et al., 2014; Schlesiger et al., 2015; Schlesiger et al., 2018). One possible interpretation of these results is that spatial input from MEC is not required for localized hippocampal firing. When input from MEC is diminished or absent, it may be that weak spatial input from other areas such as the adjacent lateral entorhinal cortex (LEC) or parasubiculum is sufficient to support hippocampal spatial firing. This explanation is consistent with models suggesting that place fields can be formed from any weakly spatial input (in conjunction with feedback inhibition or Hebbian plasticity) (Rolls et al., 2006; de Almeida et al., 2009a; Savelli and Knierim, 2010; Monaco and Abbott, 2011). Alternatively, the persistence of hippocampal spatial firing observed in these studies may have been supported by remaining tissue or compensatory reorganization following the surgical lesion. In any case, lesion studies are limited by their inability to explain how the activity of neurons in MEC impacts place cell activity in the intact brain. Excitingly, the recent development of new technologies has enabled reversible manipulations of neural activity with higher spatial and temporal precision than ever before (Lykken and Kentros, 2014). Thus, more recent studies have investigated whether MEC contributes to hippocampal remapping using chemogenetic (Miao et al., 2015; Zhao et al., 2016) or optogenetic (Miao et al., 2015; Rueckemann et al., 2016) methods to inactivate MEC. In response to these manipulations, hippocampal place cells typically remap (to varying degrees), demonstrating a clear role for MEC in hippocampal spatial firing. However, it is unclear exactly which changes in the spatial and/or directional firing patterns of each functional cell type in MEC contributed to the

observed remapping, as the responses of MEC neurons to these manipulations were not characterized. Additionally, since the aforementioned studies typically used viral injections to incorporate transgenes into MEC neurons, these manipulations lacked layer- and cell-type specificity, and likely introduced considerable variability between animals due to the complex diffusion of virus through brain tissue (Lykken and Kentros, 2014). Therefore, our understanding of how specific functionally or molecularly defined cell types in the individual layers of MEC contribute to hippocampal spatial firing is incomplete.

OBJECTIVES

The initial discovery that place cells can participate in multiple independent spatial representations (i.e., remap) was critical, as it established a link between place cells and memory. To understand the mechanism underlying hippocampal remapping, it is important to consider the activity of upstream neurons in the superficial layers of MEC, the primary source of input to the hippocampus. Recent empirical studies have done this by manipulating the activity of MEC neurons, which often elicits hippocampal remapping. While these results provide support for the idea that MEC is involved in hippocampal spatial firing, it has yet to be shown precisely *which* changes in the activity patterns of specific functional cell types in MEC are sufficient to induce remapping and impair spatial memory. Furthermore, these different functional cell types are comprised of cells that have different morphologies, express different molecular markers, and are located in different sublayers of MEC. Manipulations of MEC therefore must take this complexity into account.

To overcome these issues, we used highly specific expression of chemogenetic transgenes to bidirectionally manipulate the activity of a subset of cells in layer II of the medial entorhinal cortex (MEC LII). Using electrophysiological recordings, we aimed to characterize the response to our manipulations both locally in MEC as well as downstream in hippocampal subregions CA3 and CA1. Finally, by assessing spatial memory using the Morris Water Maze, we aimed to provide a clear demonstration of which changes in the spatial firing properties of hippocampal and MEC neurons are associated with spatial memory impairment.

For the papers contained within this thesis, we set out to address the following specific questions:

Paper 1

1. Does increasing or decreasing the activity of a subset of cells in MEC LII impact hippocampal spatial firing and/or spatial memory?
2. Which changes in the firing patterns of superficial MEC neurons are associated with hippocampal remapping and spatial memory impairment?

Paper 2

1. Are changes in grid field firing rates sufficient to induce hippocampal remapping?
2. How do grid field rate changes impact place field location and stability?
3. Does a subsequent depolarization of the same subset of MEC LII neurons produce similar changes in grid field firing rates and place field locations?

Paper 3

1. Does increasing the activity of a subset of neurons in MEC LII by various amounts have differential effects on the firing properties of place cells in CA1 and CA3?
2. Following our manipulation, does the activity of CA1 and CA3 place cells recover in a similar manner?

SUMMARY OF METHODS

Experimental Model

In Papers 1-3, we manipulated the activity of neurons using transgenic expression of DREADDs (Designer Receptors Exclusively Activated by a Designer Drug) (Armbruster et al., 2007) in mice. Here, we used the hM3Dq and hM4Di DREADDs, which are muscarinic acetylcholine G-protein-coupled receptors (GPCRs) that have been mutated so that they exhibit a low affinity for their native ligands. Instead, these receptors are highly sensitive to an otherwise inert exogenous ligand called clozapine-N-oxide (CNO). CNO binding to the Gq-coupled hM3 DREADD activates the phospholipase C (PLC) cascade, leading to calcium release and depolarization (**Figure 12**). In contrast, CNO binding to the Gi-coupled hM4 DREADD results in a decrease in cyclic AMP (cAMP) signaling and activates mitogen-activated protein kinase (MAPK) signaling and G-protein-coupled inwardly rectifying potassium (GIRK) channels, leading to hyperpolarization. Following an intraperitoneal (IP) injection, the effects of CNO develop after approximately 15 minutes, peak after approximately 30 minutes, and sharply decline over two hours (Guettier et al., 2009). Given this time course, the DREADD system is well-suited for studying steady-state network responses in vivo.

To achieve cell-type specific expression of DREADDs in MEC LII, we used the tetracycline transactivation system (**Figure 13**; Gossen et al., 1995). In this system, anatomical specificity is provided by a cell type-specific promoter in the driver line, while dispersed, high-level transgene expression is controlled by a ubiquitous promoter in the payload line. In the driver line, the tetracycline transactivator (tTA) sequence is downstream from a cell-type specific promoter. The payload line carries the transgene of interest downstream from the tetracycline-response element (TRE), which is composed of a minimal promoter and the Tet operator (tetO) sequence. In double-positive offspring, tTA is therefore expressed in a cell type-specific manner and can bind to the TRE, activating high-level transcription of the transgene.

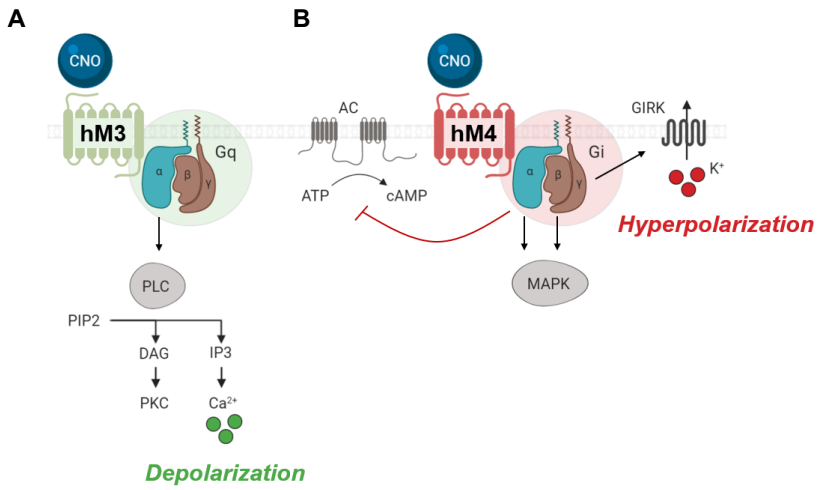

Figure 12 | Mechanisms of action for designer receptors. (A) CNO binds to the hM3Dq DREADD (green), a Gq-coupled receptor, activating a PLC-dependent pathway, which leads to calcium release and depolarization. (B) CNO binding to the hM4Di DREADD (red), a Gi-coupled receptor, decreases cAMP signaling, increases MAPK signaling, and activates GIRK channels, leading to potassium efflux and hyperpolarization. PLC, phospholipase C; MAPK, mitogen-activated protein kinase; GIRK, G-protein inwardly-rectifying potassium channels. Figure created by B. R. Kanter.

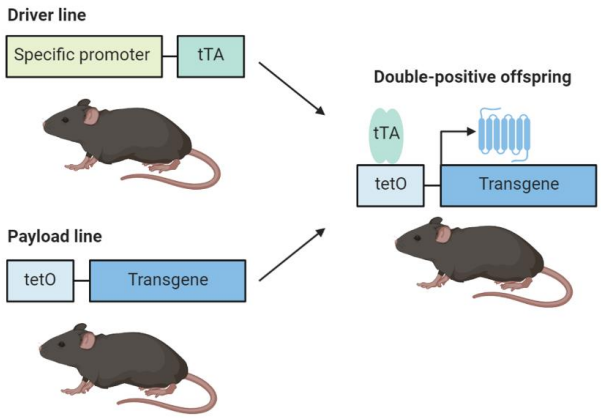

Figure 13 | Tetracycline-transactivation system for transgene expression. In the driver line, tTA expression is controlled by a cell type-specific promoter. The payload line carries the transgene of interest downstream from a minimal promoter. In double-positive offspring, tTA is available to bind the tetO sequence only in the population of cells dictated by the specific promoter, activating transcription of the transgene. tTA, tetracycline transactivator; tetO, Tet operator.

Here, we used the EC-tTA driver line (Yasuda and Mayford, 2006), which expresses almost exclusively in reelin-positive stellate cells throughout the dorsoventral extent of MEC LII, with limited expression in pre- and parasubiculum (**Figure 14**; Rowland et al., 2013; Rowland et al., 2018; Paper 1). We crossed this driver line to hM3Dq-tetO or hM4Dq-tetO payload lines (Alexander et al., 2009), enabling us to increase or decrease the activity of a subset of stellate cells in MEC LII, respectively. Using in situ hybridization for DREADD receptor mRNA, we estimated that our manipulation targeted approximately 27% of stellate cells in MEC LII.

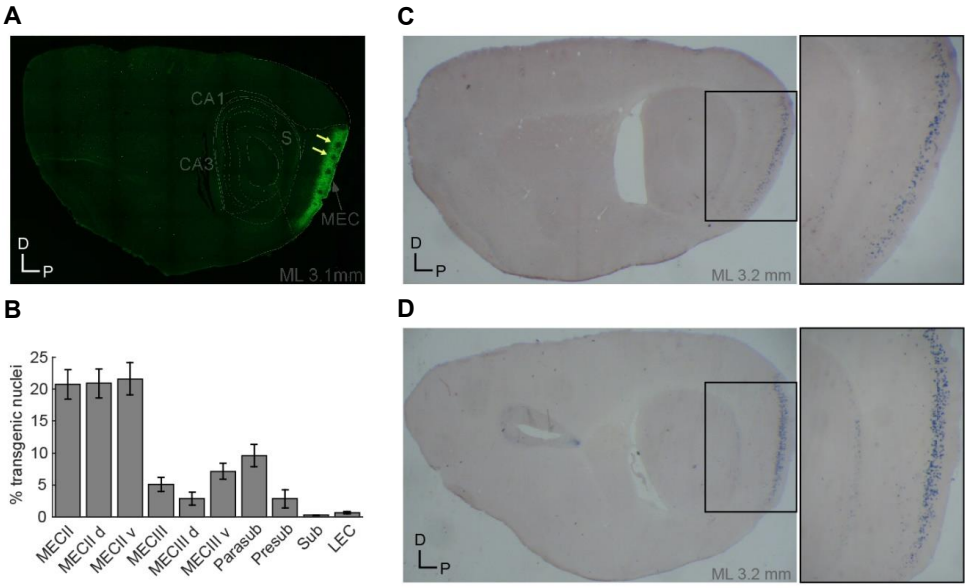

Figure 14 | Highly specific transgenic expression of DREADDs in MEC LII. (A) Expression of hM3Dq transgene (green) visualized by antibody staining in a sagittal section. Note the absence of label in presumed calbindin-positive patches (yellow arrows), consistent with expression restricted to reelin-positive stellate cells. (B) Percentage of transgenic nuclei by brain region. (C-D) In situ hybridization for hM3Dq (C) and hM4Di (D) mRNA in sagittal sections. Insets on the right show MEC. Abbreviations: D, dorsal; P, posterior; ML, medial-lateral; MEC, medial entorhinal cortex; d, dorsal; v, ventral; Parasub, parasubiculum; Presub, presubiculum; Sub, subiculum; LEC, lateral entorhinal cortex. Roman numerals refer to cell layer. Adapted from Paper 1.

Double-positive (i.e., DREADD-expressing) offspring of each cross given IP injections of the designer ligand CNO are referred to as hM3 or hM4 mice. The control group (Con) included single-positive (i.e., non-DREADD-expressing) littermates or wild-type C57 mice given IP injections of CNO, and double-positive offspring given IP injections of saline.

Electrophysiological Recordings

Experimentally naïve hM3, hM4, or Con mice were surgically implanted with four- or eight-tetrode microdrives in the dorsal hippocampus (CA1 and/or CA3) or superficial MEC. Following recovery, we screened for units as mice explored an open field environment, during which time the recording environment became highly familiar to the mice. Experiments were initiated when cells with clear spatial and/or head direction correlates were observed along with increased power in the theta range.

First, baseline activity was recorded for 30 minutes (BL1) (**Figure 15**). Mice were then removed from the open field environment and given an IP injection of CNO or saline. Immediately following the injection, mice were placed back into the open field environment and data were recorded for one to six hours (CNO). Mice were then removed from the environment and returned to their home cage in the colony room. For the majority of our experiments, mice were returned to the open field environment for an additional 30-minute baseline session (BL2) after a delay of 12+ hours. Experiments were repeated as long as activity was still present. For a subset of our experiments, a break was inserted into the CNO session after two hours. During this one- to four-hour break, mice were returned to their home cage in the colony room. Following the break, mice were reintroduced to the open field environment and data were recorded for an additional hour. We assessed the reversibility of our manipulation with a second BL session 12+ hours later (BL2). Once electrophysiological recordings were complete, mice were euthanized and perfused in order to assess the location of recording sites.

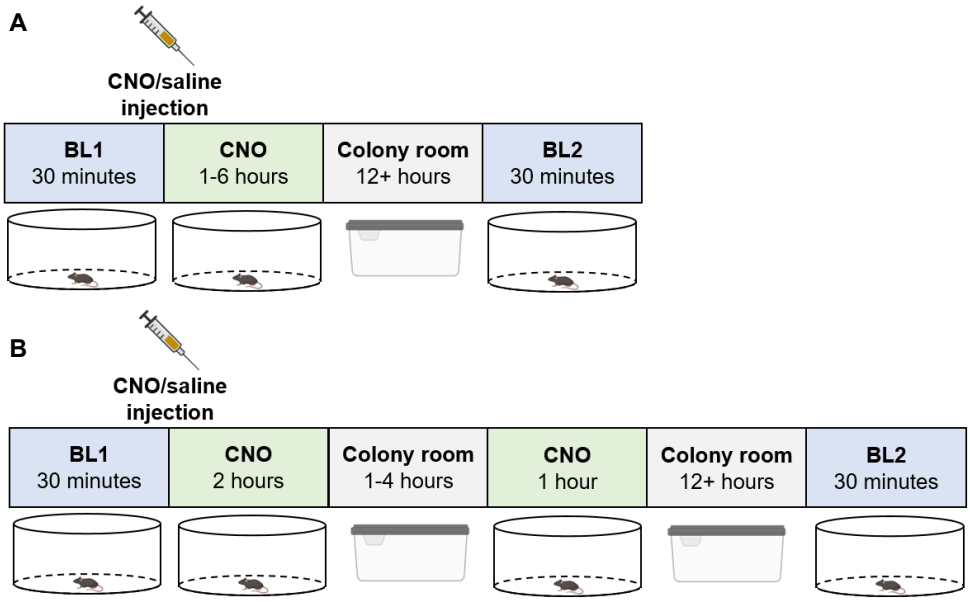

Figure 15 | Recording protocols. (A) During the initial baseline session (BL1), mice explored a circular open field environment for 30 minutes. Mice were given an injection of CNO or saline and returned to the environment for the CNO session, which ranged from one to six hours in length. Once the recording ended, mice were returned to their home cages in the colony room for 12+ hours, after which a final 30-minute baseline session (BL2) occurred. (B) After the initial baseline session (BL1), injection of CNO or saline, and a two-hour CNO session, mice were returned to their home cages in the colony room for one to four hours. Mice were then reintroduced to the open field environment for a subsequent one-hour session. After 12+ hours, a second baseline session (BL2) was conducted.

Behavior

In Paper 1, we used the Morris Water Maze task to assess spatial memory in hM3, hM4, and Con mice (**Figure 16**). In this task, mice learn to use distal spatial cues to navigate to a hidden platform located in a constant position. On each of the eight training days, the mice were given four 60-second trials separated by 120 seconds. Each trial began from a pseudorandom start location. On Days 9 and 10, mice were given a single probe trial during which the platform was absent. Thirty minutes prior to the probe trial on Days 9 and 10, mice were given an IP injection of CNO or saline, respectively.

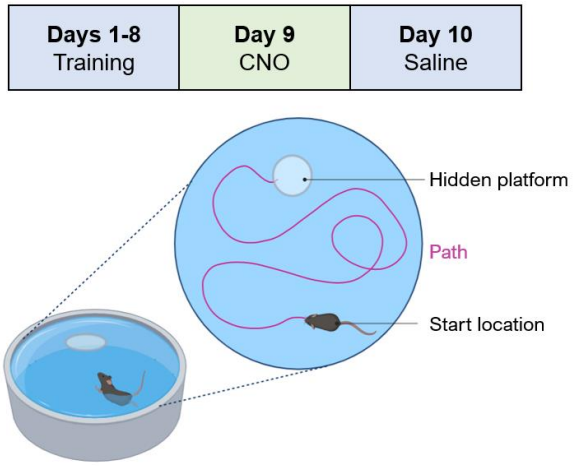

Figure 16 | Behavioral protocol for Morris Water Maze task. (A) On each training day (Days 1-8), mice were given four trials in which they were placed in a pseudorandom start location and were required to navigate to a hidden platform location using only distal cues. On Days 9 and 10, mice were given an injection of CNO or saline, respectively, 30 minutes before a single probe trial during which the hidden platform was absent.

SYNOPSIS OF RESULTS

Paper 1: A novel mechanism for the grid-to-place cell transformation revealed by transgenic depolarization of medial entorhinal cortex layer II.

In Paper 1, we demonstrated that depolarization of a subset of MEC LII neurons in hM3 mice via CNO injection produced robust remapping of CA1 place cells and impaired spatial memory in the Morris Water Maze. In contrast, hyperpolarization of the same subset of MEC LII neurons in hM4 mice did not elicit hippocampal remapping or spatial memory impairment. In both hM3 and hM4 mice, CNO administration produced significant changes in the firing rate and field size of putative excitatory neurons in MEC without causing any obvious changes to their spatial firing patterns. Notably, depolarization of MEC LII did not change the location of grid fields, which is typically observed under conditions that elicit hippocampal remapping. Instead, CNO administration in hM3 mice produced changes in the firing rate of individual grid fields that differed in magnitude and/or direction within single grid cells. In contrast, in hM4 and control mice, grid field relationships were stable before and after CNO injection. Since there were no significant changes to the spatial or directional firing patterns of other functional cell types in MEC in hM3 mice, we proposed that these changes in grid field firing rates may serve as an alternative mechanism underlying hippocampal remapping.

Paper 2: Grid field firing rate changes control the predictability and stability of hippocampal remapping.

In Paper 2, we discovered that depolarization of a subset of MEC LII neurons in hM3 mice caused place cells to remap in a predictable manner. More specifically, place cells frequently remapped to locations that contained small amounts of activity during an initial baseline session prior to CNO injection. By adapting a model of the grid-to-place cell transformation, we demonstrated that this predictable hippocampal remapping could result from changes in the firing rates of individual grid fields. Following CNO injection, grid field rates in hM3 mice continued to fluctuate, eventually disrupting the relationship between individual grid fields, and the magnitude of these fluctuations was tightly correlated to place cell stability. Over time, the magnitude of grid field rate changes increased, and the spatial stability of hippocampal place cells decreased, a result that was recapitulated in our model of the grid-to-place cell transformation. Grid field rates and place field locations in hM3 mice continued to evolve, without returning to baseline, as long as the mice remained in the environment following CNO injection. Returning the mice to the colony room for periods as short as 60 minutes often caused both grid field relationships and place field locations to reset, even at timepoints associated with strong CNO-induced changes during continuous recordings. The following day, 12+ hours after CNO injection, grid field rates and place field locations in hM3 mice completely reverted to baseline. By readministering CNO, we could assess whether depolarization of the same subset of MEC LII neurons multiple times would produce the same network response. Our manipulation elicited changes in place field locations and grid field rates that were highly similar across days. Incorporating the grid field rate changes we observed on each day into our model also yielded highly similar hippocampal remappings, supporting our conclusion that grid field rates control the location and stability of hippocampal place cells.

Paper 3: Distinct remappings in CA3 and CA1 elicited by depolarization of medial entorhinal cortex layer II.

In Paper 3, we reported that depolarization of a subset of MEC LII neurons via CNO injection in hM3 mice causes robust remapping of CA3 place cells, as we had observed previously in CA1. Previous studies aiming to characterize the functional role of these hippocampal subregions have typically compared the responses of CA1 and CA3 place cells to incremental alterations of the sensory environment. In contrast, our manipulation induced place cell remapping in both regions even though the mice explored a stable environmental context. Thus, we had a unique opportunity to compare the responses of CA1 and CA3 place cells to systematic manipulations of MEC LII input using different doses of CNO, thereby mimicking these varying degrees of contextual change. Before doing so, we confirmed that higher doses of CNO substantially increased activity in MEC LII relative to lower doses using double-label in situ hybridization for hM3Dq and Arc, an immediate-early gene used as a marker for recent neural activity. At the single cell level, CA1 neurons remapped more strongly and exhibited greater changes in both firing rate and place field size at higher doses of CNO than at lower doses of CNO. In contrast, CA3 neurons strongly remapped and exhibited high levels of firing rate and field size change at both low and high doses of CNO. At the population level, however, we observed that the hippocampal representation in both subregions was more orthogonalized after higher doses of CNO. CNO-induced changes in place cell activity were generally reversible after low doses of CNO in CA1 and CA3, as well as after high doses of CNO in CA1. Following high doses of CNO, CA3 place cells frequently remapped a second time, rather than reverting to baseline. Therefore, we suggest that high doses of CNO are sufficient to induce plasticity between monosynaptically connected neurons in MEC LII and CA3, and that these changes in synaptic strength are capable of altering the spatial input to CA3 place cells even when CNO is absent.

EXPERIMENTAL CONSIDERATIONS

We used a chemogenetic approach to bidirectionally manipulate the activity of a subset of neurons in MEC LII. We coupled this with in vivo electrophysiology to monitor the response of our manipulation both locally in MEC and downstream in the hippocampus. Chemogenetics involves the use of engineered receptors to reversibly and remotely control neural activity through the administration of an otherwise inert designer ligand. The ideal chemogenetic receptor should meet the following criteria: (1) the receptor is insensitive to endogenous ligands; (2) the receptor has a high affinity for the designer ligand; (3) the receptor exhibits little or no basal activity in the absence of ligand. The ideal designer ligand (1) should not exhibit off-target effects at endogenous receptors, and (2) should cross the blood-brain barrier following peripheral administration. While the DREADD system used here improves upon the shortcomings of its predecessors (Lykken and Kentros, 2014), recent reports have questioned whether this system fulfills these criteria (Gomez et al., 2017), as originally suggested (Armbruster et al., 2007).

The hM3Dq and hM4Di DREADDs were engineered by introducing random mutations into human M3 and M4 muscarinic receptors, respectively, which reduced their affinity for the endogenous ligand acetylcholine and increased their affinity for the exogenous designer ligand CNO (Armbruster et al., 2007). In the absence of ligand, the DREADDs lack any detectable constitutive activity (Armbruster et al., 2007; Alexander et al., 2009). However, a major drawback of using CNO as a designer ligand is that a small proportion of systemically administered CNO is rapidly metabolized to clozapine (Jann et al., 1994; MacLaren et al., 2016), an antipsychotic drug which exhibits activity at serotonin and dopamine receptors (Meltzer, 1994), among other targets (Gomez et al., 2017; Jendryka et al., 2019). Although DREADD receptors exhibit lower affinity for many endogenous ligands (including acetylcholine) than for CNO, the affinity of clozapine for DREADD receptors greatly exceeds that of CNO (Armbruster et al., 2007; Gomez et al., 2017). In contrast to earlier reports (Ji et al., 2016), a recent study questioned whether CNO crosses the blood-brain barrier following systemic injection (Gomez et al., 2017). Since converted clozapine readily permeates the blood-brain barrier (Cremers et al., 2012; Hellman et al., 2016) and exhibits high affinity for DREADD receptors, the authors concluded that clozapine may be primarily responsible for activating DREADD receptors following systemic injection of CNO (Gomez et al., 2017). Although the concentration of clozapine is high in brain tissue following systemic injection of CNO (Gomez et al., 2017; Jendryka et al., 2019), one study reported that its concentration in cerebrospinal fluid remains below the detection limit, indicating that clozapine may be bound unspecifically to brain tissue and would therefore be unable to bind to DREADD receptors

(Jendryka et al., 2019). This study also demonstrated that CNO does indeed cross the blood-brain barrier in mice (Jendryka et al., 2019).

In any case, to control for any potential off-target effects of CNO and/or clozapine, we administered CNO to non-DREADD-expressing littermates. Given that clozapine accumulates over time, reaching its highest concentration two or more hours after CNO injection (Gomez et al., 2017), the inclusion of a non-DREADD-expressing control group was particularly important for our long-duration recordings, which continued up to six hours after CNO injection. Critically, we did not observe any significant electrophysiological or behavioral differences between the non-DREADD-expressing control group given CNO and a second control group of double-positive mice injected with saline. These results are in agreement with prior studies that reported no behavioral effects of CNO in non-DREADD-expressing animals using doses as high as 20 mg/kg (Mahler et al., 2014). Similarly, we confirmed that CNO did not cause any obvious behavioral or locomotor effects in non-DREADD-expressing mice with CNO doses as high as 20 mg/kg (unpublished data from B. R. Kanter). The majority of our experiments used a 1 mg/kg dose of CNO, and the highest dose of CNO that we used was 15 mg/kg. Thus, we conclude that our results cannot be explained by off-target effects of CNO and/or clozapine. In the future, the use of non-CNO designer ligands, such as compound C21 (Chen et al., 2015), could circumvent these issues entirely.

Another important concern for our experiments relates to the strength of inactivation achieved using the DREADD system. First, it is important to acknowledge that the suppression of neural activity that results from CNO injection in hM4 mice is unlikely to be as robust as the suppression resulting from optogenetic inhibition or traditional pharmacological inactivation. Second, the magnitude of excitation in hM3 mice would likely exceed the magnitude of suppression in hM4 mice given the same dose of CNO. A previous report indicated that local application of CNO to hM3Dq-expressing neurons produces 150% excitation above baseline firing rates (Vazey and Aston-Jones, 2014). In contrast, firing rates in hM4Di-expressing neurons were reduced to approximately 60% of their baseline firing rate, suggesting that inhibitory DREADDs dampen, rather than eliminate, neural activity (Mahler et al., 2014). Similar results have been obtained following systemic delivery of CNO (Vazey and Aston-Jones, 2014; Chang et al., 2015). As a consequence, administration of higher doses of CNO in hM4 animals are often required to induce behavioral effects (Farrell and Roth, 2013; Mahler et al., 2014; Yau and McNally, 2015). Thus, it is important to note that for our experiments using hM4 mice in Paper 1, we used a 10 mg/kg dose of CNO, rather than the 1 mg/kg dose used for hM3 mice. Even at this higher dose, hyperpolarization

of MEC LII neurons in hM4 mice did not induce remapping in CA1 or impair spatial memory. We confirmed that 10 mg/kg CNO did in fact suppress neural activity in hM4 mice by recording locally from the superficial layers of MEC. The strength of firing rate suppression in hM4 mice was roughly equal to the firing rate elevation in hM3 mice, ameliorating this concern.

An additional consideration for our experiments relates to the repeatability of our manipulation, since we administered CNO multiple times to individual mice. This was a concern because DREADDs are modified GPCRs, which can be desensitized, internalized, and downregulated following activation (DeWire et al., 2007). However, transgenic expression of DREADDs likely results in much higher expression levels than native GPCRs, reducing the likelihood of desensitization following repeated activation (Roth, 2016). In line with previous findings (Alexander et al., 2009), we did not observe any desensitization in our electrophysiological recordings. Instead, repeated administration of CNO continued to induce the same electrophysiological changes in MEC and CA1 neurons that we observed following its initial administration. Thus, we concluded that our manipulation could be repeated multiple times within a single animal.

Despite these limitations, DREADDs remain a highly effective tool for manipulating neural activity in vivo, and they offer several important advantages for our experiments relative to other chemogenetic or optogenetic (i.e., controlling neural activity with light) methods. First, due to the pharmacokinetics of CNO, DREADDs can be used to modify neural activity for a prolonged period (i.e., minutes to hours). Although this approach lacks the millisecond timescale precision of optogenetics, it is ideal for studying steady-state hippocampal network response to the manipulation of MEC activity. Optogenetic methods are difficult to use for extended periods due to the production of heat associated with sustained illumination, which can be detrimental to cell health and can alter the activity patterns of neurons. The onset and reversibility of other chemogenetic methods, such as the use of modified receptors activated by ivermectin (Lerchner et al., 2007; Lynagh and Lynch, 2010), are much slower (i.e., hours to days) than DREADDs, limiting their applicability in this context. A second benefit of the DREADD system is that CNO can be administered noninvasively via systemic injection. Following delivery, CNO diffuses widely and is capable of binding uniformly to DREADD receptors distributed throughout a large or elongated structure like MEC. In contrast, optogenetics typically requires the invasive implantation of a light source, and the scattering of light could differentially impact opsin-expressing neurons located at various distances from the light source. An alternative chemogenetic method, selective expression of the allatostatin GPCR (Lechner et al., 2002), also requires invasive intracranial delivery of ligand

because allatostatin does not cross the blood-brain barrier and its activity is limited by diffusion. Finally, using the DREADD system, we are able to increase or decrease the activity of the same population of neurons in hM3 and hM4 mice, respectively, while other chemogenetic methods (including those described above) mediate neural silencing alone. Thus, DREADDs are ideally suited for bidirectionally manipulating the activity of a specific population of MEC neurons, especially given the ease of combining this approach with electrophysiological recordings and behavior.

GENERAL DISCUSSION

Mechanisms for place cell remapping

Not long after the discovery of grid cells, it was demonstrated that the grid pattern shifts and/or rotates between distinct environments, when place cells undergo global remapping (Fyhn et al., 2007). Simultaneously recorded grid cells (i.e., within a module) realigned coherently such that the relationship in their spatial phases was preserved between environments (Fyhn et al., 2007). If the entire population of grid cells realigned coherently, this would not result in global remapping. Instead, place field locations would shift and/or rotate in concert with the grid pattern. Thus, it was proposed that grid cells in different modules might realign independently, which would change the coactivity patterns between neurons in a manner that is capable of generating strong hippocampal global remapping (**Figure 11**; Fyhn et al., 2007; Monaco and Abbott, 2011).

In support of this proposal, there is accumulating evidence that grid modules can operate independently under certain conditions. For example, it was shown recently that spike-time correlations between pairs of grid cells are weaker between modules than within a module during several behavioral states (Gardner et al., 2019). Additionally, grid modules have been shown to respond independently to the compression of a familiar environment (Stensola et al., 2012). Following this manipulation, cells in three of four simultaneously recorded modules completely rescaled their grid patterns, even though cells in the module with the smallest spacing showed only minimal rescaling (**Figure 17A**).

Given the difficulty of simultaneously recording large numbers of grid cells across multiple modules, these results provided an important step forward by demonstrating that modules are capable of operating independently. However, place cells do not exhibit global remapping under these conditions. Instead, when an environment is rescaled by extending its length in one dimension, place fields are stretched or pulled apart in that direction while remaining a fixed distance from the wall (**Figure 17B**; O'Keefe and Burgess, 1996). To resolve whether modules realign (rather than simply rescale) independently under conditions that elicit place cell remapping, it will be necessary to record from multiple modules simultaneously in distinct environments.

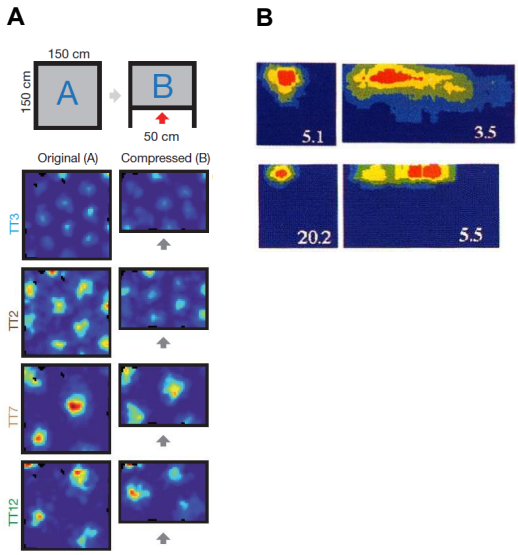

Figure 17 | Grid modules respond independently to the rescaling of a familiar environment. (A) Grid cells in the module with the smallest spacing do not rescale following the compression of the environment, whereas simultaneously recorded grid cells in three modules with larger spacing rescaled completely. (B) When an environment is elongated in the horizontal direction, place fields are stretched (top row) or pulled apart (bottom row) in that direction while maintaining a fixed distance from an environmental boundary. Peak firing rate is indicated at the bottom right of each rate map. (A-B) Activity is color coded from blue to red. Panel A adapted from Stensola et al., 2012. Panel B adapted from O'Keefe and Burgess, 1996.

Although computational evidence indicates that independent realignment of grid modules would be sufficient to induce hippocampal remapping (Monaco and Abbott, 2011), we demonstrated in Paper 1 that it is not necessary for hippocampal remapping. Much to our surprise, depolarization of a subset of MEC LII neurons produced robust hippocampal remapping even though grid vertices remained in a fixed position. For many months, we struggled to understand how this could occur. First, we focused our attention on how the activity of other cell types in the superficial MEC was affected by our manipulation, but we found no compelling explanation for the observed remapping. Eventually, instead of considering the grid pattern as a whole by examining its hexagonal regularity, spacing, or spatial position, as is typically done, we thought to consider whether our manipulation produced changes at the level of individual grid fields. Once we began to evaluate the cells in this manner, we immediately noticed that the firing rates of individual grid fields seemed to be stable over time in control mice. In contrast, in hM3 mice, the firing rates of individual grid

fields varied independently in response to our manipulation. Thus, we proposed that the corresponding changes in grid field relationships could serve as an alternative mechanism for place cell remapping. Subsequently, in Paper 2, by adapting a model of the grid-to-place cell transformation, we provided strong support for this conclusion by confirming that grid field rate changes are sufficient to induce the same type of hippocampal remapping we observed in vivo.

It is important to note that these potential mechanisms of remapping do not have to operate in isolation. Instead, it seems likely that independent grid realignment between environments could be accompanied by grid field rate changes, which would aid in the orthogonalization of hippocampal representations. Demonstrating this in vivo will be quite difficult, however, as it is currently unclear how to track the location of individual grid fields as they shift and/or rotate between distinct environments. Thus, we had a unique opportunity in our experiments to examine how grid field rate changes impact the hippocampal representation of space when grid vertices remain in a fixed position.

If grid modules do not realign independently between environments (or do so only under certain conditions), high levels of grid field rate change alone could in fact produce a completely orthogonal hippocampal representation, as we demonstrated in Paper 2 (Figure S7D). Given the recent accumulation of evidence indicating that changes in grid field relationships occur following a variety of contextual manipulations, including changes in the shape, color, and/or odor of the environment (Diehl et al., 2017; Ismakov et al., 2017), this mechanism could underlie place cell remapping under conditions that would not be expected to induce grid realignment. For instance, place cell remapping has been observed following changes in behavioral task (Wiener et al., 1989; Markus et al., 1995; Hallock and Griffin, 2013), changes in memory demands (Ferbinteanu and Shapiro, 2003; Kennedy and Shapiro, 2009; Ferbinteanu et al., 2011), and changes in goal location (Fyhn et al., 2002; Dupret et al., 2010), even though the animals occupy the same physical space.

Additionally, under some conditions, the place cell network undergoes partial remapping, meaning that some cells remap while others maintain stable place field locations (Anderson and Jeffery, 2003). Partial remapping has always posed a challenge for attractor hypotheses, which conceptualize place cell remapping as a sudden and coherent transition of the network from one state to another (McNaughton et al., 1996). Grid field rate changes could potentially circumvent this issue and account for the heterogeneity of partial remapping in a number of ways. First, if grid field rates change in a localized manner (e.g., increasing in a restricted portion of the environment), as was observed recently (Butler et al., 2019), place

cells that originally received subthreshold input in that location might remap there (assuming a linear summation model of the grid-to-place cell transformation) (**Figure 18A**, top row). Place cells receiving grid inputs that do not overlap in that location would be unaffected and could continue to represent another salient feature of the environment (**Figure 18A**, bottom row). Second, it could be that some place cells remap because grid inputs decrease in the current place field location and increase in a location that receives subthreshold input (**Figure 18B**, top row). Other place cells receiving grid inputs that exhibit little or no change in activity levels in the current place field location may not remap (**Figure 18B**, bottom row).

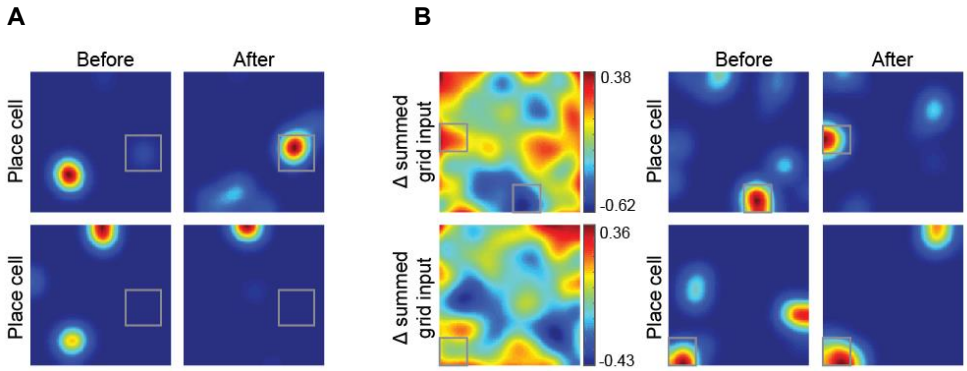

Figure 18 | Partial remapping can be explained by changes in grid field rates. (A) If grid field rates increase in a restricted portion of the environment, a place cell with subthreshold input in that location may remap there (top row), whereas a place cell with subthreshold input in other locations may not remap (bottom row). Gray boxes indicate the location where grid field rates increase. (B) If grid input decreases in the original place field location and increases in a location that previously received subthreshold input, a place cell may remap to that location (top row). When there is little or no change in grid input in the original place field location, a place cell may not remap (bottom row). Gray boxes surround place field locations before and after grid field rate changes. (A-B) Activity is color coded from blue to red. Panels A and B depict simulated place cells and grid inputs from Paper 2.

Do place cells rely on grid cell input?

Both of the mechanisms of remapping described above assume that grid cells are the primary determinant of place cell firing. However, many studies have called this assumption into question. The location-specific activity of place cells persists following manipulations that disrupt grid cell firing, such as lesions (Van Cauter et al., 2008; Hales et al., 2014; Schlesiger et al., 2015; Schlesiger et al., 2018) and inactivations of MEC (Miao et al., 2015; Ormond and McNaughton, 2015; Rueckemann et al., 2016; Zhao et al., 2016) or medial septum

(Koenig et al., 2011; Brandon et al., 2014). Furthermore, interfering with the grid signal does not prevent hippocampal remapping (Brandon et al., 2014; Schlesiger et al., 2018). In contrast, our results clearly support a role for grid cells in the generation and remapping of place fields. One possible explanation for these disparate patterns of results is that grid cells are the strongest contributor to place cell firing when they are *intact*. When the grid signal is absent, other functional cell types in MEC, such as border or spatial nongrid cells, which also project directly to the hippocampus (Zhang et al., 2013), might contribute to the generation and remapping of place cells (Barry et al., 2006). Alternatively, spatial input may come from MEC neurons that have not yet been functionally characterized, or from neurons that do not fit neatly into a specific functionally defined cell type, but nevertheless convey information about space to the hippocampus (Hardcastle et al., 2017). Another possibility is that a contextual signal for place cell remapping is provided by a subset of MEC neurons referred to as “context cells” (which may or may not include specific functionally defined cells), that exhibit drastic changes in firing rate between environments (Kitamura et al., 2015). Finally, it may be that other weakly spatial inputs to the hippocampus, such as those from the LEC, could support place cell firing following complete lesions of MEC.

Place fields could persist when MEC is inactivated via chemogenetic or optogenetic methods because these manipulations may not completely disrupt grid cell firing. For instance, a recent study reported that the firing rates of MEC neurons were reduced by approximately 60% using chemogenetic or optogenetic inactivation of this region (Miao et al., 2015). In other studies, the degree and/or the extent of inactivation were not quantified, making it more difficult to interpret the results (Rueckemann et al., 2016; Zhao et al., 2016). In any case, inactivation of MEC using these methods typically produces hippocampal remapping in a familiar environment (to varying degrees) (Miao et al., 2015; Rueckemann et al., 2016; Zhao et al., 2016). Given that grid cell activity likely persists following these manipulations, it may be that remapping in these studies could even be explained by changes in the firing rates of individual grid fields. Since the impact of these manipulations on grid cell firing patterns was not characterized, it is unclear precisely which changes in MEC neurons were associated with the observed remapping.

Here, it is important to note a key difference between the results of the aforementioned studies and our own work. While these studies observed remapping following MEC inactivation, we observed remapping following depolarization, but *not* hyperpolarization, of MEC LII neurons. A plausible explanation for this difference is that the strength of the manipulation differs across studies in terms of the number of neurons infected, their cell type, or their anatomical location within MEC. One study reported that over 90% of neurons

within the target region expressed the transgene throughout all layers of MEC (Miao et al., 2015), whereas our manipulation targeted a subset (~27%) of stellate cells that were largely confined to a specific layer of MEC. Other viral or transgenic approaches used to perturb the relationship between grid cells and place cells have not achieved comparable specificity.

Does remapping differ between hippocampal subregions?

The use of this highly specific transgenic line enabled us to determine the specific contribution of MEC LII to hippocampal remapping. This was particularly valuable because few studies have tested the impact of a particular sublayer of MEC on hippocampal function. Instead, they have investigated the role of this area more generally by lesioning or inactivating cells throughout all sublayers (Van Cauter et al., 2008; Hales et al., 2014; Miao et al., 2015; Ormond and McNaughton, 2015; Rueckemann et al., 2016; Schlesiger et al., 2018). Studies that have removed trisynaptic or monosynaptic input from MEC LII or MEC LIII, respectively, have shown that CA1 place cells remain intact, yet diffuse, making the contribution of a specific sublayer unclear (Brun et al., 2002; Brun et al., 2008; Nakashiba et al., 2008). Even fewer studies have investigated how individual sublayers of MEC are involved in hippocampal remapping in a manner that leaves hippocampal subregions CA1 and CA3 intact.

Thus, in Paper 3, we took advantage of a unique opportunity to manipulate the activity of a subset of stellate cells in MEC LII and compare the responses of CA1 and CA3 neurons. In these experiments, we used different doses of CNO to mimic varying degrees of contextual change. Depolarization of a subset of MEC LII neurons elicited qualitatively similar place cell remapping in both subregions across a range of CNO doses. However, CA1 place cells responded to our manipulation in a dose-dependent manner (i.e., remapping more strongly after high doses of CNO), whereas the strength of remapping in CA3 was similar after low and high doses of CNO (**Figure 19**). Our results agree with previous work indicating that CA1 neurons represent changes in input in a linear fashion (for review, see Guzowski et al., 2004). For example, it has been shown that the CA1 representation is more orthogonalized when the similarity between testing enclosures is low than when testing enclosures are highly similar (Leutgeb et al., 2004). In contrast, the activity patterns of CA3 neurons are highly orthogonalized regardless of the similarity of the testing enclosure (Leutgeb et al., 2004). This is consistent with our observation of near-complete orthogonalization of the CA3 representation even after low doses of CNO. Other studies have examined how CA1 and CA3 neurons respond to more subtle alterations of proximal or distal cues alone (Lee et al.,

2004; Vazdarjanova and Guzowski, 2004). Under these conditions, the degree of orthogonalization is greater in CA1 than in CA3. Thus, it is possible that in response to even lower doses of CNO than we used in our experiments, we would have obtained a similar pattern of results. Overall, our results corroborate previous work showing that CA1 and CA3 representations can emerge independently. We also extend these results in an important way by demonstrating that changing the activity of a subset of MEC LII neurons is sufficient to produce independent responses in CA1 and CA3 neurons. This differs from previous proposals that independence of the CA1 representation arises by virtue of direct input from MEC LIII (Leutgeb et al., 2004). We suggest that a contextual signal that triggers remapping is conveyed throughout the trisynaptic loop immediately following depolarization of MEC LII neurons, but that the process of orthogonalization in CA3 continues in an iterative fashion via activity in its recurrent collaterals. This conclusion is supported by evidence indicating that new representations emerge more slowly in CA3 than in CA1 (Leutgeb et al., 2004). Given the coarse timescale of our manipulation, however, this proposal remains speculative at this time.

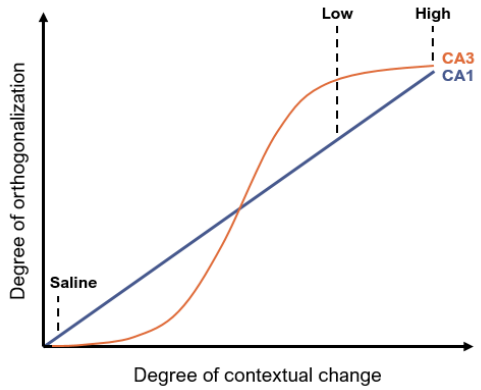

Figure 19 | Degree of orthogonalization of hippocampal representations in CA1 and CA3 in response to varying degrees of contextual change. As reported previously (Leutgeb et al., 2004), the degree of orthogonalization in CA1 (blue) increased with increasing levels of contextual change (i.e., increasing CNO dose). CA3 representations (orange) were highly orthogonalized after both low and high doses of CNO but could potentially exhibit less orthogonalization following even lower doses of CNO. Adapted from Guzowski et al., 2004.

What do grid cells contribute to place cell firing?

In Paper 2, we were able to predict where place cells in hM3 mice would remap to following our manipulation using the baseline activity of the neurons *before* the manipulation occurred. In order to determine whether grid field rate changes were sufficient to drive the observed remapping, we adapted a model of the grid-to-place cell transformation by incorporating the grid field rate changes we observed empirically in hM3 mice. The remapping that we observed in simulated place cells was remarkably similar to the remapping we observed empirically following depolarization of a subset of MEC LII neurons, in terms of both its extent and its degree of predictability. This similarity allowed us to draw several important conclusions about how grid cells influence the location of place fields.

First, our simulation demonstrated that changes in grid field rates *alone* were sufficient to induce hippocampal remapping, suggesting that this same mechanism could have produced the hippocampal remapping we observed in vivo. Moreover, any other changes induced by our manipulation (i.e., changes in other functional cell types or changes in the mean firing rate of grid cells) were therefore not necessary for hippocampal remapping to occur. Our simulation did not incorporate return projections from the hippocampus to the EC, providing additional support for the idea that remapping was driven directly by changes in grid field rates. Given its coarse timescale, we are not able to make strong claims about the directionality of our manipulation from our in vivo experiments alone. For instance, one could envision that depolarization of a subset of MEC LII neurons produced a change in local network activity that caused downstream place cells to remap, and that feedback from remapped place cells was in fact responsible for modifying grid field rates. This would be consistent with evidence demonstrating that excitatory drive from the hippocampus is required to maintain the grid pattern (Bonnevie et al., 2013). Instead, our results suggest that altered local network activity following CNO injection led to changes in grid field rates, which then drove remapping downstream. That being said, it seems plausible that subsequent fluctuations in grid field rates that occurred over time could have been driven by feedback from place cells, as information continually flows around the entorhinal-hippocampal loop (Rennó-Costa and Tort, 2017).

Second, our results demonstrate that remapping elicited by grid field rate change is predictable in nature, with place fields frequently shifting to locations that previously received subthreshold input. In our simulation, changing grid field rates modified the height of existing peaks in the summed grid input pattern, rather than generating new peaks in discrete

locations, as we observed following the independent realignment of grid modules (**Figure 20**). Thus, simulated place cells frequently remapped to locations that previously received subthreshold input following a change in grid field rates, whereas independent realignment of grid modules resulted in the random reallocation of place field locations.

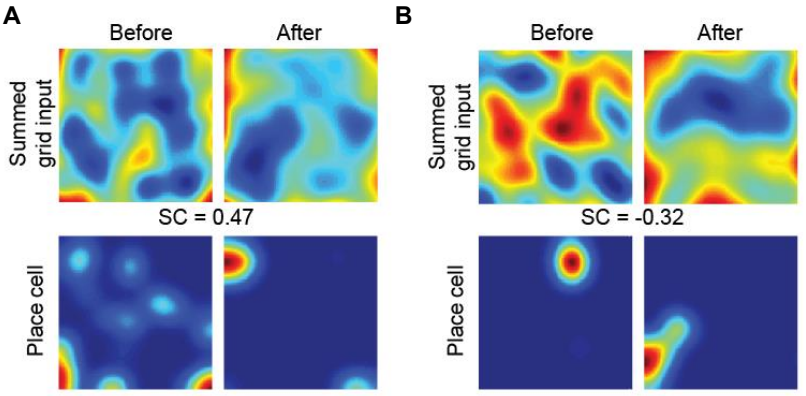

Figure 20 | Predictable remapping results from changes in grid field rates, whereas independent realignment of grid modules results in the random reallocation of place field locations. (A) Grid field rate changes modified the height of existing peaks in summed grid input pattern, producing predictable shifts in place field location. (B) Independent realignment of grid modules resulted in the generation of new peaks in discrete locations in the summed grid input pattern, producing unpredictable shifts in place field location. (A-B) Activity is color coded from blue to red. SC denotes spatial correlation between summed grid inputs before and after grid field rate changes or independent realignment. Adapted from Paper 2.

Other intracellular and extracellular recordings of place cells have also demonstrated that place cells receive subthreshold drive at particular locations in the environment. Intracellular recordings of place cells have shown that there is an elevation in the somatic membrane potential (Vm) under their place field spiking (Epsztein et al., 2011; Lee et al., 2012). In one such study, recordings of CA1 neurons in head-fixed mice navigating a novel virtual maze revealed that the mean Vm was elevated inside the eventual place field location on laps even before spiking occurred (**Figure 21A**; Cohen et al., 2017). These results are reminiscent of our own and suggest that place cells may receive spatial input biased towards the eventual place field location, rather than receiving broadly distributed input tuning. Similarly, a recent study demonstrated that local optogenetic stimulation of CA1 place cells while mice explored a familiar linear track induced remapping, and that the location of the induced fields could be predicted from the baseline activity of the neurons (McKenzie et al., 2019). The authors reported that the firing rate inside the future place field location was

significantly higher than expected by chance, suggesting the prior existence of subthreshold place field drive at that location. A third study juxtacellularly stimulated hippocampal neurons in mice exploring a familiar circular track (Diamantaki et al., 2018). Stimulation outside of the original place field location caused approximately half of the cells to remap to the stimulated location (**Figure 21B**). Two observations in this study were consistent with our own. First, in some cases, an additional place field was induced at the stimulation site, and both the induced and original fields persisted throughout the recording. Second, in other cases, the original field and the induced field were co-expressed for several minutes following stimulation. These results are consistent with the idea that remapping can result from a redistribution in the strength of existing inputs.

It is important to note here that the grid-to-place cell model we adapted in Paper 2 simulates place fields in CA3 (de Almeida et al., 2012), whereas the empirical evidence we obtained in that paper came from recordings of CA1 place cells. In Paper 3, however, we demonstrated that CA3 place cells also remapped in hM3 mice following depolarization of a subset of MEC LII neurons. In response to a low dose of CNO, place cells in both CA1 and CA3 exhibited large changes in firing rate, field size, and the spatial location of their place fields. Moreover, we observed that CA3 place cells also remapped in a predictable manner following our manipulation after a low dose of CNO (**Figure 21C**), just as we observed in CA1. Given the similarity of the remapping that we induced in these two subregions, along with the similarity of the simulated and empirically observed remappings, adapting this model was a reasonable method for better understanding how grid field rates impact place field location.

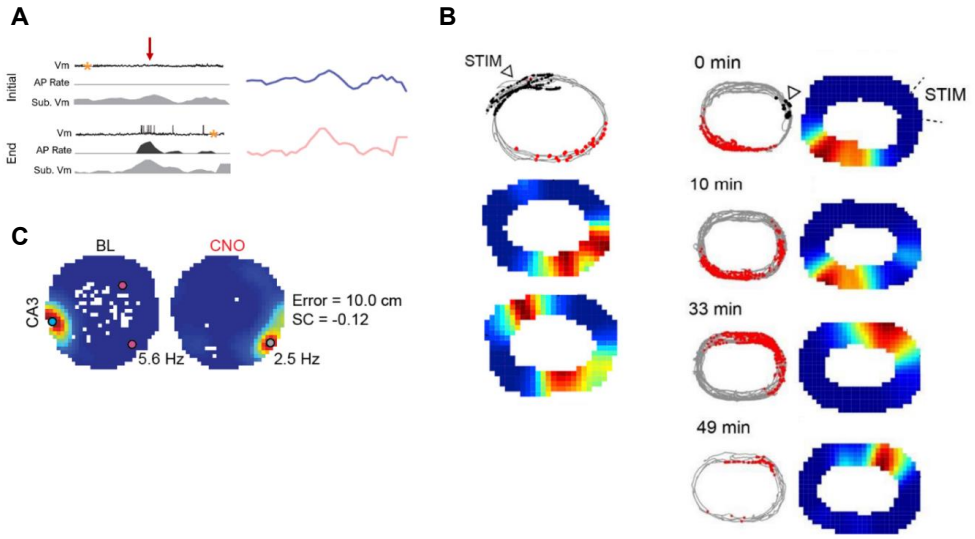

Figure 21 | Evidence of subthreshold drive to place cells in intracellular, juxtacellular, and extracellular recordings. (A) During the initial laps on a linear track in a novel environment, some place cells did not fire any action potentials (AP). However, the subthreshold membrane potential (Sub Vm) of these cells was elevated in the eventual location of the place field (indicated by red arrow). (B) Following juxtacellular stimulation on a familiar circular track, co-expression of the original field and the induced field persisted throughout the duration of the recording (leftmost column) or for several minutes following stimulation (right columns). Gray lines indicate the animal's trajectory. Red dots indicate spontaneous activity. Black dots indicate activity resulting from stimulation (STIM). (C) CA3 place cells in hM3 mice remapped to predictable locations following CNO injection. Error denotes minimum distance between predicted locations (pink dots) and eventual place field location (gray dot). SC denotes the spatial correlation between rate maps from BL and CNO sessions. Peak rate is indicated at the bottom right of each rate map. (B-C) Activity is color coded from blue to red. Panel A adapted from Cohen et al., 2017. Panel B adapted from Diamantaki et al., 2018. Panel C is unpublished data from B. R. Kanter analyzed by C. Lykken.

Several lines of evidence have confirmed that the stability of place cells also seems to depend on cells in MEC. As previously discussed, lesions of MEC do not eliminate the location-specific activity of hippocampal place cells, but they do result in more diffuse place fields that lack spatial stability over periods as short as two minutes (Van Cauter et al., 2008; Hales et al., 2014; Schlesiger et al., 2018). Although disrupting the grid signal via medial septal inactivation does not interfere with place cell remapping in a novel environment, the newly established place cell representation is significantly less stable following this manipulation relative to control animals (Brandon et al., 2014). Finally, during development, place cells are present in larger proportions than grid cells the first time that pre-weanling rat

pups leave the nest, yet their spatial stability does not approach adult-like levels until several days later, when a larger proportion of grid cells has matured (Wills et al., 2010; Langston et al., 2010). Together, these results support the conclusion that grid cell activity is important for the stability of place cells. The results of Paper 2 build upon this conclusion by providing strong evidence that a specific aspect of the grid pattern might control place cell stability. Both grid field rates and place field locations were highly stable across behaviorally relevant timescales (as long as 12 hours). However, depolarization of a subset of MEC LII neurons in hM3 mice caused grid field rates to fluctuate, and across all timepoints we measured, the magnitude of these fluctuations was tightly correlated with the degree of place cell stability.

What causes grid field rates to change?

An important question to consider here is why our manipulation causes grid field rates to change, particularly in response to the depolarization, but not hyperpolarization, of a subset of MEC LII neurons. As discussed in Paper 1, we propose that this difference may reflect the involvement of the local interneuron network. MEC LII contains two largely distinct populations of principal cells: reelin-expressing stellate cells and calbindin-expressing pyramidal cells. We expressed hM3Dq and hM4Di DREADDs almost exclusively in stellate cells, a substantial fraction of which are grid cells (Rowland et al., 2018). Stellate cells are primarily connected via fast-spiking parvalbumin-positive (PV) interneurons (Couey et al., 2013). A small percentage of PV cells exhibit high spatial selectivity, and although the remainder exhibit low spatial selectivity, the stability of their spatial firing patterns is significantly higher than is expected by chance, indicating that PV interneurons may provide varying degrees of spatially specific inhibition onto downstream stellate cells (Buetfering et al., 2014). Further, it has been proposed that the spatial selectivity of these neurons could be generated through the integration of inputs from multiple grid cells with variable grid field rates (**Figure 22A**; Buetfering et al., 2014).

Given this information, we can speculate how the activity of PV interneurons could change grid field rates following the depolarization, but not hyperpolarization, of MEC LII neurons. We hypothesize that activating a subset of hM3Dq-expressing stellate cells would strongly drive PV interneurons and alter the pattern of inhibition they provide onto downstream grid cells, thereby modifying individual grid field rates while also decreasing their overall firing rates. A recent study examined how activating PV interneurons in MEC LII impacted grid cells in MEC, which serves as a test for our hypothesis that increasing PV interneuron activity could produce changes in grid field rates. This manipulation reduced the overall firing

rate of grid cells, and the magnitude of rate changes seemed to differ between individual grid fields (**Figure 22B**), although the authors did not specifically quantify this aspect of the grid pattern (Buetfering et al., 2014).

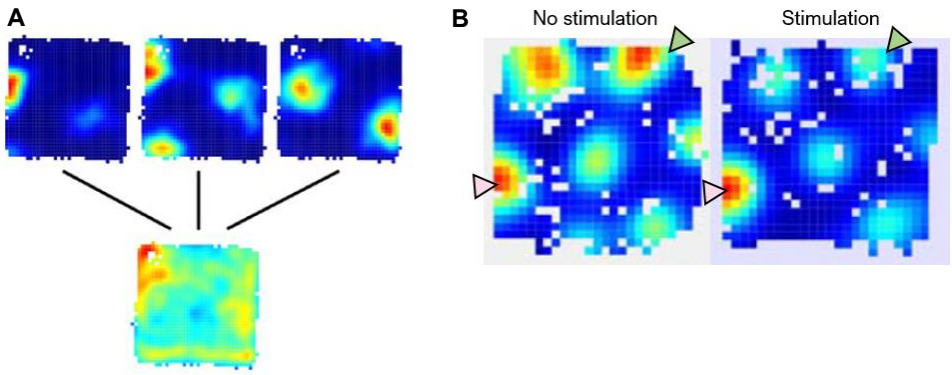

Figure 22 | The activity of PV interneurons may impact individual grid field firing rates. (A) Spatial firing patterns of PV interneurons (bottom) could be generated by the integration of inputs from grid cells with variable field rates (top). PV interneurons could then provide some level of spatially specific inhibition onto downstream grid cells. (B) Optogenetic stimulation of PV interneurons resulted in independent changes in the firing rate of individual grid fields. Green arrowheads indicate a grid field that exhibited a strong decrease in firing rate following the activation of PV interneurons. Pink arrowheads indicate a grid field that exhibited a negligible change in firing rate following the activation of PV interneurons. (A-B) Activity is color coded from blue to red. Adapted from Buetfering et al., 2014.

In contrast, we propose that decreasing the activity of hM4Di-expressing stellate cells would reduce the activity of the PV interneurons to which they are directly connected, but that this would not be sufficient to disinhibit downstream excitatory neurons, since most of the excitatory drive onto PV interneurons would remain intact. In this case, the correlated reduction in grid field rates we observed in hM4 mice should only occur in hM4Di-expressing stellate cells because they are directly hyperpolarized, whereas there would be negligible field rate changes in the rest of the grid cell population. The fact that we cannot identify which of the neurons we record from express our transgene is a limitation of our approach. Contrary to this proposal, however, a recent study demonstrated that inactivating PV interneurons in MEC actually reduced the spatial periodicity of grid cells by increasing spiking activity *outside* the original grid field boundaries (Miao et al., 2017). However, in this study, over 75% of PV cells in layers II and III of MEC were directly targeted with the hM4Di DREADD (Miao et al., 2017). In contrast, we expressed this receptor in just 27% of stellate

cells in MEC LII, which would inhibit a smaller proportion of PV cells in an indirect manner. Therefore, we would not expect PV interneurons to be inhibited to the same extent in these two studies. Indeed, the authors of the aforementioned study observed that inactivation of PV neurons increased the mean firing rate of grid cells, whereas in our study, hyperpolarization of a subset of stellate cells either decreased or did not change the mean firing rates of grid cells, potentially indicating the direct and indirect effects of our manipulation, respectively. Although this scheme is clearly an oversimplification of the complex microcircuit computations and multitude of cell types involved, it is undoubtedly worth investigating whether the activity of different subpopulations of interneurons can control grid field rates.

Does place field formation require plasticity?

An enduring question regarding place cells has been whether the formation of place fields is a result of experience and therefore requires plasticity mechanisms, or if the network is hard-wired such that the connectivity between neurons is established during development. This question has been tested experimentally by investigating whether place fields are immediately expressed when an animal explores a novel environment, as would be expected from a pre-existing hard-wired network. On the contrary, several minutes of exploration are generally required for new and stable place fields to form (Wilson and McNaughton, 1993; Frank et al., 2004). Once formed, it has been shown that place fields can continue to change over the course of several days (Lever et al., 2002). These results are consistent with a role for plasticity in place field formation. Others have addressed this question of “soft-wiring” versus “hard-wiring” by investigating whether the formation and/or stabilization of place fields requires N-Methyl-D-Aspartate receptors (NMDARs), which play a critical role in hippocampal LTP. Pharmacological blockade of NMDARs (Kentros et al., 1998) or targeted deletion of their NR1 subunit in CA1 (McHugh et al., 1996) or CA3 (Nakazawa et al., 2002; Nakazawa et al., 2003) does not abolish place fields in familiar environments or prevent remapping in novel environments, suggesting that hard-wired connections may be sufficient for place field formation. Newly remapped place fields have even been shown to exhibit short-term stability on the order of one or two hours that is independent of NMDAR activation (Kentros et al., 1998). Instead, it seems that only the long-term stability of newly developed place fields relies on NMDAR-dependent plasticity (Kentros et al., 1998). Given these results, the extent to which place field formation depends on learned versus hard-wired connections between neurons is still unclear.

The similarity in hippocampal remapping that we observed across days following depolarization of a subset of MEC LII neurons in hM3 mice (Paper 2) could have been due to hard-wired connectivity or rapid, CNO-induced plasticity. On one hand, our simulation perfectly recapitulates our empirical results, even though no plasticity has taken place. We simply changed the firing rates of individual grid fields between runs of the simulation by the amounts we observed experimentally. The incorporation of similar levels of grid field rate change caused place cells to remap in a similar manner in each run of the simulation, just as we observed in vivo. Thus, these results suggest that changes in synaptic weights are not required for similar remappings to occur. On the other hand, if the CNO-induced map is indeed consolidated through plasticity, one would expect that mice could eventually use this representation to navigate to a learned reward location. Preliminary evidence from our behavioral experiments in hM3 mice supports this idea (Kveim et al., 2018, Soc. Neurosci., abstract [689.11]). In these experiments, mice were trained to navigate toward a constant reward location from a randomized start location using only distal cues surrounding a Y-shaped track. After an injection of CNO, hM3 mice exhibited impaired performance on the task relative to control mice, and their place cells remapped extensively. However, hM3 mice made fewer errors toward the end of the session (linear correlation between trial number and total of errors: $n = 101$, $r = -0.58$, $p = 1.0 \times 10^{-3}$). Additionally, when hM3 mice that exhibited a task impairment were given a subsequent injection of CNO the following day, they exhibited a large increase in performance ($n = 5$, mean degree of impairment: first experiment = -18.3%, second experiment = -4.7%). In fact, during this second experiment, three of the five mice tested were no longer impaired on the task, even though the extent of place cell remapping was similar after a second injection of CNO. Taken together, these behavioral results suggest that the CNO-induced map is consolidated without interfering with the original map, and that the animal can then flexibly use either map to guide behavior.

To provide a conclusive answer to the question of soft-wiring versus hard-wiring, future experiments could use co-administration of CNO and an NMDAR antagonist to test whether plasticity is required for the stabilization of a CNO-induced remapping. If a subsequent injection of CNO produced similar remapping even under these conditions, that would provide strong support for hard-wired connectivity in the entorhinal-hippocampal network. On a related note, we observed in Paper 2 that grid field rates were highly stable over long periods (12+ hours). Thus, it is of interest to determine how quickly grid field rates stabilize in a novel environment, and whether the time course of stabilization is similar to what has been observed for place cells in a novel environment. If grid field rates do indeed control place field stability, as discussed above, we would expect the time course of stabilization to be similar. Finally, it will also be important to test whether the stabilization of grid field rates in a

novel environment requires NMDAR-dependent plasticity, as has been previously observed for place field locations (Kentros et al., 1998).

Beyond the representation of space: a role for place cells and grid cells

Since the hippocampal formation is critical for memory, and memories are an integral part of who we are, it may seem surprising that neurons of the hippocampal formation are mainly responsible for building simple spatial representations. I will now discuss evidence that place cells and grid cells support not only navigation and memory in physical space, but also navigation and memory in more abstract, cognitive spaces.

Not long after their discovery, it became evident that the activity of place cells strongly depends on environmental context (Muller and Kubie, 1987). Place cells exhibit global remapping between distinct environments and rate remapping in response to more subtle environmental manipulations (Leutgeb et al., 2005). In contrast, grid cells have traditionally been thought to provide a universal, context-independent metric of space, consistent with the proposal that these neurons support path integration (i.e., the use of self-motion information to update position). Support for this idea came from the early observation that the phase relationship among simultaneously recorded grid cells is maintained between environments (Fyhn et al., 2007). Subsequent observations strengthened this conclusion by demonstrating that grid cells within a module also exhibit coherent changes in orientation, ellipiticity, and spacing in response to a variety of environmental manipulations (Yoon et al., 2013; Marozzi et al., 2015; Wernle et al., 2018; Butler et al., 2019).

Several lines of evidence, including the results contained within this thesis, have now converged upon the notion that, like place cells, the activity of grid cells is context-dependent and can be modulated by cognitive factors. First, it was demonstrated that the boundaries and geometry of an environment influence grid cell firing. For instance, when the size of a familiar recording environment was changed, the grid pattern rescaled along the same direction as the environmental distortion, reflecting an influence of environmental boundaries on the grid pattern (**Figure 23A**; Barry et al., 2007). Initial recordings of grid cells in a circular environment suggested that the orientation of the grid pattern is controlled by distal cues in the environment since the rotation of a distal cue produced an equal rotation of the grid (Hafting et al., 2005). More recently, it was shown that rotation of a polarized square environment elicits an equal rotation of the grid pattern even if distal cues remain fixed, confirming an influence of environmental boundaries on grid cell firing (**Figure 23B**; Krupic et al., 2015). In a familiar square environment, the orientation of grid cells is highly clustered so

that it aligns with the walls of the environment at an angle of ~7-9° (**Figure 23C**; Stensola et al., 2015; Krupic et al., 2015). This rotational offset is accompanied by an elliptic distortion of the grid pattern, implying that environmental boundaries exert a deforming influence even if the environment is stable (Stensola et al., 2015). Finally, in a familiar trapezoidal environment, the grid pattern is rotated and stretched across the length of the environment such that the pattern is distorted near the compressed end while retaining its regularity near the noncompressed end, revealing an influence of the geometry of the environment on the regularity of the grid pattern (**Figure 23D**; Krupic et al., 2015).

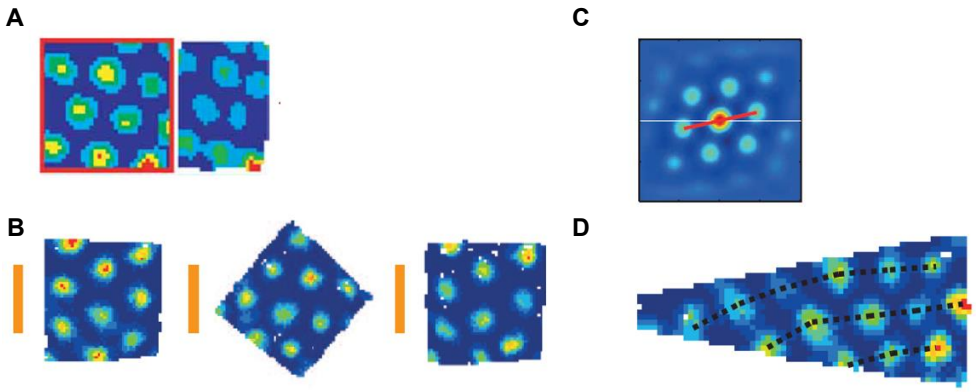

Figure 23 | Environmental boundaries and geometry influence the grid pattern. (A) Rescaling a familiar environment along the horizontal axis resulted in a rescaling of the grid pattern along that axis. (B) Rotation of a square recording environment produced in an equal rotation of the grid pattern. (C) In a familiar square environment, the orientation of the grid pattern was offset from the cardinal axis by ~7-9° and exhibited an elliptic distortion. (D) In a trapezoidal environment, the grid pattern was distorted near the compressed end. (A-D) Activity is color coded from blue to red. Panel A adapted from Barry et al., 2007. Panels B and D adapted from Krupic et al., 2015. Panel C adapted from Stensola et al., 2015.

When grid cells were first discovered, it was acknowledged that there were “small, but reliable rate differences between the vertices” (Hafting et al., 2005). However, until recently, this aspect of the grid pattern has largely been ignored. Computational models of the grid to place cell transformation typically have not incorporated this feature (but see Lyttle et al., 2013; Dunn et al., 2017), and instead use idealized grid cells with uniform rates across their fields. In Paper 1, we provided the first empirical evidence that the firing rates of individual grid fields in mice differ from one another but are stable over time. Grid field rates were stable not only within a session, but also between repeated exposures to a familiar

environment (**Figure 24A**). These results were quickly corroborated by subsequent work in wild-type rats, which clearly illustrated that grid field rates are more variable than is expected by chance, and that this variability does not result from the animal's heading direction, running speed, or overdispersion (Ismakov et al., 2017). Further, grid field rates in wild-type rats exhibited a high degree of stability within a single recording session, between sessions in matching box shapes or colors, and even following the rescaling of a familiar environment (**Figure 24B**; Diehl et al., 2017; Ismakov et al., 2017). Taken together, these results indicate that grid field location and rate may be coded independently. Rescaling an environment produced changes in the location of the grid pattern without changing grid field rates (Ismakov et al., 2017), while changing the environmental context (Diehl et al., 2017) or the activity of a subset of MEC LII neurons (Paper 1) redistributed grid field rates without changing the spatial location of the fields. Most recently, it has even been shown that individual grid fields independently encode head direction (Gerlei et al., 2019). Head direction tuning varied across individual grid fields but was stable between sessions (Gerlei et al., 2019), just as we observed for grid field rates.

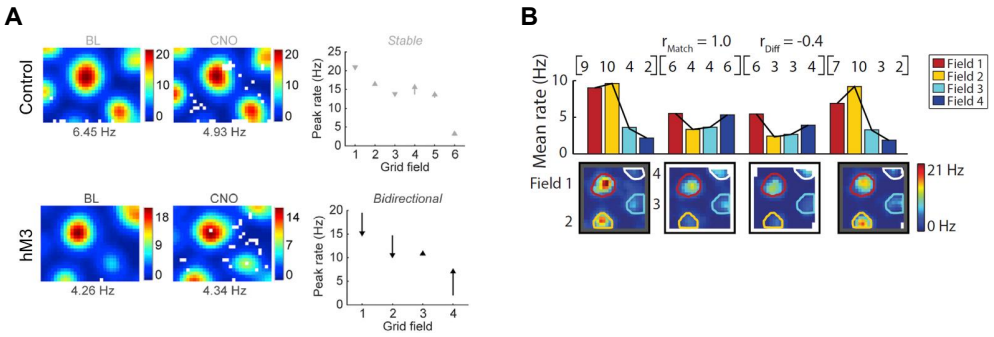

Figure 24 | Independent changes in individual grid field rates. (A) Grid field rates were stable between BL and CNO sessions in control mice (top row). Bidirectional changes in grid field rates in hM3 mice (bottom) were associated with hippocampal remapping. Peak firing rate is indicated below each rate map. (B) Grid field rates were stable between repeated exposures to the same environment. A redistribution of grid field rates was observed when the color of the recording environment changed from black to white. Panel A adapted from Paper 1. Panel B adapted from Diehl et al., 2017.

In Paper 1, we demonstrated that depolarization of a subset of MEC LII neurons in hM3 mice not only produced changes in grid field rates, but also caused them to vary independently, thus modifying the relative rankings between the individual fields (**Figure 24A**). This disruption in grid field relationships was associated with robust hippocampal remapping that was characterized by changes in both place field location and firing rate. In a related study,

adjustments in the shape or color of the environment resulted in a redistribution of grid field relationships and rate remapping in place cells (Diehl et al., 2017). These subtle contextual modifications produced only small fluctuations in grid field rates, as opposed to the substantial changes in grid field rates we observed in hM3 mice following our manipulation. Thus, inducing large changes in grid field rates may result in a more drastic reconfiguration of grid field relationships, which reorganizes the pattern of spatial input provided by grid cells and elicits the strong remapping we observed in hM3 mice. In contrast, minor contextual changes may prompt a less extensive reorganization of grid field relationships, which initiates rate remapping in place cells. In both cases, the redistribution of grid field rates may serve as a contextual signal that triggers remapping with the extent of that redistribution dictating which type of remapping occurs downstream.

Since there was activity in the eventual place field location during the baseline session, the predictable remapping we observed in hM3 mice following depolarization of MEC LII neurons could even be considered to be an extreme form of rate remapping. Yet, it is important to highlight a key difference between predictable remapping and rate remapping: rate remapping does not involve a change in the location of peak firing activity. Instead, it is characterized by large changes in firing rate at a single spatial location. In contrast, predictable remapping in hM3 mice involved changes in the location of peak firing. Accordingly, in Paper 2, we observed substantial increases in firing rate at the new place field location and substantial decreases in firing rate at the previous place field location. Despite this difference, these phenomena may be intimately related, potentially reflecting the ends of a continuum, as both are produced following a reconfiguration of grid field relationships.

The influence of grid field relationships on place field location was particularly evident in Paper 2, where we demonstrated that place fields frequently reverted to their original locations when grid field relationships (but not individual field rates) were reset. The possible mechanisms underlying this resetting are described in detail in the discussion section for Paper 2.

The firing rate and location of individual grid fields are also influenced by cognitive factors, including task demands and the presence of reward. In a recent study, rats randomly foraged for food rewards in one environment, and navigated toward an unmarked, remembered zone for a food reward in a second environment (**Figure 25A**; Butler et al., 2019). This change in task demands resulted in changes in the orientation, spacing, and ellipticity of the grid pattern that were not observed in rats that randomly foraged for food

rewards in both environments. Additionally, individual grid fields located near the reward zone exhibited higher peak firing rates (**Figure 25B**). In a related study, rats learned three new reward locations on a cheeseboard maze each day. Following training, the authors observed that the grid pattern was distorted on the maze because individual grid fields in over 80% of grid cells recorded shifted toward a rewarded goal location (**Figure 25C**; Boccara et al., 2019).

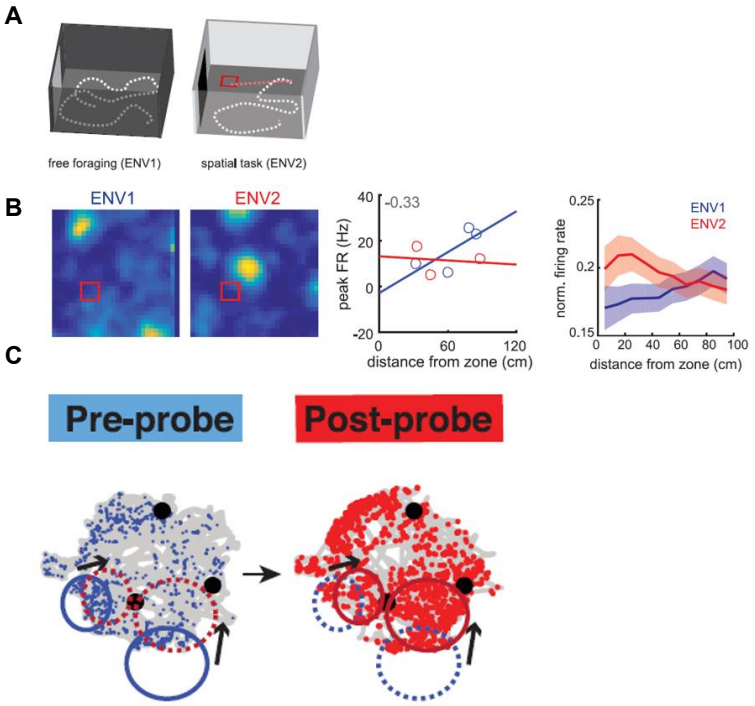

Figure 25 | Changes in the firing rate or location of individual grid fields near reward locations. (A) In ENV1, rats randomly foraged for food rewards. In ENV2, rats navigated toward an unmarked, remembered zone for a food reward following an auditory cue. (B) The firing rates of individual grid fields were highest near the reward zone in ENV2 (red), but not ENV1 (blue). This was observed in single grid cells (two left panels) as well as across the population of grid cells (center and right panels). Activity is color coded from blue to yellow. (C) On each day, rats were trained to navigate toward three rewarded locations on a cheeseboard maze (black dots). Individual grid fields moved toward newly learned goal locations. Colored circles indicate grid field locations before (pre-probe, blue) and after (post-probe, red) training. Arrows depict independent translation of grid fields. Panels A and B adapted from Butler et al., 2019. Panel C adapted from Boccara et al., 2019.

Finally, recent evidence indicates that the function of the spatial code provided by place and grid cells may not be limited to the representation of physical space and could extend more broadly to the representation of nonspatial dimensions, as well as conceptual or cognitive spaces. Electrophysiological recordings in rodents have demonstrated that place cells and grid cells exhibit frequency-specific firing fields during performance of a task that involved adjusting the frequency of an auditory stimulus to match a target frequency (Aronov et al., 2017). The preferred frequencies of the neurons spanned the entire behavioral task, indicating that these cells can provide a continuous representation of a one-dimensional nonspatial variable (**Figure 26A**; Aronov et al., 2017). Others have reported the existence of "time cells" in the hippocampus (Pastalkova et al., 2008; MacDonald et al., 2011; Mau et al., 2018) and MEC (Kraus et al., 2013; Kraus et al., 2015; Heys and Dombeck, 2018). These cells are reliably active at specific time points during a delay period, even as rats run in place on a treadmill (**Figure 26B**). The population of time cells includes place cells and grid cells that fired at successive moments during the delay, such that the activity of a small ensemble of cells bridged the entire delay period, providing a continuous representation of elapsed time. More recently, human participants learned to associate bird stimuli with variable neck and leg lengths with specific Christmas symbols (Constantinescu et al., 2016). Subsequently during functional magnetic resonance imaging (fMRI) scanning, hexadirectional modulation of the blood-oxygen-level-dependent (BOLD) signal in the EC (a proxy for grid cell activity) was observed while participants watched videos of bird stimuli morphing along these dimensions and imagined the outcome of trajectories through this conceptual feature space (**Figure 26C**). In light of these recent results, it has been proposed that place cells and grid cells could map the dimensions of cognitive spaces, in addition to providing a continuous code for space that supports spatial navigation (Bellmund et al., 2018). In this framework, similar stimuli are mapped to neighboring locations in cognitive space, while distinct stimuli are mapped to distant locations (**Figure 26D**; Bellmund et al., 2018). Akin to their roles in the mapping of physical space, place cells could represent specific locations in feature space, while grid cells provide a metric for that space (Bellmund et al., 2018). As the number of similarities between encoding physical space and cognitive space grows, it becomes more plausible that grid field rates may also be used to encode features in cognitive space.

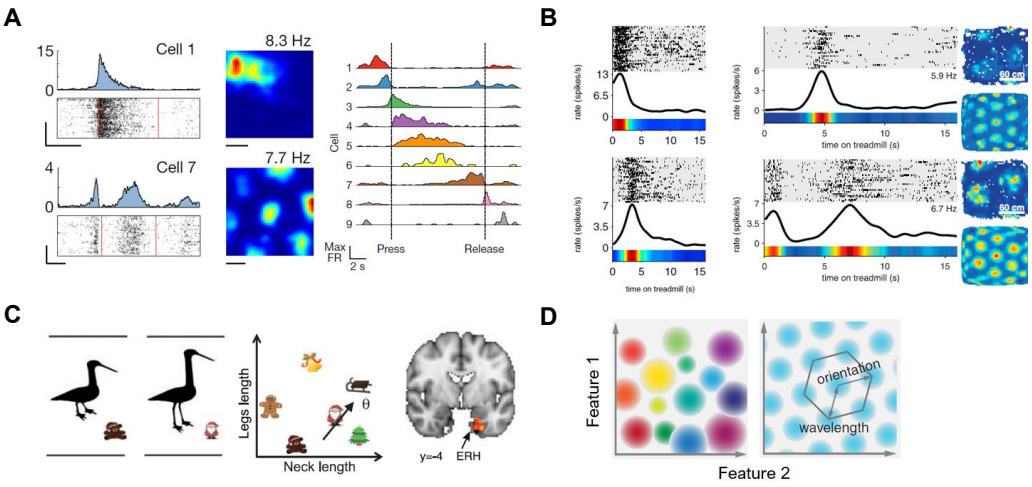

Figure 26 | A role for place cells and grid cells beyond the representation of space. (A) In a sound manipulation task, animals were trained to deflect a lever to adjust the frequency of a tone and release it in a target zone. Left: Place cells (top row) and grid cells (bottom row) exhibited "frequency fields" during the performance of the task. Peristimulus histograms and raster plots depict activity as a function of sound frequency. Rate maps depict activity of each cell in an open field environment. Peak firing rate is indicated above each rate map. Right: The activity of an ensemble of cells in CA1 tiled the entire sound manipulation task. (B) Place cells (left) and grid cells (right) fired at specific times during a delay period while rats ran in place on a treadmill. (A-B) Activity is color coded from blue to red. (C) Human participants learned to associate bird stimuli with variable neck and leg lengths with Christmas symbols. During scanning, subjects watched the stimuli morph along these dimensions and were asked to imagined the outcome of trajectories through this feature space. Hexadirectional signals were observed in the entorhinal cortex (ERH), as previously shown during navigation (Doeller et al., 2010). (D) Abstract features of stimuli are mapped in cognitive space in two (or more) dimensions. Similar stimuli are mapped to neighboring locations and distinct stimuli are mapped to distant locations. In this framework, place cells may represent specific locations in feature space (left), while grid cells provide a metric for that space (right). Panel A adapted from Aronov et al., 2017. Panel B adapted from Kraus et al., 2013; Kraus et al., 2015. Panel C adapted from Constantinescu et al., 2016. Panel D adapted from Bellmund et al., 2018.

CONCLUSION

The hippocampus is critical for navigation and memory, and its primary cell type, the place cell, links these two functions together. Place cells maintain a stable representation of space within an environment, but they drastically remap between distinct environments, thus enabling the formation of distinct spatial memories. To understand the mechanism that underlies place cell remapping, we must consider the activity of neurons immediately upstream in MEC, the dominant source of spatial input to the hippocampus. In this thesis, we used highly specific expression of chemogenetic transgenes to manipulate the activity of a subset of stellate cells in MEC LII. While prior work has shown a link between remapping and changes in MEC activity, we showed precisely *which* changes in the activity of MEC neurons were associated with remapping and spatial memory impairment. Contrary to our initial expectations, altering the activity of a subset of stellate cells did not change the spatial position of the grid pattern or impact its hexagonal regularity, providing strong evidence that these types of changes are not required for hippocampal remapping to occur. Instead, we uncovered a novel mechanism: independent changes in the grid field firing rates are sufficient to cause remapping. Thus, we showed for the first time that grid field firing rates provide a third dimension to the grid code, enabling a more detailed representation of two-dimensional space. This discovery could have far reaching implications, affecting not only place field formation and remapping, but also the encoding of reward locations, and more broadly, the use of multi-dimensional Euclidean spaces to organize cognitive processes.

REFERENCES

ALEXANDER, G. M., ROGAN, S. C., ABBAS, A. I., ARMBRUSTER, B. N., PEI, Y., ALLEN, J. A., NONNEMAN, R. J., HARTMANN, J., MOY, S. S., NICOLELIS, M. A., MCNAMARA, J. O. & ROTH, B. L. 2009. Remote control of neuronal activity in transgenic mice expressing evolved G protein-coupled receptors. *Neuron,* 63**,** 27-39.

ALME, C. B., MIAO, C., JEZEK, K., TREVES, A., MOSER, E. I. & MOSER, M. B. 2014. Place cells in the hippocampus: Eleven maps for eleven rooms. *Proc Natl Acad Sci USA,* 111**,** 18428-18435.

ANDERSON, M. I. & JEFFERY, K. J. 2003. Heterogeneous modulation of place cell firing by changes in context. *J Neurosci,* 23**,** 8827-8835.

ARANTIUS, G. 1587. *De humano foetu . . . Ejusdem anatomicorum observationum liber*. Venice.

ARMBRUSTER, B. N., LI, X., PAUSCH, M. H., HERLITZE, S. & ROTH, B. L. 2007. Evolving the lock to fit the key to create a family of G protein-coupled receptors potently activated by an inert ligand. *Proc Natl Acad Sci USA,* 104**,** 5163-5168.

ARONOV, D., NEVERS, R. & TANK, D. W. 2017. Mapping of a non-spatial dimension by the hippocampal-entorhinal circuit. *Nature,* 543**,** 719-722.

BAHAR, A. S., SHIRVALKAR, P. R. & SHAPIRO, M. L. 2011. Memory-guided learning: CA1 and CA3 neuronal ensembles differentially encode the commonalities and differences between situations. *J Neurosci,* 31**,** 12270-12281.

BARNES, C. A. 1979. Memory deficits associated with senescence: A neurophysiological and behavioral study in the rat. *J Comp Physiol Psychol,* 93**,** 74-104.

BARNES, C. A., MCNAUGHTON, B. L., MIZUMORI, S. J., LEONARD, B. W. & LIN, L. H. 1990. Comparison of spatial and temporal characteristics of neuronal activity in sequential stages of hippocampal processing. *Prog Brain Res,* 83**,** 287-300.

BARNES, C. A., SUSTER, M. S., SHEN, J. & MCNAUGHTON, B. L. 1997. Multistability of cognitive maps in the hippocampus of old rats. *Nature,* 388**,** 272-275.

BARRY, C., GINZBERG, L. L., O'KEEFE, J. & BURGESS, N. 2012. Grid cell firing patterns signal environmental novelty by expansion. *Proc Natl Acad Sci USA,* 109**,** 17687-17692.

BARRY, C., HAYMAN, R., BURGESS, N. & JEFFERY, K. J. 2007. Experience-dependent rescaling of entorhinal grids. *Nat Neurosci,* 10**,** 682-684.

BARRY, C., LEVER, C., HAYMAN, R., HARTLEY, T., BURTON, S., O'KEEFE, J., JEFFERY, K. & BURGESS, N. 2006. The boundary vector cell model of place cell firing and spatial memory. *Rev Neurosci,* 17**,** 71-97.

BELLMUND, J. L. S., GÄRDENFORS, P., MOSER, E. I. & DOELLER, C. F. 2018. Navigating cognition: Spatial codes for human thinking. *Science,* 362**,** eaat6766.

BJERKNES, T. L., MOSER, E. I. & MOSER, M. B. 2014. Representation of geometric borders in the developing rat. *Neuron,* 82**,** 71-78.

BLISS, T. V. P. & LØMO, T. 1973. Long-lasting potentiation of synaptic transmission in the dentate area of the anaesthetized rabbit following stimulation of the perforant path. *J Physiol,* 232**,** 331-356.

BOCCARA, C. N., NARDIN, M., STELLA, F., O'NEILL, J. & CSICSVARI, J. 2019. The entorhinal cognitive map is attracted to goals. *Science,* 363**,** 1443-1447.

BONNEVIE, T., DUNN, B., FYHN, M., HAFTING, T., DERDIKMAN, D., KUBIE, J. L., ROUDI, Y., MOSER, E. I. & MOSER, M. B. 2013. Grid cells require excitatory drive from the hippocampus. *Nat Neurosci,* 16**,** 309-317.

BOSTOCK, E., MULLER, R. & KUBIE, J. 1991. Experience-dependent modifications of hippocampal place cell firing. *Hippocampus,* 1**,** 193-206.

BRANDON, M. P., KOENIG, J., LEUTGEB, J. K. & LEUTGEB, S. 2014. New and distinct hippocampal place codes are generated in a new environment during septal inactivation. *Neuron,* 82**,** 789-796.

BROCA, P. 1861. Remarks on the seat of the faculty of articulate speech, followed by the report of a case of aphemia (loss of speech). Translated by C. WASTERLAIN & D.A. ROTTENBERG. *Bulletin de la Société Anatomique,* 6, 330-357.

BRUN, V. H., LEUTGEB, S., WU, H. Q., SCHWARCZ, R., WITTER, M. P., MOSER, E. I. & MOSER, M. B. 2008. Impaired spatial representation in CA1 after lesion of direct input from entorhinal cortex. *Neuron,* 57**,** 290-302.

BRUN, V. H., OTNASS, M. K., MOLDEN, S., STEFFENACH, H. A., WITTER, M. P., MOSER, M. B. & MOSER, E. I. 2002. Place cells and place recognition maintained by direct entorhinal-hippocampal circuitry. *Science,* 296**,** 2243-2246.

BUETFERING, C., ALLEN, K. & MONYER, H. 2014. Parvalbumin interneurons provide grid cell-driven recurrent inhibition in the medial entorhinal cortex. *Nat Neurosci,* 17**,** 710-718.
BUSH, D., BARRY, C. & BURGESS, N. 2014. What do grid cells contribute to place cell firing? *Trends Neurosci,* 37**,** 136-145.
BUTLER, W. N., HARDCASTLE, K. & GIOCOMO, L. M. 2019. Remembered reward locations restructure entorhinal spatial maps. *Science,* 363**,** 1447-1452.
CASH, S. & YUSTE, R. 1998. Input summation by cultured pyramidal neurons is linear and position-independent. *J Neurosci,* 18**,** 10-15.
CASH, S. & YUSTE, R. 1999. Linear summation of excitatory inputs by CA1 pyramidal neurons. *Neuron,* 22**,** 383-394.
CHANG, S. E., TODD, T. P., BUCCI, D. J. & SMITH, K. S. 2015. Chemogenetic manipulation of ventral pallidal neurons impairs acquisition of sign-tracking in rats. *Eur J Neurosci,* 42**,** 3105-3116.
CHEN, X., CHOO, H., HUANG, X. P., YANG, X., STONE, O., ROTH, B. L. & JIN, J. 2015. The first structure-activity relationship studies for designer receptors exclusively activated by designer drugs. *ACS Chem Neurosci,* 6**,** 476-484.
COHEN, J. D., BOLSTAD, M. & LEE, A. K. 2017. Experience-dependent shaping of hippocampal CA1 intracellular activity in novel and familiar environments. *eLife,* 6**,** e23040.
CONSTANTINESCU, A. O., O'REILLY, J. X. & BEHRENS, T. E. J. 2016. Organizing conceptual knowledge in humans with a gridlike code. *Science,* 352**,** 1464-1468.
CORKIN, S. 2002. What's new with the amnesic patient H.M.? *Nat Rev Neurosci,* 3**,** 153-160.
COUEY, J. J., WITOELAR, A., ZHANG, S. J., ZHENG, K., YE, J., DUNN, B., CZAJKOWSKI, R., MOSER, M. B., MOSER, E. I., ROUDI, Y. & WITTER, M. P. 2013. Recurrent inhibitory circuitry as a mechanism for grid formation. *Nat Neurosci,* 16**,** 318-324.
CREMERS, T. I., FLIK, G., HOFLAND, C. & STRATFORD, R. E., JR. 2012. Microdialysis evaluation of clozapine and N-desmethylclozapine pharmacokinetics in rat brain. *Drug Metab Dispos,* 40**,** 1909-1916.
DANIELSON, N. B., ZAREMBA, J. D., KAIFOSH, P., BOWLER, J., LADOW, M. & LOSONCZY, A. 2016. Sublayer-specific coding dynamics during spatial navigation and learning in hippocampal area CA1. *Neuron,* 91**,** 652-665.
DANJO, T., TOYOIZUMI, T. & FUJISAWA, S. 2018. Spatial representations of self and other in the hippocampus. *Science,* 359**,** 213-218.
DE ALMEIDA, L., IDIART, M. & LISMAN, J. E. 2009a. The input-output transformation of the hippocampal granule cells: from grid cells to place fields. *J Neurosci,* 29**,** 7504-7512.
DE ALMEIDA, L., IDIART, M. & LISMAN, J. E. 2009b. A second function of gamma frequency oscillations: An E%-max winner-take-all mechanism selects which cells fire. *J Neurosci,* 29**,** 7497-7503.
DE ALMEIDA, L., IDIART, M. & LISMAN, J. E. 2012. The single place fields of CA3 cells: a two-stage transformation from grid cells. *Hippocampus,* 22**,** 200-208.
DEWIRE, S. M., AHN, S., LEFKOWITZ, R. J. & SHENOY, S. K. 2007. B-arrestins and cell signaling. *Annu Rev Physiol,* 69**,** 483-510.
DIAMANTAKI, M., COLETTA, S., NASR, K., ZERAATI, R., LATURNUS, S., BERENS, P., PRESTON-FERRER, P. & BURGALOSSI, A. 2018. Manipulating hippocampal place cell activity by single-cell stimulation in freely moving mice. *Cell Rep,* 23**,** 32-38.
DIEHL, G. W., HON, O. J., LEUTGEB, S. & LEUTGEB, J. K. 2017. Grid and nongrid cells in medial entorhinal cortex represent spatial location and environmental features with complementary coding schemes. *Neuron,* 94**,** 83-92.
DOELLER, C. F., BARRY, C. & BURGESS, N. 2010. Evidence for grid cells in a human memory network. *Nature,* 463**,** 657-661.
DUNN, B., WENNBERG, D., HUANG, Z. & ROUDI, Y. 2017. Grid cells show field-to-field variability and this explains the aperiodic response of inhibitory interneurons. *bioRxiv,* 101899.
DUPRET, D., O'NEILL, J., PLEYDELL-BOUVERIE, B. & CSICSVARI, J. 2010. The reorganization and reactivation of hippocampal maps predict spatial memory performance. *Nat Neurosci,* 13**,** 995-1002.
EICHENBAUM, H. & COHEN, N. J. 2001. *From Conditioning to Conscious Recollection*. New York, NY: Oxford University Press.
EICHENBAUM, H., KUPERSTEIN, M., FAGAN, A. & NAGODE, J. 1987. Cue-sampling and goal-approach correlates of hippocampal unit activity in rats performing an odor-discrimination task. *J Neurosci,* 7**,** 716-732.

EPSZTEIN, J., BRECHT, M. & LEE, A. K. 2011. Intracellular determinants of hippocampal CA1 place and silent cell activity in a novel environment. *Neuron,* 70**,** 109-120.
FARRELL, M. S. & ROTH, B. L. 2013. Pharmacosynthetics: Reimagining the pharmacogenetic approach. *Brain Res,* 1511**,** 6-20.
FERBINTEANU, J. & SHAPIRO, M. L. 2003. Prospective and retrospective memory coding in the hippocampus. *Neuron,* 40**,** 1227-1239.
FERBINTEANU, J., SHIRVALKAR, P. & SHAPIRO, M. L. 2011. Memory modulates journey-dependent coding in the rat hippocampus. *J Neurosci,* 31**,** 9135-9146.
FRANK, L. M., BROWN, E. N. & WILSON, M. 2000. Trajectory encoding in the hippocampus and entorhinal cortex. *Neuron,* 27**,** 169-178.
FRANK, L. M., STANLEY, G. B. & BROWN, E. N. 2004. Hippocampal plasticity across multiple days of exposure to novel environments. *J Neurosci,* 24**,** 7681-7689.
FUHS, M. C. & TOURETZKY, D. S. 2006. A spin glass model of path integration in rat medial entorhinal cortex. *J Neurosci,* 26**,** 4266-4276.
FYHN, M., HAFTING, T., TREVES, A., MOSER, M. B. & MOSER, E. I. 2007. Hippocampal remapping and grid realignment in entorhinal cortex. *Nature,* 446**,** 190-194.
FYHN, M., MOLDEN, S., HOLLUP, S., MOSER, M. B. & MOSER, E. 2002. Hippocampal neurons responding to first-time dislocation of a target object. *Neuron,* 35**,** 555-566.
FYHN, M., MOLDEN, S., WITTER, M. P., MOSER, E. I. & MOSER, M. B. 2004. Spatial representation in the entorhinal cortex. *Science,* 305**,** 1258-1264.
GALL, F. & SPURZHEIM, J. C. 1810-1819. *Anatomie et Physiologie du Systeme Nerveux*. Paris, FR: Shoell.
GARDNER, R. J., LU, L., WERNLE, T., MOSER, M.-B. & MOSER, E. I. 2019. Correlation structure of grid cells is preserved during sleep. *Nat Neurosci,* 22**,** 598-608.
GASPARINI, S. & MAGEE, J. C. 2006. State-dependent dendritic computation in hippocampal CA1 pyramidal neurons. *J Neurosci,* 26**,** 2088-2100.
GERLEI, K., PASSLACK, J., STEVENS, H., PAPASTATHOPOULOS, I. & NOLAN, M. F. 2019. Grid cells implement a location-dependent directional code. *bioRxiv***,** 681312.
GOMEZ, J. L., BONAVENTURA, J., LESNIAK, W., MATHEWS, W. B., SYSA-SHAH, P., RODRIGUEZ, L. A., ELLIS, R. J., RICHIE, C. T., HARVEY, B. K., DANNALS, R. F., POMPER, M. G., BONCI, A. & MICHAELIDES, M. 2017. Chemogenetics revealed: DREADD occupancy and activation via converted clozapine. *Science,* 357**,** 503-507.
GOSSEN, M., FREUNDLIEB, S., BENDER, G., MULLER, G., HILLEN, W. & BUJARD, H. 1995. Transcriptional activation by tetracyclines in mammalian cells. *Science,* 268**,** 1766-1769.
GUETTIER, J.-M., GAUTAM, D., SCARSELLI, M., RUIZ DE AZUA, I., LI, J. H., ROSEMOND, E., MA, X., GONZALEZ, F. J., ARMBRUSTER, B. N., LU, H., ROTH, B. L. & WESS, J. 2009. A chemical-genetic approach to study G protein regulation of cell function in vivo. *Proc Natl Acad Sci USA*.
GUZOWSKI, J. F., KNIERIM, J. J. & MOSER, E. I. 2004. Ensemble dynamics of hippocampal regions CA3 and CA1. *Neuron,* 44**,** 581-584.
HAFTING, T., FYHN, M., MOLDEN, S., MOSER, M. B. & MOSER, E. I. 2005. Microstructure of a spatial map in the entorhinal cortex. *Nature,* 436**,** 801-806.
HALES, J. B., SCHLESIGER, M. I., LEUTGEB, J. K., SQUIRE, L. R., LEUTGEB, S. & CLARK, R. E. 2014. Medial entorhinal cortex lesions only partially disrupt hippocampal place cells and hippocampus-dependent place memory. *Cell Rep,* 9**,** 893-901.
HALLOCK, H. L. & GRIFFIN, A. L. 2013. Dynamic coding of dorsal hippocampal neurons between tasks that differ in structure and memory demand. *Hippocampus,* 23**,** 169-186.
HARDCASTLE, K., MAHESWARANATHAN, N., GANGULI, S. & GIOCOMO, L. M. 2017. A multiplexed, heterogeneous, and adaptive code for navigation in medial entorhinal cortex. *Neuron,* 94**,** 1-13.
HEBB, D. O. 1949. *The organization of behavior; a neuropsychological theory.* Oxford, UK: Wiley.
HELLMAN, K., AADAL NIELSEN, P., EK, F. & OLSSON, R. 2016. An ex vivo model for evaluating blood-brain barrier permeability, efflux, and drug metabolism. *ACS Chem Neurosci,* 7**,** 668-680.
HEYS, J. G. & DOMBECK, D. A. 2018. Evidence for a subcircuit in medial entorhinal cortex representing elapsed time during immobility. *Nat Neurosci*, 21, 1574-1582.
HUBEL, D. H. & WIESEL, T. N. 1962. Receptive fields, binocular interaction and functional architecture in the cat's visual cortex. *J Physiol,* 160**,** 106-154.
HØYDAL, Ø. A., SKYTØEN, E. R., ANDERSSON, S. O., MOSER, M.-B. & MOSER, E. I. 2019. Object-vector coding in the medial entorhinal cortex. *Nature,* 568**,** 400-404.

IGARASHI, K. M., LU, L., COLGIN, L. L., MOSER, M. B. & MOSER, E. I. 2014. Coordination of entorhinal-hippocampal ensemble activity during associative learning. *Nature,* 510**,** 143-147.
ISMAKOV, R., BARAK, O., JEFFERY, K. & DERDIKMAN, D. 2017. Grid cells encode local positional information. *Curr Biol,* 27**,** 2337-2343.
JANN, M. W., LAM, Y. W. & CHANG, W. H. 1994. Rapid formation of clozapine in guinea-pigs and man following clozapine-N-oxide administration. *Arch Int Pharmacodyn Ther,* 328**,** 243-250.
JARRARD, L. E. 1978. Selective hippocampal lesions: differential effects on performance by rats of a spatial task with preoperative versus postoperative training. *J Comp Physiol Psychol,* 92, 1119-1127.
JEFFERY, K. J., GILBERT, A., BURTON, S. & STRUDWICK, A. 2003. Preserved performance in a hippocampal-dependent spatial task despite complete place cell remapping. *Hippocampus*, 13, 175-189.
JENDRYKA, M., PALCHAUDHURI, M., URSU, D., VAN DER VEEN, B., LISS, B., KÄTZEL, D., NISSEN, W. & PEKCEC, A. 2019. Pharmacokinetic and pharmacodynamic actions of clozapine-N-oxide, clozapine, and compound 21 in DREADD-based chemogenetics in mice. *Sci Rep,* 9**,** 4522.
JI, B., KANEKO, H., MINAMIMOTO, T., INOUE, H., TAKEUCHI, H., KUMATA, K., ZHANG, M. R., AOKI, I., SEKI, C., ONO, M., TOKUNAGA, M., TSUKAMOTO, S., TANABE, K., SHIN, R. M., MINAMIHISAMATSU, T., KITO, S., RICHMOND, B. J., SUHARA, T. & HIGUCHI, M. 2016. Multimodal imaging for DREADD-expressing neurons in living brain and their application to implantation of iPSC-derived neural progenitors. *J Neurosci,* 36**,** 11544-11558.
KENNEDY, P. J. & SHAPIRO, M. L. 2009. Motivational states activate distinct hippocampal representations to guide goal-directed behaviors. *Proc Natl Acad Sci USA,* 106**,** 10805-10810.
KENTROS, C., HARGREAVES, E., HAWKINS, R. D., KANDEL, E. R., SHAPIRO, M. & MULLER, R. V. 1998. Abolition of long-term stability of new hippocampal place cell maps by NMDA receptor blockade. *Science,* 280**,** 2121-2126.
KINSBOURNE, M. & WOOD, F. 1975. Short-term memory and the amnesic syndrome, in D. DEUTSCH & J.A. DEUTSCH (eds.). *Short-Term Memory*. New York, NY: Academic Press, 257-291.
KITAMURA, T., SUN, C., MARTIN, J., KITCH, L. J., SCHNITZER, M. J. & TONEGAWA, S. 2015. Entorhinal cortical ocean cells encode specific contexts and drive context-specific fear memory. *Neuron,* 87**,** 1317-1331.
KJELSTRUP, K. B., SOLSTAD, T., BRUN, V. H., HAFTING, T., LEUTGEB, S., WITTER, M. P., MOSER, E. I. & MOSER, M. B. 2008. Finite scale of spatial representation in the hippocampus. *Science,* 321**,** 140-143.
KOENIG, J., LINDER, A. N., LEUTGEB, J. K. & LEUTGEB, S. 2011. The spatial periodicity of grid cells is not sustained during reduced theta oscillations. *Science,* 332**,** 592-595.
KRAUS, B. J., BRANDON, M. P., ROBINSON, R. J., CONNERNEY, M. A., HASSELMO, M. E. & EICHENBAUM, H. 2015. During running in place, grid cells integrate elapsed time and distance run. *Neuron,* 88**,** 578-589.
KRAUS, B. J., ROBINSON, R. J., 2ND, WHITE, J. A., EICHENBAUM, H. & HASSELMO, M. E. 2013. Hippocampal "time cells": time versus path integration. *Neuron,* 78**,** 1090-1101.
KROPFF, E., CARMICHAEL, J. E., MOSER, M. B. & MOSER, E. I. 2015. Speed cells in the medial entorhinal cortex. *Nature,* 523**,** 419-424.
KRUPIC, J., BAUZA, M., BURTON, S., BARRY, C. & O'KEEFE, J. 2015. Grid cell symmetry is shaped by environmental geometry. *Nature,* 518**,** 232-235.
KRUPIC, J., BURGESS, N. & O'KEEFE, J. 2012. Neural representations of location composed of spatially periodic bands. *Science,* 337**,** 853-857.
KUBIE, J. L. & MULLER, R. U. 1991. Multiple representations in the hippocampus. *Hippocampus,* 1**,** 240-242.
KUBIE, J. L. & RANCK, J. B., JR. 1983. Sensory-behavioral correlates in individual hippocampal neurons in three situations: space and context, in W. SEIFERT (ed.) *Neurobiology of the Hippocampus.* San Diego, CA: Academic Press, 433-447.
LANGSTON, R. F., AINGE, J. A., COUEY, J. J., CANTO, C. B., BJERKNES, T. L., WITTER, M. P., MOSER, E. I. & MOSER, M. B. 2010. Development of the spatial representation system in the rat. *Science,* 328**,** 1576-1580.
LASHLEY, K. S. 1929. *Brain Mechanisms and Intelligence: A Quantitative Study of Injuries to the Brain.* Chicago, IL: University of Chicago Press.

LASHLEY, K. S. 1950. In search of the engram. *Symposiums of the Society for Experimental Biology*, 4, 454-482.
LECHNER, H. A. E., LEIN, E. S. & CALLAWAY, E. M. 2002. A genetic method for selective and quickly reversible silencing of mammalian neurons. *J Neurosci,* 22**,** 5287-5290.
LEE, D., LIN, B. J. & LEE, A. K. 2012. Hippocampal place fields emerge upon single-cell manipulation of excitability during behavior. *Science,* 337**,** 849-853.
LEE, I., RAO, G. & KNIERIM, J. J. 2004. A double dissociation between hippocampal subfields: differential time course of CA3 and CA1 place cells for processing changed environments. *Neuron,* 42**,** 803-815.
LEE, J. Q., LEDUKE, D. O., CHUA, K., MCDONALD, R. J. & SUTHERLAND, R. J. 2018. Relocating cued goals induces population remapping in CA1 related to memory performance in a two-platform water task in rats. *Hippocampus*, 6, 431-440.
LENCK-SANTINI, P. P., MULLER, R. U., SAVE, E. & POUCET, B. 2002. Relationships between place cell firing fields and navigational decisions by rats. *J Neurosci,* 22**,** 9035-47.
LENCK-SANTINI, P. P., SAVE, E. & POUCET, B. 2001. Evidence for a relationship between place-cell spatial firing and spatial memory performance. *Hippocampus,* 11**,** 377-90.
LERCHNER, W., XIAO, C., NASHMI, R., SLIMKO, E. M., VAN TRIGT, L., LESTER, H. A. & ANDERSON, D. J. 2007. Reversible silencing of neuronal excitability in behaving mice by a genetically targeted, ivermectin-gated Cl- channel. *Neuron,* 54**,** 35-49.
LEUTGEB, S., LEUTGEB, J. K., BARNES, C. A., MOSER, E. I., MCNAUGHTON, B. L. & MOSER, M. B. 2005. Independent codes for spatial and episodic memory in hippocampal neuronal ensembles. *Science,* 309**,** 619-623.
LEUTGEB, S., LEUTGEB, J. K., TREVES, A., MOSER, M. B. & MOSER, E. I. 2004. Distinct ensemble codes in hippocampal areas CA3 and CA1. *Science,* 305**,** 1295-1298.
LEVER, C., WILLS, T., CACUCCI, F., BURGESS, N. & O'KEEFE, J. 2002. Long-term plasticity in hippocampal place-cell representation of environmental geometry. *Nature,* 416**,** 90-94.
LYKKEN, C. & KENTROS, C. G. 2014. Beyond the bolus: transgenic tools for investigating the neurophysiology of learning and memory. *Learn Mem,* 21**,** 506-518.
LYNAGH, T. & LYNCH, J. W. 2010. An improved ivermectin-activated chloride channel receptor for inhibiting electrical activity in defined neuronal populations. *J Biol Chem,* 285**,** 14890-14897.
LYTTLE, D., GEREKE, B., LIN, K. K. & FELLOUS, J. M. 2013. Spatial scale and place field stability in a grid-to-place cell model of the dorsoventral axis of the hippocampus. *Hippocampus,* 23**,** 729-744.
MACDONALD, C. J., LEPAGE, K. Q., EDEN, U. T. & EICHENBAUM, H. 2011. Hippocampal "time cells" bridge the gap in memory for discontiguous events. *Neuron,* 71**,** 737-749.
MACLAREN, D. A. A., BROWNE, R. W., SHAW, J. K., KRISHNAN RADHAKRISHNAN, S., KHARE, P., ESPAÑA, R. A. & CLARK, S. D. 2016. Clozapine N-oxide administration produces behavioral effects in Long-Evans rats: Implications for designing DREADD experiments. *eNeuro,* 3**,** ENEURO.0219-16.2016.
MAHLER, S. V., VAZEY, E. M., BECKLEY, J. T., KEISTLER, C. R., MCGLINCHEY, E. M., KAUFLING, J., WILSON, S. P., DEISSEROTH, K., WOODWARD, J. J. & ASTON-JONES, G. 2014. Designer receptors show role for ventral pallidum input to ventral tegmental area in cocaine seeking. *Nat Neurosci,* 17**,** 577-585.
MARKUS, E. J., QIN, Y. L., LEONARD, B., SKAGGS, W. E., MCNAUGHTON, B. L. & BARNES, C. A. 1995. Interactions between location and task affect the spatial and directional firing of hippocampal neurons. *J Neurosci,* 15**,** 7079-7094.
MAROZZI, E., GINZBERG, L. L., ALENDA, A. & JEFFERY, K. J. 2015. Purely translational realignment in grid cell firing patterns following nonmetric context change. *Cereb Cortex,* 25**,** 4619-4627.
MAU, W., SULLIVAN, D. W., KINSKY, N. R., HASSELMO, M. E., HOWARD, M. W. & EICHENBUAM, H. 2018. The same hippocampal CA1 population simultaneously codes temporal information over multiple timescales. *Curr Biol*, 28, 1499-1508.
MCHUGH, T. J., BLUM, K. I., TSIEN, J. Z., TONEGAWA, S. & WILSON, M. A. 1996. Impaired hippocampal representation of space in CA1-specific NMDAR1 knockout mice. *Cell,* 87**,** 1339-1349.
MCKENZIE, S., HUSZÁR, R., ENGLISH, D. F., KIM, K., YOON, E. & BUZSÁKI, G. 2019. Preexisting hippocampal network dynamics constrain optogenetically induced place fields. *bioRxiv***,** 803577.
MCNAUGHTON, B. L., BARNES, C. A., GERRARD, J. L., GOTHARD, K., JUNG, M. W., KNIERIM, J. J., KUDRIMOTI, H., QIN, Y., SKAGGS, W. E., SUSTER, M. & WEAVER, K. L. 1996.

Deciphering the hippocampal polyglot: the hippocampus as a path integration system. *J Exp Biol,* 199**,** 173-185.
MCNAUGHTON, B. L., BATTAGLIA, F. P., JENSEN, O., MOSER, E. I. & MOSER, M.-B. 2006. Path integration and the neural basis of the 'cognitive map'. *Nat Rev Neurosci,* 7**,** 663-678.
MELTZER, H. Y. 1994. An overview of the mechanism of action of clozapine. *J Clin Psychiatry,* 55 Suppl B**,** 47-52.
MIAO, C., CAO, Q., ITO, H. T., YAMAHACHI, H., WITTER, M. P., MOSER, M. B. & MOSER, E. I. 2015. Hippocampal remapping after partial inactivation of the medial entorhinal cortex. *Neuron,* 88**,** 590-603.
MIAO, C., CAO, Q., MOSER, M. B. & MOSER, E. I. 2017. Parvalbumin and somatostatin interneurons control different space-coding networks in the medial entorhinal cortex. *Cell,* 171**,** 507-521.
MILLER, V. M. & BEST, P. J. 1980. Spatial correlates of hippocampal unit activity are altered by lesions of the fornix and endorhinal cortex. *Brain Res,* 194**,** 311-323.
MILNER, B. 1962. Les trouble de la mémoire accompagnant les lésions hippocampiques bilatérales, in P. PASSOUANT. *Physiologie de l'Hippocampe, Colloques Internationaux, No. 107.* Paris, FR: Centre National de la Recherche Scientifique, 257-272.
MILNER, B., SQUIRE, L. R. & KANDEL, E. R. 1998. Cognitive neuroscience and the study of memory. *Neuron,* 20**,** 445-468.
MISHKIN, M. 1978. Memory in monkeys severely impaired by combined but not by separate removal of amygdala and hippocampus. *Nature,* 273**,** 297-298.
MONACO, J. D. & ABBOTT, L. F. 2011. Modular realignment of entorhinal grid cell activity as a basis for hippocampal remapping. *J Neurosci,* 31**,** 9414-9425.
MORRIS, R. G. M. 1981. Spatial localization does not require the presence of local cues. *Learning and Motivation,* 12**,** 239-260.
MORRIS, R. G. M., GARRUD, P., RAWLINS, J. N. P. & O'KEEFE, J. 1982. Place navigation impaired in rats with hippocampal lesions. *Nature,* 297**,** 681-683.
MOSER, E. I., MOSER, M. B. & MCNAUGHTON, B. L. 2017. Spatial representation in the hippocampal formation: a history. *Nat Neurosci,* 20**,** 1448-1464.
MOSER, E. I., ROUDI, Y., WITTER, M. P., KENTROS, C., BONHOEFFER, T. & MOSER, M. B. 2014. Grid cells and cortical representation. *Nat Rev Neurosci,* 15**,** 466-481.
MULLER, R. U. & KUBIE, J. L. 1987. The effects of changes in the environment on the spatial firing of hippocampal complex-spike cells. *J Neurosci,* 7**,** 1951-1968.
MULLER, R. U., KUBIE, J. L. & RANCK, J. B., JR. 1987. Spatial firing patterns of hippocampal complex-spike cells in a fixed environment. *J Neurosci,* 7**,** 1935-1950.
NAKASHIBA, T., YOUNG, J. Z., MCHUGH, T. J., BUHL, D. L. & TONEGAWA, S. 2008. Transgenic inhibition of synaptic transmission reveals role of CA3 output in hippocampal learning. *Science,* 319**,** 1260-1264.
NAKAZAWA, K., QUIRK, M. C., CHITWOOD, R. A., WATANABE, M., YECKEL, M. F., SUN, L. D., KATO, A., CARR, C. A., JOHNSTON, D., WILSON, M. A. & TONEGAWA, S. 2002. Requirement for hippocampal CA3 NMDA receptors in associative memory recall. *Science,* 297**,** 211-218.
NAKAZAWA, K., SUN, L. D., QUIRK, M. C., RONDI-REIG, L., WILSON, M. A. & TONEGAWA, S. 2003. Hippocampal CA3 NMDA receptors are crucial for memory acquisition of one-time experience. *Neuron,* 38**,** 305-315.
NEVES, G., COOKE, S. F. & BLISS, T. V. P. 2008. Synaptic plasticity, memory and the hippocampus: a neural network approach to causality. *Nat Neurosci,* 9**,** 65-75.
O'KEEFE, J. & BURGESS, N. 1996. Geometric determinants of the place fields of hippocampal neurons. *Nature,* 381**,** 425-428.
O'KEEFE, J. & BURGESS, N. 2005. Dual phase and rate coding in hippocampal place cells: theoretical significance and relationship to entorhinal grid cells. *Hippocampus,* 15**,** 853-866.
O'KEEFE, J. & CONWAY, D. 1978. Hippocampal place units in the freely moving rat: why they fire where they fire. *Exp Brain Res,* 31**,** 573-590.
O'KEEFE, J. & DOSTROVSKY, J. 1971. The hippocampus as a spatial map. Preliminary evidence from unit activity in the freely-moving rat. *Brain Res,* 34**,** 171-175.
O'KEEFE, J. & NADEL, L. 1978. *The Hippocampus as a Cognitive Map*. Oxford, UK: Oxford University Press.
O'KEEFE, J., NADEL, L., KEIGHTLEY, S. & KILL, D. 1975. Fornix lesions selectively abolish place learning in the rat. *Exp Neurol,* 48**,** 152-166.
O'KEEFE, J & SPEAKMAN, A. 1987. Single unit activity in the rat hippocampus during spatial memory tasks. *Exp Brain Res,* 68, 1-27.

OLTON, D. S., WALKER, J. A. & GAGE, F. H. 1978. Hippocampal connections and spatial discrimination. *Brain Research,* 139**,** 295-308.
OMER, D. B., MAIMON, S. R., LAS, L. & ULANOVSKY, N. 2018. Social place-cells in the bat hippocampus. *Science,* 359**,** 218-224.
ORMOND, J. & MCNAUGHTON, B. L. 2015. Place field expansion after focal MEC inactivations is consistent with loss of Fourier components and path integrator gain reduction. *Proc Natl Acad Sci USA,* 112**,** 4116-4121.
PASTALKOVA, E., ITSKOV, V., AMARASINGHAM, A. & BUZSAKI, G. 2008. Internally generated cell assembly sequences in the rat hippocampus. *Science,* 321**,** 1322-1327.
PFEIFFER, B. E. & FOSTER, D. J. 2013. Hippocampal place-cell sequences depict future paths to remembered goals. *Nature,* 497**,** 74-79.
QUIRK, G. J., MULLER, R. U. & KUBIE, J. L. 1990. The firing of hippocampal place cells in the dark depends on the rat's recent experience. *J Neurosci,* 10**,** 2008-2017.
QUIRK, G. J., MULLER, R. U., KUBIE, J. L. & RANCK, J. B., JR. 1992. The positional firing properties of medial entorhinal neurons: description and comparison with hippocampal place cells. *J Neurosci,* 12**,** 1945-1963.
RANCK, J. B., JR. 1985. Head direction cells in the deep layer of dorsal presubiculum in freely moving rats, in G. BUZSAKI & C. H. VANDERWOLF (eds.). *Electrical Activity of the Archicortex*. Budapest, HU: Akademiai Kiado.
RENNÓ-COSTA, C. & TORT, A. B. L. 2017. Place and grid cells in a loop: implications for memory function and spatial coding. *J Neurosci,* 37**,** 8062-8076.
ROLLS, E. T., STRINGER, S. M. & ELLIOT, T. 2006. Entorhinal cortex grid cells can map to hippocampal place cells by competitive learning. *Network,* 17**,** 447-465.
ROTH, B. L. 2016. DREADDs for neuroscientists. *Neuron,* 89**,** 683-694.
ROWLAND, D. C., OBENHAUS, H. A., SKYTØEN, E. R., ZHANG, Q., KENTROS, C. G., MOSER, E. I. & MOSER, M. B. 2018. Functional properties of stellate cells in medial entorhinal cortex layer II. *eLife,* 7**,** e36664.
ROWLAND, D. C., WEIBLE, A. P., WICKERSHAM, I. R., WU, H., MAYFORD, M., WITTER, M. P. & KENTROS, C. G. 2013. Transgenically targeted rabies virus demonstrates a major monosynaptic projection from hippocampal area CA2 to medial entorhinal layer II neurons. *J Neurosci,* 33**,** 14889-14898.
RUECKEMANN, J. W., DIMAURO, A. J., RANGEL, L. M., HAN, X., BOYDEN, E. S. & EICHENBAUM, H. 2016. Transient optogenetic inactivation of the medial entorhinal cortex biases the active population of hippocampal neurons. *Hippocampus,* 26**,** 246-260.
SAREL, A., FINKELSTEIN, A., LAS, L. & ULANOVSKY, N. 2017. Vectorial representation of spatial goals in the hippocampus of bats. *Science,* 355**,** 176-180.
SARGOLINI, F., FYHN, M., HAFTING, T., MCNAUGHTON, B. L., WITTER, M. P., MOSER, M. B. & MOSER, E. I. 2006. Conjunctive representation of position, direction, and velocity in entorhinal cortex. *Science,* 312**,** 758-762.
SAVE, E., CRESSANT, A., THINUS-BLANC, C. & POUCET, B. 1998. Spatial firing of hippocampal place cells in blind rats. *J Neurosci,* 18**,** 1818-1826.
SAVELLI, F. & KNIERIM, J. J. 2010. Hebbian analysis of the transformation of medial entorhinal grid-cell inputs to hippocampal place fields. *J Neurophysiol,* 103**,** 3167-3183.
SAVELLI, F., YOGANARASIMHA, D. & KNIERIM, J. J. 2008. Influence of boundary removal on the spatial representations of the medial entorhinal cortex. *Hippocampus,* 18**,** 1270-1282.
SCHLESIGER, M. I., BOUBLIL, B. L., HALES, J. B., LEUTGEB, J. K. & LEUTGEB, S. 2018. Hippocampal global remapping can occur without input from the medial entorhinal cortex. *Cell Rep,* 22**,** 3152-3159.
SCHLESIGER, M. I., CANNOVA, C. C., BOUBLIL, B. L., HALES, J. B., MANKIN, E. A., BRANDON, M. P., LEUTGEB, J. K., LEIBOLD, C. & LEUTGEB, S. 2015. The medial entorhinal cortex is necessary for temporal organization of hippocampal neuronal activity. *Nat Neurosci,* 18**,** 1123-1132.
SCOVILLE, W. B. & MILNER, B. 1957. Loss of recent memory after bilateral hippocampal lesions. *J Neurol Neurosurg Psychiatry,* 20**,** 11-21.
SI, B. & TREVES, A. 2009. The role of competitive learning in the generation of DG fields from EC inputs. *Cogn Neurodynamics,* 3**,** 177-187.
SKAGGS, W. E. & MCNAUGHTON, B. L. 1996. Replay of neuronal firing sequences in rat hippocampus during sleep following spatial experience. *Science,* 271**,** 1870-1873.
SOLSTAD, T., BOCCARA, C. N., KROPFF, E., MOSER, M. B. & MOSER, E. I. 2008. Representation of geometric borders in the entorhinal cortex. *Science,* 322**,** 1865-1868.

SOLSTAD, T., MOSER, E. I. & EINEVOLL, G. T. 2006. From grid cells to place cells: a mathematical model. *Hippocampus,* 16**,** 1026-1031.
SQUIRE, L. R. & ZOLA-MORGAN, S. 1991. The medial temporal lobe memory system. *Science,* 253**,** 1380-1386.
STENSOLA, H., STENSOLA, T., SOLSTAD, T., FROLAND, K., MOSER, M. B. & MOSER, E. I. 2012. The entorhinal grid map is discretized. *Nature,* 492**,** 72-78.
STENSOLA, T., STENSOLA, H., MOSER, M. B. & MOSER, E. I. 2015. Shearing-induced asymmetry in entorhinal grid cells. *Nature,* 518**,** 207-212.
STRANGE, B. A., WITTER, M. P., LEIN, E. S. & MOSER, E. I. 2014. Functional organization of the hippocampal longitudinal axis. *Nat Neurosci,* 15**,** 655-669.
TAUBE, J. S. & BURTON, H. L. 1995. Head direction cell activity monitored in a novel environment and during a cue conflict situation. *J Neurophysiol,* 74**,** 1953-1971.
TAUBE, J. S., MULLER, R. U. & RANCK, J. B., J.R. 1990a. Head-direction cells recorded from the postsubiculum in freely moving rats. I. Description and quantitative analysis. *J Neurosci,* 10**,** 420-435.
TAUBE, J. S., MULLER, R. U. & RANCK, J. B., J.R. 1990b. Head-direction cells recorded from the postsubiculum in freely moving rats. II. Effects of environmental manipulations. *J Neurosci,* 10**,** 436-447.
THOMPSON, L. T. & BEST, P. J. 1990. Long-term stability of the place-field activity of single units recorded from the dorsal hippocampus of freely behaving rats. *Brain Res,* 509**,** 299-308.
TOLMAN, E. C. 1948. Cognitive maps in rats and men. *Psychological Review,* 55**,** 189-208.
TULVING, E. 1983. *Elements of Episodic Memory*. Oxford, UK: Oxford University Press.
VAN CAUTER, T., POUCET, B. & SAVE, E. 2008. Unstable CA1 place cell representation in rats with entorhinal cortex lesions. *Eur J Neurosci,* 27**,** 1933-1946.
VARGHA-KHADEM, F., GADIAN, D. G., WATKINS, K. E., CONNELLY, A., VAN PAESSCHEN, W. & MISHKIN, M. 1997. Differential effects of early hippocampal pathology on episodic and semantic memory. *Science,* 277**,** 376-380.
VAZDARJANOVA, A. & GUZOWSKI, J. F. 2004. Differences in hippocampal neuronal population responses to modifications of an environmental context: evidence for distinct, yet complementary, functions of CA3 and CA1 ensembles. *J Neurosci,* 24**,** 6489-6496.
VAZEY, E. M. & ASTON-JONES, G. 2014. Designer receptor manipulations reveal a role of the locus coeruleus noradrenergic system in isoflurane general anesthesia. *Proc Natl Acad Sci USA,* 111**,** 3859-3864.
WERNLE, T., WAAGA, T., MØRREAUNET, M., TREVES, A., MOSER, M. B. & MOSER, E. I. 2018. Integration of grid maps in merged environments. *Nat Neurosci,* 21**,** 92-101.
WIENER, S. I., PAUL, C. A. & EICHENBAUM, H. 1989. Spatial and behavioral correlates of hippocampal neuronal activity. *J Neurosci,* 9**,** 2737-2763.
WILLS, T. J., CACUCCI, F., BURGESS, N. & O'KEEFE, J. 2010. Development of the hippocampal cognitive map in preweanling rats. *Science,* 328**,** 1573-1576.
WILSON, M. A. & MCNAUGHTON, B. L. 1993. Dynamics of the hippocampal ensemble code for space. *Science,* 261**,** 1055-1058.
WOOD, E., ET AL. 1999. The global record of memory in hippocampal neuronal activity. *Nature,* 397**,** 613-616.
WOOD, E. R., DUDCHENKO, P. A., ROBITSEK, R. J. & EICHENBAUM, H. 2000. Hippocampal neurons encode information about different types of memory episodes occurring in the same location. *Neuron,* 27**,** 623-633.
YASUDA, M. & MAYFORD, M. R. 2006. CaMKII activation in the entorhinal cortex disrupts previously encoded spatial memory. *Neuron,* 50**,** 309-318.
YAU, J. O. & MCNALLY, G. P. 2015. Pharmacogenetic excitation of dorsomedial prefrontal cortex restores fear prediction error. *J Neurosci,* 35**,** 74-83.
YOGANARASIMHA, D., YU, X. & KNIERIM, J. J. 2006. Head direction cell representations maintain internal coherence during conflicting proximal and distal cue rotations: comparison with hippocampal place cells. *J Neurosci,* 26**,** 622-631.
YOON, K., BUICE, M. A., BARRY, C., HAYMAN, R., BURGESS, N. & FIETE, I. R. 2013. Specific evidence of low-dimensional continuous attractor dynamics in grid cells. *Nat Neurosci,* 16**,** 1077-1084.
YOUNG, B. J., FOX, G. D. & EICHENBAUM, H. 1994. Correlates of hippocampal complex-spike cell activity in rats performing a nonspatial radial maze task. *J Neurosci,* 14**,** 6553-6563.

ZHANG, S. J., YE, J., MIAO, C., TSAO, A., CERNIAUSKAS, I., LEDERGERBER, D., MOSER, M. B. & MOSER, E. I. 2013. Optogenetic dissection of entorhinal-hippocampal functional connectivity. *Science,* 340**,** 1232627.

ZHAO, R., GRUNKE, S. D., KERALAPURATH, M. M., YETMAN, M. J., LAM, A., LEE, T. C., SOUSOUNIS, K., JIANG, Y., SWING, D. A., TESSAROLLO, L., JI, D. & JANKOWSKY, J. L. 2016. Impaired recall of positional memory following chemogenetic disruption of place field stability. *Cell Rep,* 16**,** 793-804.

ZOLA, S. M. & SQUIRE, L. R. 2001. Declarative Memory, Neural Basis of, in: N. J. SMELSER & P. B. BALTES (eds.). *International Encyclopedia of the Social & Behavioral Sciences.* Oxford, UK: Pergamon, 3340-3343.

Paper 1

Article

Neuron

A Novel Mechanism for the Grid-to-Place Cell Transformation Revealed by Transgenic Depolarization of Medial Entorhinal Cortex Layer II

Highlights

- Depolarization of MECII neurons produces remapping in CA1 and impairs spatial memory
- Hyperpolarization of a similar number of MECII neurons produces neither
- Both manipulations change the firing rate, but not firing location, of MEC neurons
- Depolarization of MECII differentially changes firing rates of individual grid fields

Authors

Benjamin R. Kanter, Christine M. Lykken, Daniel Avesar, ..., Nils Z. Borgesius, Yasser Roudi, Clifford G. Kentros

Correspondence

clifford.kentros@ntnu.no

In Brief

Kanter et al. show that depolarization, but not hyperpolarization, of MECII neurons produces hippocampal remapping and impairs memory. Since MEC neurons do not change firing location, these results are likely due to changes in firing rate of individual grid fields.

Kanter et al., 2017, Neuron *93*, 1480–1492
March 22, 2017
http://dx.doi.org/10.1016/j.neuron.2017.03.001

CellPress

Neuron
Article

A Novel Mechanism for the Grid-to-Place Cell Transformation Revealed by Transgenic Depolarization of Medial Entorhinal Cortex Layer II

Benjamin R. Kanter,[1,2] Christine M. Lykken,[1,2] Daniel Avesar,[2] Aldis Weible,[2] Jasmine Dickinson,[2] Benjamin Dunn,[1] Nils Z. Borgesius,[1] Yasser Roudi,[1] and Clifford G. Kentros[1,2,3,*]
[1]Kavli Institute for Systems Neuroscience and Centre for Neural Computation, Norwegian University of Science and Technology, Olav Kyrres gate 9, 7030 Trondheim, Norway
[2]Institute of Neuroscience, University of Oregon, 1254 University of Oregon, Eugene, OR 97403, USA
[3]Lead Contact
*Correspondence: clifford.kentros@ntnu.no
http://dx.doi.org/10.1016/j.neuron.2017.03.001

SUMMARY

The spatial receptive fields of neurons in medial entorhinal cortex layer II (MECII) and in the hippocampus suggest general and environment-specific maps of space, respectively. However, the relationship between these receptive fields remains unclear. We reversibly manipulated the activity of MECII neurons via chemogenetic receptors and compared the changes in downstream hippocampal place cells to those of neurons in MEC. Depolarization of MECII impaired spatial memory and elicited drastic changes in CA1 place cells in a familiar environment, similar to those seen during remapping between distinct environments, while hyperpolarization did not. In contrast, both manipulations altered the firing rate of MEC neurons without changing their firing locations. Interestingly, only depolarization caused significant changes in the relative firing rates of individual grid fields, reconfiguring the spatial input from MEC. This suggests a novel mechanism of hippocampal remapping whereby rate changes in MEC neurons lead to locational changes of hippocampal place fields.

INTRODUCTION

Neurons in the hippocampal formation exhibit spatially selective activity patterns that are thought to support episodic memory and spatial navigation. Hippocampal place cells (O'Keefe and Dostrovsky, 1971) typically display single environment-specific spatial receptive fields that change drastically between different environments, a process referred to as remapping (Muller and Kubie, 1987). In contrast, grid cells in medial entorhinal cortex (MEC), one of two major inputs to the hippocampus, have multiple regularly spaced firing fields (Fyhn et al., 2004; Hafting et al., 2005) that are largely similar between environments (Fyhn et al., 2007). Other directionally modulated and speed-modulated cell types in MEC also retain their basic firing patterns between environments (Taube et al., 1990; Kropff et al., 2015). Thus, it appears that MEC neurons encode space in general, while hippocampal neurons encode particular locations in space.

Much of the excitement surrounding the discovery of grid cells came from their presumed ability to generate place cells. Under conditions that elicit remapping in place cells, grid cells shift and rotate their axes (Fyhn et al., 2007) and transiently increase in size and scale (Barry et al., 2012). Theoretical models have elucidated how such changes may lead to remapping in downstream hippocampal place cells (Rolls et al., 2006; Solstad et al., 2006; de Almeida et al., 2009; Savelli and Knierim, 2010). Demonstrating causality is more challenging because it is difficult to determine which changes in MEC are critical for place cell remapping, and which are epiphenomena evoked by changes in sensory inputs.

Several recent studies bring the assumption that grid cells are the primary determinant of place cell firing into question. Notably, pharmacological inactivation of the medial septum reduces theta power and disrupts the hexagonal regularity of grid cells, yet has surprisingly little effect on the stability of place fields in familiar environments (Koenig et al., 2011), or on their development in novel environments (Brandon et al., 2014). In addition, place fields are present several days before the emergence of grid firing patterns during development (Langston et al., 2010; Wills et al., 2010). Finally, a recent study reported that while grid cells form the majority of the direct projections from MEC to the hippocampus, other functionally specialized cell types such as border and head direction cells project directly to the hippocampus as well (Zhang et al., 2013). These findings lead to the counterintuitive suggestion that the spatial receptive fields of place cells do not rely on their major spatial input.

Indeed, it is still unclear exactly how the MEC network is involved in hippocampal spatial firing and spatial memory. Nearly complete entorhinal lesions do not prevent location-selective activity in the hippocampus, though the resulting place fields lack precision and spatial stability (Miller and Best, 1980; Brun et al., 2008; Van Cauter et al., 2008; Hales et al., 2014; Schlesiger et al., 2015). In addition, genetic disruptions and lesions of the entorhinal cortex produce impairments on some hippocampus-dependent tasks, but they can be milder than those

observed following lesions of the hippocampus (Parron et al., 2004; Steffenach et al., 2005; Yasuda and Mayford, 2006; Hales et al., 2014). A possible reason for these inconsistent results is that it is extremely difficult to surgically destroy the entirety of a structure without also damaging surrounding brain areas. Even ideal surgical lesions are irreversible and temporally diffuse, as the brain gradually adapts to the insult. More recent work has shown that hippocampal place fields change their firing properties to varying degrees following pharmacological (Ormond and McNaughton, 2015), chemogenetic (Miao et al., 2015; Zhao et al., 2016), and optogenetic (Miao et al., 2015; Rueckemann et al., 2016) inactivation of MEC. While these results provide support for the idea that MEC is involved in hippocampal spatial firing, the changes in the firing patterns of MEC neurons in response to these manipulations are not well characterized. Therefore, it is difficult to determine precisely which changes in the firing patterns of MEC neurons lead to changes in hippocampal place fields and spatial memory deficits. Finally, most of these interventions depend upon the complex diffusion of a bolus within the brain, which generates variability in the number and types of neurons affected in each animal (Lykken and Kentros, 2014).

To overcome these issues, we designed experiments using transgenic mice expressing DREADDs (Designer Receptors Exclusively Activated by Designer Drugs) (Alexander et al., 2009) almost exclusively in stellate cells of MEC layer II (MECII), where grid cells are most abundant (Sargolini et al., 2006). By using transgenic crosses rather than stereotactic injections into brain tissue, expression of the transgene was similar in all mice and we were able to estimate the percentage of each cell type being manipulated. Here, we present the electrophysiological and behavioral results of reversibly increasing or decreasing the membrane potential of a subset of MECII neurons, yielding insight into the relationship between the spatial firing properties of MEC and hippocampal neurons, and their relationship to spatial memory.

RESULTS

Anatomical Specificity of the Transgenic Crosses

One of the most attractive features of transgenic crosses is that they are anatomically restricted in a more uniform manner than injections of pharmacological or viral agents. Here, we crossed the EC-tTA driver line (Yasuda and Mayford, 2006) to hM3Dq- or hM4Di-tetO DREADD lines (Alexander et al., 2009) to enable control of neurons in the superficial layers of MEC via intraperitoneal injection of the designer ligand clozapine N-oxide (CNO). Double-positive offspring are referred to as hM3 and hM4 mice, respectively. The driver line expresses primarily throughout the dorsoventral extent of MECII, as well as in other brain regions such as pre- and parasubiculum, depending on the particular cross (Rowland et al., 2013; Yetman et al., 2016). DREADD receptor expression restricted to superficial MEC was revealed by antibody labeling of a heme-agglutinin (HA) epitope tag (Figure 1A), but localization of the receptor to processes made quantification nearly impossible. Therefore, to visualize somatic transgene expression, we performed in situ hybridization using a custom probe targeting DREADD receptor mRNA (hM3Dq: Figure 1B, hM4Di: Figure 1D). We quantified expression levels by counting the number of hM3Dq RNA-positive nuclei (Figure S1) within all brain regions with detectable expression levels (Figure 1C). We estimated that 20% of nuclei in MECII expressed the DREADD receptor in each transgenic cross. Our prior work (Rowland et al., 2013) demonstrated that this driver line expresses in stellate cells of MECII, which form the majority (74%) of nuclei in layer II (Gatome et al., 2010). Therefore, our manipulation targeted approximately 27% of layer II stellate cells, and relatively few other cell types. Since the only other areas with significant expression levels (pre- and parasubiculum) have very weak projections to the hippocampus (Köhler, 1985), we ascribe the vast majority of our effects on hippocampal neurons to the manipulation of MECII activity.

Depolarization, but Not Hyperpolarization, of MECII Causes "Artificial Remapping" in CA1

Naive adult mice were implanted with chronic tetrode arrays targeting hippocampal area CA1 (Figures S2A, S2C, S2E, and S2G) to record the effect of manipulating MECII activity on place cells. Depolarizing MECII inputs by CNO injection (1 mg/kg) in hM3 mice had striking effects on CA1 place cells in a stable, familiar environment (Figure 2). A large proportion of cells shifted the location of their place fields (28/105, or 27%, Figures 2A–2C), or had fields that turned on (9/105, or 9%, Figure 2D) or off (5/105, or 5%, Figure 2E), closely resembling the remapping observed between distinct environments. Other simultaneously recorded cells changed their firing rate and/or field size, but maintained the position of their primary field (19/105, or 18%, Figure 2F), much like the rate remapping seen between similar environments (Leutgeb et al., 2005). We refer to the above changes collectively as "artificial remapping." The remaining cells did not change significantly in any of these dimensions (Figure 2G), suggesting that some degree of the initial hippocampal representation was still intact.

At the population level, depolarization of MECII significantly increased firing rate (Figure 3A) and field size (Figure 3B) of CA1 place cells compared to littermate controls (rate: hM3 n = 80, Con n = 91, p = 0.02; size: hM3 n = 76, Con n = 91, $p = 8.04 \times 10^{-5}$; two-sided independent t tests). As a result of the increased field size, there was a concomitant decrease in spatial information relative to controls (Table S1), but the Gaussian structure of the fields remained intact (coherence: hM3 n = 80, Con n = 91, p = 0.72, one-sided Wilcoxon rank sum test). These firing rate and field size effects alone could indicate that MECII neurons simply provide gain control to the hippocampus. However, the spatial correlation of firing rate maps before and after CNO injection was significantly lower in hM3 mice relative to controls (hM3 n = 80, Con n = 91, $p = 4.31 \times 10^{-7}$, one-sided Wilcoxon rank sum test, Figure 3C), suggesting that substantial hippocampal remapping occurred even though the mouse remained in a stable, familiar environment. An alternative method of quantifying the extent of remapping revealed that while 83% (77/93) of place cells had spatial correlation values between the first and second halves of the baseline session that exceeded the 95th percentile of a shuffled distribution, only 26% (21/80) of place cells had correlation values between baseline and CNO sessions that passed the

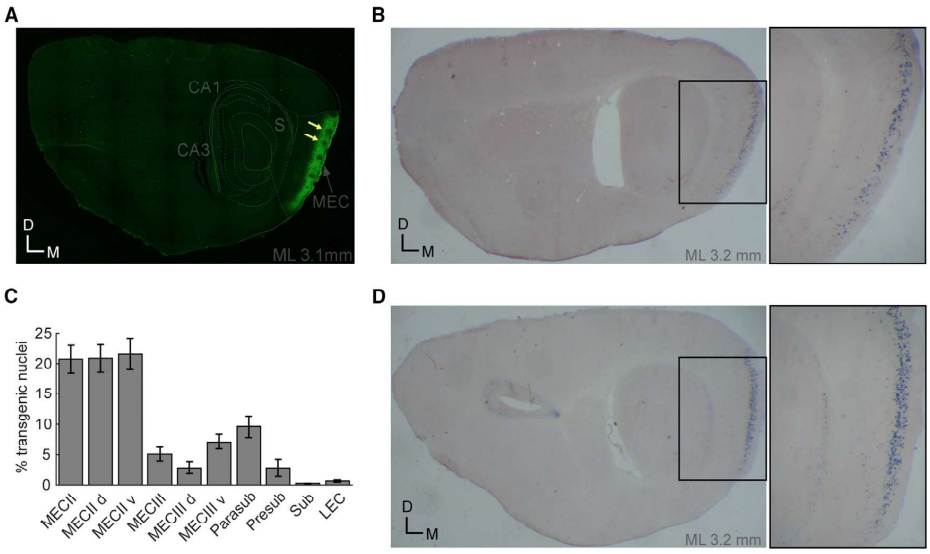

Figure 1. Transgenic Expression of DREADD Receptors Is Highly Specific to MECII

(A) Expression of hM3Dq transgene visualized by heme-agglutinin antibody in sagittal section. Note the absence of label in presumed calbindin-positive patches (yellow arrows), consistent with expression restricted to reelin-positive stellate cells. D, dorsal; M, medial; S, subiculum; ML, medial/lateral relative to midline.

(B) RNA in situ hybridization targeted to hM3Dq. Inset on right shows MEC.

(C) Percentage of hM3Dq-positive nuclei by brain region (mean ± SEM; n = 9 mice). MEC, medial entorhinal cortex; d, dorsal; v, ventral; Parasub, parasubiculum; Presub, presubiculum; Sub, subiculum; LEC, lateral entorhinal cortex. Roman numerals refer to cell layer.

(D) RNA in situ hybridization targeted to hM4Di. Inset on right shows MEC.

Magnification is 1.25×, and 4× for insets.

same threshold. To determine the time course of remapping, we divided the data into smaller temporal bins and found that the decrease in spatial correlation occurred 10–15 min post-injection (hM3 n = 81, Con n = 84, $p = 7.66 \times 10^{-5}$, one-sided Wilcoxon rank sum test, Figure S3A). Interestingly, this CNO-induced remapping stabilized over the duration of the 2-hr recording session (Figure S4). In addition, the effects were generally reversible, as the firing rate, field size, and spatial correlations were not significantly different from controls 12+ hr post-CNO injection (rate: hM3 n = 77, Con n = 91, p = 0.07, two-sided independent t test, Figure 3A; size: hM3 n = 72, Con n = 91, p = 0.83, two-sided independent t test, Figure 3B; spatial correlation: hM3 n = 77, Con n = 37, p = 1.00, one-sided Wilcoxon rank sum test, Figure 3C). While this may indicate that the altered place cell map is not consolidated, it is possible that it would be reinstated following a subsequent injection of CNO.

Given that depolarizing MECII produced these qualitative changes in place cell activity, we predicted that hyperpolarization of the same MECII inputs would yield similar results. However, we found that hyperpolarizing MECII had a negligible effect on CA1 place cells (e.g., Figure 2H), despite using a much higher dose of CNO (10 mg/kg) in an attempt to elicit an effect. Changes in mean firing rate, field size, and spatial information in hM4 mice were not significantly different from controls (rate: hM4 n = 106, Con n = 91, p = 0.28, Figure 3A; size: hM4 n = 102, Con n = 91, p = 0.46, Figure 3B; spatial information: hM4 n = 106, Con n = 91, p = 0.44, Table S1; two-sided independent t tests). In addition, there was no change in the spatial correlation between firing rate maps before and after injection of CNO relative to littermate controls (hM4 n = 106, Con n = 91, p = 0.93, one-sided Wilcoxon rank sum test, Figure 3C), indicating that this manipulation did not cause hippocampal remapping. Furthermore, the majority (78/106, or 74%) of place cells had spatial correlation values between baseline and CNO sessions that exceeded the 95th percentile of the shuffled distribution (BL first versus second half: 119/127, or 94%). Thus, it seems that place cells are not affected by transgenic hyperpolarization of MECII stellate cells, even though depolarization of a similar number of them results in drastic changes.

Behavioral Significance of Artificial Remapping

Since artificial remapping appears to reflect a major reorganization of the place cell code, we wanted to examine its impact on spatial memory. We trained naive cohorts of hM3, hM4, and littermate control mice (hM3 n = 13, hM4 n = 13, Con n = 25) in the Morris water maze. As expected, learning rates for both cued (non-spatial, Days 1–2) and hidden (spatial, Days 6–8) versions of the task did not differ between groups (cued: p = 0.71; hidden: p = 0.17; one-between one-within ANOVA; Figure 4A). However, CNO injection 30 min before the probe test on Day 9 significantly increased the escape latency in hM3, but not hM4,

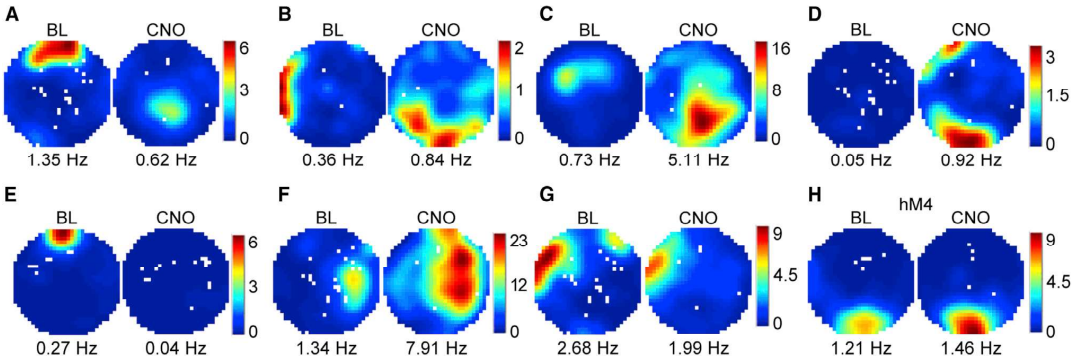

Figure 2. Artificial Remapping of CA1 Place Cells following Depolarization, but Not Hyperpolarization, of MECII

(A–G) Firing rate maps of seven representative CA1 place cells in hM3 mice before and after CNO injection. Rate maps show that place cells changed location and shape (A–C), turned on (D), turned off (E), expanded (F), or were unaffected (G) following CNO injection. Cells in (A), (D), (F), and (G) were simultaneously recorded. (H) Rate maps of a representative place cell from an hM4 mouse that was unaffected by CNO injection.

BL, baseline; CNO, 30–60 min post-CNO injection. Maps are scaled to maximum rate between sessions. Red represents maximum firing, blue is silent, and white represents unvisited pixels. Mean rate indicated below rate maps.

mice relative to controls (hM3: $p = 0.02$; hM4: $p = 0.31$; one-sided Wilcoxon rank sum tests; Figure 4B). This increased latency cannot be explained by reduced swimming speed in hM3 mice (hM3 versus Con: $p = 0.30$, one-sided Wilcoxon rank sum test). Moreover, hM3 mice spent significantly less time in the target quadrant compared to control mice ($p = 0.01$, one-sided Wilcoxon rank sum test). When injected with vehicle on Day 10, hM3 mice found the target as quickly as hM4 and control mice (hM3 versus hM4: $p = 0.47$; hM3 versus Con: $p = 0.83$; one-sided Wilcoxon rank sum tests; Figure 4C), indicating that they were able to successfully retrieve the memory of the platform location. This result is consistent with the return to baseline firing patterns observed after CNO has worn off. Thus, artificial remapping of place cells via depolarization, but *not* hyperpolarization, of a subset of hippocampal inputs is sufficient to impair recall of a previously formed spatial memory.

Manipulation of MECII Activity Leads Only to Quantitative Changes in MEC Neurons

The surprising dichotomy between these manipulations made it imperative to uncover exactly how upstream MEC neurons respond to CNO administration. Naive cohorts of hM3 and hM4 mice were implanted with chronic tetrode arrays targeting the superficial layers of dorsal MEC (Figures S2B, S2D, S2F, and S2H). Recordings of MEC neurons before and after CNO administration were performed under conditions nearly identical to those of the hippocampal recordings. Depolarization of MECII neurons in hM3 mice significantly increased firing rate (e.g., Figures 5A, 5C, and 5D) and field size (e.g., Figure 5A) of putative excitatory MEC neurons relative to controls (e.g., Figure 5E) (rate: hM3 $n = 86$, Con $n = 28$, $p = 4.79 \times 10^{-3}$, Figure 6A; size: hM3 $n = 74$, Con $n = 40$, $p = 2.14 \times 10^{-7}$, Figure 6B; one-sided Wilcoxon rank sum tests). The time course of this rate increase closely mirrored that of the CNO-induced remapping in CA1, occurring 10–15 min post-injection (hM3 $n = 95$, Con $n = 25$, $p = 0.01$, one-sided Wilcoxon rank sum test, Figure S3B). Surprisingly, CNO administration did not alter the location of the firing fields of excitatory MEC neurons (e.g., Figures 5A–5C) (hM3 $n = 82$, Con $n = 49$, $p = 0.29$, one-sided Wilcoxon rank sum test, Figure 6C). Counterintuitively, this result implies that the extensive hippocampal remapping observed in hM3 mice is caused by nonspatial changes in MEC inputs.

Since CNO injection in hM4 mice did not lead to hippocampal remapping, we assumed that its direct effects on MEC neurons would also be minimal. However, transgenic hyperpolarization of MECII in hM4 mice significantly decreased firing rate (e.g., Figure 5F) and field size of putative excitatory MEC neurons compared to controls (rate: hM4 $n = 71$, Con $n = 28$, $p = 2.15 \times 10^{-5}$, Figure 6A; size: hM4 $n = 61$, Con $n = 40$, $p = 0.01$, Figure 6B; one-sided Wilcoxon rank sum tests). Similarly, there was no significant difference in the spatial correlation of firing rate maps before and after CNO injection between hM4 and control mice (hM4 $n = 69$, Con $n = 49$, $p = 0.16$, one-sided Wilcoxon rank sum test, Figure 6C). Therefore, our manipulations of MECII neurons bidirectionally affected firing rate and field size of excitatory MEC neurons without any obvious changes to their spatial firing patterns. This raises the question of how depolarization and hyperpolarization of a similar number of MECII neurons have comparable effects on the firing of MEC neurons, yet drastically different effects on the hippocampus.

The simplest explanation would be that depolarization of MECII stellate cells leads to larger quantitative changes in putative excitatory MEC neurons than their hyperpolarization, but the magnitude of firing rate and field size changes were nearly identical between hM3 and hM4 mice (Figures 6A and 6B). A more detailed analysis revealed a subtle difference between the crosses. As expected, hyperpolarization of MECII neurons led to an overall decrease in firing rate of excitatory MEC neurons, with cells either firing less or not changing (Figure 6D), presumably reflecting cells that did or did not express the transgene,

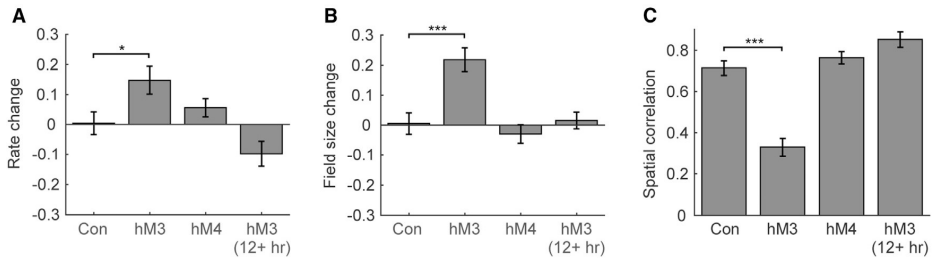

Figure 3. Depolarization, but Not Hyperpolarization, of MECII Reversibly Increases Firing Rate and Field Size of CA1 Place Cells and Induces Artificial Remapping

(A and B) Change in mean firing rate (A) and field size (B) following CNO injection in littermate control (Con), hM3, and hM4 mice.

(C) Spatial correlation between baseline and CNO sessions in Con, hM3, and hM4 mice.

Rightmost bars compare the baseline and 12+ hr post-CNO injection sessions in hM3 mice and show return to baseline firing patterns. Data represented as median ± SEM. *p < 0.05, ***p < 0.001. Change refers to a difference score (see STAR Methods).

respectively. Surprisingly, depolarization elicited bidirectional changes in firing rate (Figure 6D). The majority of excitatory cells increased their firing rate, but a substantial number of cells decreased their rate after CNO injection, resulting in significantly larger variance in rate changes in hM3 versus hM4 mice (hM3 n = 86, hM4 n = 71, $p = 3.35 \times 10^{-3}$, Levene's test). A recent imaging study (Kitamura et al., 2015) also reported that MEC cells drastically increased or decreased their firing rates between distinct environments. Approximately 36% of MECII stellate cells were significantly more active in one environment and were dubbed "context cells." When we calculated an analogous firing rate threshold, we found that merely 7% (6/90) of cells in hM3 mice and only 1% (1/84) of cells in hM4 mice were significantly more active either before or after CNO injection (includes putative excitatory and inhibitory cells, Figure S5). While Kitamura et al. (2015) did not address the functional characteristics of the neurons they imaged, the cells we identified were not of a particular functional class of MEC neurons. Furthermore, the observed firing rate changes appear to be the tails of a continuous distribution, rather than representing a separate population of MEC cells.

If artificial remapping is driven by changes in a specific functional cell type or set of cell types in MEC, the above analyses may have occluded differences between hM3 and control mice by grouping all putative excitatory neurons together. Since we do not know which functional cell types express our transgenic receptors, we examined the previously characterized functional classes individually. Surprisingly, we did not observe any large changes in the location of grid cell firing fields by translation or rotation (Figures 7A–7C; Table S2), which are the most obvious effects observed under conditions that elicit hippocampal remapping (Fyhn et al., 2007). Furthermore, grid regularity and scale, which have previously been shown to change upon introduction to a novel environment (Barry et al., 2012), remained essentially unchanged following transgenic depolarization (Table S2). Interestingly, we discovered that the average change in firing rate of grid cells following CNO injection in hM3 mice was not significantly different from controls (Table S2) because grid cells were among the MEC neurons described above that exhibited bidirectional rate changes (increase: 9/21; decrease 8/21; compared to 95th percentile of control distribution; e.g., Figures 5A and 5B). This was not the case for grid field size, which increased or remained stable (max field size: increase = 11/18, stable = 7/18; compared to 95th percentile of control distribution). Border (or boundary-vector) cells (e.g., Figure 5C) increased in firing rate (n = 14, Table S2) and field size (n = 13, median difference score = 0.34) following transgenic depolarization, but did not shift their preferred environmental boundary (n = 14, median spatial correlation = 0.67). Finally, head direction cells (e.g., Figure 5D) significantly increased their firing rate without changing their directional preference (n = 58, Table S2), which is in direct contrast to changes observed during hippocampal remapping (Taube et al., 1990). Taken together, these results suggest that the changes in place field location observed in CA1 were likely not a result of changes in the spatial or directional properties of a specific functional cell type in MEC. Instead, it appears that depolarizing MECII neurons caused the majority of excitatory MEC neurons to change their firing rate and/or field size (i.e., quantitative, not qualitative changes), unlike the drastic spatial reorganization observed downstream in the hippocampus (Figures 2 and 3).

Potential Mechanisms of Artificial Remapping

Given that grid cells are the most abundant spatial input to the hippocampus, and that they exhibited bidirectional firing rate changes following depolarization of MECII, we focused our subsequent analyses on grid cells. To determine whether the observed changes in grid cell firing rates alone were capable of eliciting remapping in hM3 mice, we simulated our results in a simple linear summation model of the grid-to-place cell transformation (Solstad et al., 2006). The simulation was run once where each grid cell had uniform peak firing rates, as previously published. The simulation was then repeated after scaling 20% (consistent with transgene expression levels) of the grid cells' firing rates to match the empirical data from hM3 and control mice following injection of CNO. These firing rate changes were not sufficient to cause place cell remapping (median spatial correlations: hM3 = 0.96, Con = 1.00), demonstrating the need

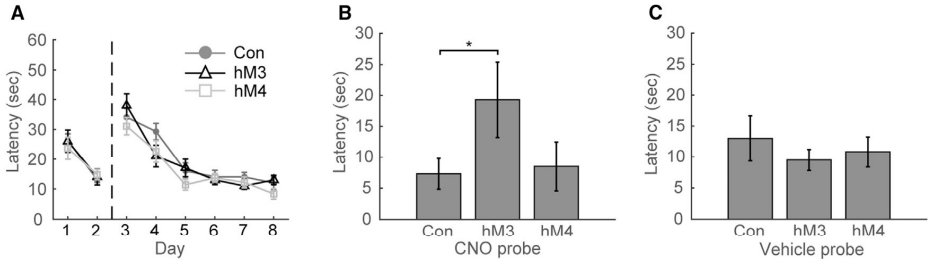

Figure 4. Spatial Memory Is Transiently Impaired following Depolarization, but Not Hyperpolarization, of MECII

(A) No difference in escape latency across training days between Con (dark gray circles), hM3 (black triangles), and hM4 mice (light gray squares). Vertical dashed line divides cued and hidden versions of task.

(B) Significant increase in escape latency following CNO injection during probe test on Day 9 in hM3, but not hM4 or Con mice.

(C) No difference in escape latency following vehicle injection during probe test on Day 10 between Con, hM3, and hM4 mice.

Data represented as median ± SEM. *$p < 0.05$.

for a shift in the location of grids relative to each other to cause remapping in this model.

Thus, the above analyses of MEC activity do not provide a clear explanation for the artificial remapping observed in hM3 mice. Since our sole manipulation was the depolarization of a minority of MECII stellate cells, there must be some aspect of MEC activity that produces sufficient change in spatial input to the hippocampus to elicit remapping. As previously described, we observed significant CNO-induced changes in firing rate without changes in firing location in MEC (i.e., rate remapping, Figures 6 and 7). While we initially examined these measures at the level of single neurons, the relevant information about space may be encoded at the population level. We therefore computed a population vector (PV) correlation of all recorded MEC neurons, which captures changes in both firing rate and location (Leutgeb et al., 2005). As expected, PV correlations for excitatory MEC neurons in hM3 mice were significantly lower than in controls, reflecting the CNO-induced firing rate changes reported above (Table S2). In order to determine whether grid cells in particular convey spatial change through firing rate alone, we computed PV correlations for grid cells and all other excitatory (non-grid) cells separately. Interestingly, while PV correlations for grid and non-grid cells were very similar in both control and hM4 mice, they were much lower for grid versus non-grid cells in hM3 mice (median PV correlation: Con grid = 0.94, Con non-grid = 0.88, hM4 grid = 0.76, hM4 non-grid = 0.79, hM3 grid = 0.35, hM3 non-grid = 0.63; Figures 7D and 7E). These results demonstrate that grid cell firing rates are very stable between repeated exposures to the same environment, yet change drastically during hippocampal remapping. We thus provide the first empirical evidence that grid cells can encode spatial change without changing spatial location (i.e., translation or rotation of grid fields).

This seeming contradiction is resolved if the firing rates of individual grid fields change independently. We calculated the CNO-induced rate changes of individual grid fields, rather than looking at each grid pattern as a whole, as is typically done. In hM3 mice, CNO administration led to changes in individual grid field firing rates that differed in magnitude and/or direction within a single cell. Some hM3 grid cells had fields that responded bidirectionally to CNO, thus changing the relative rankings between fields (5/17 cells, Figure 8A). The remaining hM3 grid cells had fields that all changed rate in the same direction, but to varying degrees (12/17; 9/12 increase, 3/12 decrease; Figure 8A). In control mice, there was a negligible change in firing rate within the fields (Figure 8A), consistent with the idea that the rates of individual grid fields are stable across repeated exposures to a familiar environment. This disruption in the relationship between grid field firing rates in hM3 mice can be observed at the population level by comparing the grid field rate changes within the baseline session to those between the baseline and CNO sessions. The peak firing rates of individual fields were highly correlated between the first and second halves of the baseline session for hM3, hM4, and control mice (hM3: $n = 77$, $p = 1.86 \times 10^{-23}$; hM4: $n = 23$, $p = 3.96 \times 10^{-8}$; Con: $n = 37$, $p = 6.05 \times 10^{-13}$; linear correlations). However, the firing rates of individual grid fields before and after CNO injection were not correlated for hM3 mice ($n = 75$, $p = 0.11$, linear correlation, Figure 8B), yet remained strongly correlated for control ($n = 40$, $p = 2.25 \times 10^{-13}$, linear correlation, Figure 8B) and hM4 mice ($n = 28$, $p = 0.01$, linear correlation). We then examined the relationship between grid field firing rates on a cell-by-cell basis. For each grid cell, the variance of the CNO-induced rate changes of individual fields indicates the degree to which the fields change independently. In hM3 mice, grid cells had significantly greater field rate change variability compared to those of control mice (hM3 $n = 16$, Con $n = 8$, $p = 0.02$, one-sided Wilcoxon rank sum test, Figure 8C), which was not the case in hM4 mice (hM4 $n = 6$, Con $n = 8$, rank sum = 46, $p = 0.47$, one-sided Wilcoxon rank sum test).

This striking difference in individual grid field rates in hM3 mice is potentially very significant. If the firing rate relationships of grid fields are stable in a familiar environment, but change under conditions that elicit place cell remapping, then grid cells may provide a contextual signal that triggers remapping. One should therefore be able to decode context by sampling a sufficient number of grid cells. We tested this hypothesis by creating population vectors of all grid cells from hM3 and control mice for three recording epochs: baseline (BL), 30–60 min post-CNO

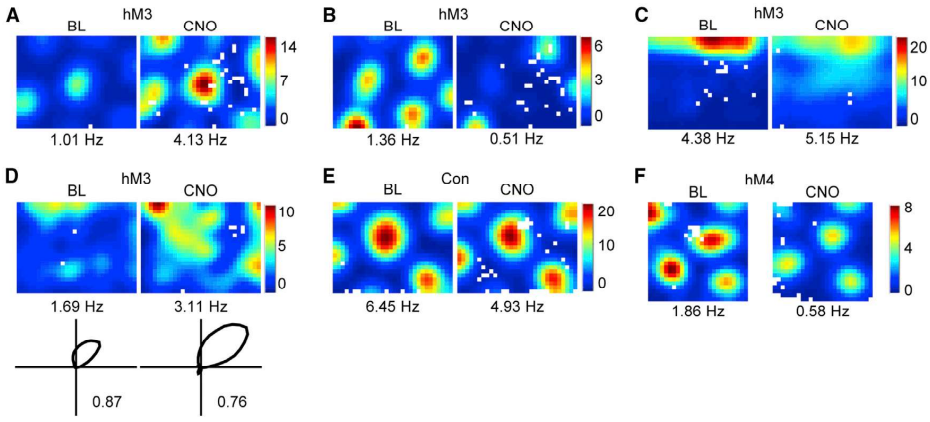

Figure 5. Altered Firing Rate of MEC Neurons following CNO Injection in hM3 and hM4 Mice

(A and B) Rate maps of grid cells in hM3 mice with increased (A) or decreased (B) firing rate and stable grid field locations following CNO injection.

(C) Border cell in an hM3 mouse with increased firing rate and preserved border representation following CNO injection.

(D) Head direction cell in an hM3 mouse with increased firing rate and preserved directional tuning following CNO injection. Mean vector length indicated below polar plots.

(E) Grid cell in a Con mouse that was unaffected by CNO injection.

(F) Grid cell in an hM4 mouse with decreased firing rate and stable grid field locations following CNO injection.

(A–F) Same convention used for Figure 2.

injection (CNO1), and 60–90 min post-CNO injection (CNO2). We reasoned that if grid field firing rates in hM3 mice change after CNO injection and then remain stable, the firing rates during CNO1 should be more similar to CNO2 than to BL. We sampled increasing numbers of grid cells and calculated the proportion of spatial bins for which this is true in hM3 and control mice. A decoding performance of 1 indicates that all CNO1 bins are more similar to CNO2, 0 indicates that all CNO1 bins are more similar to BL, and 0.5 indicates a failure to distinguish between BL and CNO2. Remarkably, we were able to successfully decode context in hM3 mice (Figure 8D), even with a small number of grid cells. However, we were not able to do so in control mice, indicating that simply removing the mouse from the environment to give it an injection is not sufficient to alter grid field firing rates. It is important to note that any changes in the relationship between the firing rates of individual grid fields is in fact a change in the spatial information conveyed by that cell, even without any change in the location of the fields. Thus, if this happens during "natural" remapping as well, grid cells could provide sufficiently distinct spatial input to the hippocampus to cause remapping without shifting relative to each other, consistent with all evidence to date (Fyhn et al., 2007; Barry et al., 2012).

DISCUSSION

We bidirectionally manipulated the excitability of a subset of hippocampal input neurons in MECII while examining the effects locally in MEC, downstream in CA1, and behaviorally in the water maze. We found that MEC neurons responded *quantitatively* to transgenic depolarization or hyperpolarization of MECII neurons by altering their firing rate and field size without changing the spatial location of their firing fields or their directional preferences. Two synapses downstream, however, hippocampal place cells in CA1 exhibited *qualitative* changes in their firing fields (i.e., remapping) in response to transgenic depolarization, but not hyperpolarization, of MECII neurons. The fact that depolarizing MECII neurons had drastically stronger downstream effects than hyperpolarizing the same cell types provides insight into the network mechanisms by which changes in MEC activity lead to remapping. Moreover, only depolarization of MECII caused spatial memory deficits in the water maze, highlighting the link between place cell activity and memory.

Our results are arguably the clearest demonstration to date of how manipulating the activity of MEC neurons produces hippocampal remapping and which changes in these two brain regions are associated with impairments in spatial memory. Lesions of the entorhinal cortex have previously been shown to result in imprecise and unstable place fields (Miller and Best, 1980; Brun et al., 2008; Van Cauter et al., 2008; Hales et al., 2014; Schlesiger et al., 2015), as well as spatial memory impairments on hippocampus-dependent tasks (Parron et al., 2004; Steffenach et al., 2005; Hales et al., 2014). While these studies indicate a clear role for the entorhinal cortex in hippocampal spatial firing and spatial memory, they are limited by their inability to determine precisely how the entorhinal cortex is involved in these functions in the intact brain. Additionally, several recent studies have demonstrated that inactivating MEC to varying degrees leads to hippocampal remapping (Miao et al., 2015; Ormond and McNaughton, 2015; Rueckemann et al., 2016). However, it is difficult to make strong conclusions about the mechanisms underlying remapping without fully understanding the effects of the manipulations in MEC. Moreover, these experiments rely upon

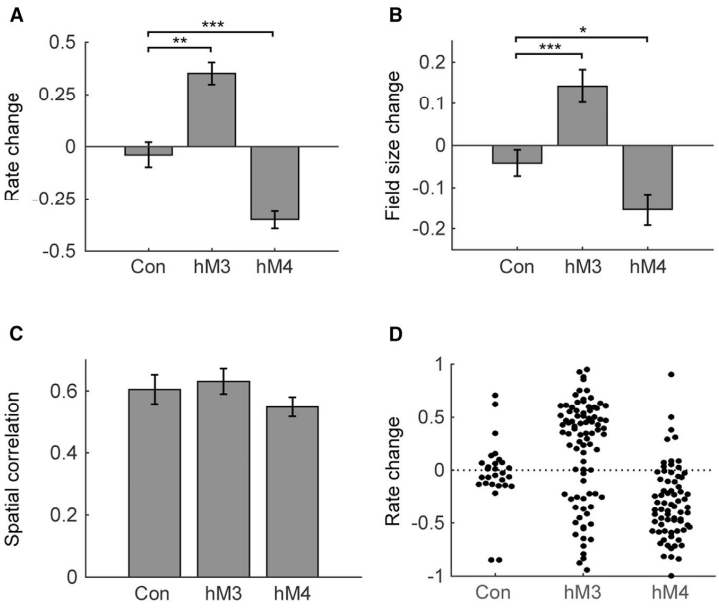

Figure 6. Depolarization and Hyperpolarization of MECII Neurons Produce Changes in Firing Rate and Field Size of Putative Excitatory MEC Neurons without Changing Spatial Location of Firing Fields

(A and B) Change in mean firing rate (A) and field size (B) following CNO injection in Con, hM3, and hM4 mice.

(C) Spatial correlation between baseline and CNO sessions in Con, hM3, and hM4 mice.

(A–C) Data represented as median ± SEM. $^{*}p < 0.05$, $^{**}p < 0.01$, $^{***}p < 0.001$.

(D) Change in mean firing rate for each cell following CNO injection in Con, hM3, and hM4 mice. Note bidirectional rate changes in hM3, but not hM4, mice. Dashed line indicates no rate change.

the diffusion of drugs or virus so the affected cell types cannot be precisely determined, nor do they address the relationship between remapping and spatial memory impairment. Only one study (Zhao et al., 2016) used a transgenic approach analogous to that presented here to hyperpolarize MEC neurons. This manipulation produced hippocampal remapping and disrupted spatial memory performance in the water maze. However, the expression pattern was not restricted to MEC, and most importantly, the authors did not characterize the in vivo responses of MEC neurons during their manipulation. It is unclear why these studies observed remapping after hyperpolarization of MEC, while we found that only depolarization causes remapping. The difference may be due to a combination of which cell types are affected and the strength of the inactivation of those neurons. A strength of our study is that we not only know the extent to which we manipulated a defined subset of stellate cells, but we also show which changes in the MEC network cause remapping and spatial memory impairment, and which changes do not. We clearly demonstrate that only the MECII manipulation that causes hippocampal remapping impairs spatial memory.

Other studies have infused drugs into the medial septum, thereby disrupting cholinergic signaling throughout the brain (Brandon et al., 2011, 2014; Koenig et al., 2011). This manipulation diminishes the spatial periodicity of grid cells and reduces the firing rate of all functional types of MEC neurons (except head direction cells). Nevertheless, place cells remain stable in familiar environments (Koenig et al., 2011), suggesting that intact grid firing patterns are not needed for the existence of place fields. Furthermore, their results demonstrate that decreasing the firing rate of MEC neurons does not necessarily elicit hippocampal remapping, as we observed in hM4 mice. In a subsequent study using a similar manipulation, they found that place cells can still remap in a novel environment (Brandon et al., 2014), indicating that the generation of new place fields also does not require spatially periodic grid cells. An important distinction between the aforementioned studies and our own work is that our manipulations do not degrade the grid pattern or change the location of grid fields. Thus, it may be that when the hippocampus is deprived of its dominant spatial input (through lesions or disruption of grid periodicity), it is capable of generating place fields on its own, as is the case during development. However, the hippocampus is likely sensitive to changes in MEC activity when its spatial inputs remain intact. Indeed, it is difficult to believe that spatial firing fields in the hippocampus do not depend upon their dominant spatial inputs.

Although artificial remapping is inherently distinct from natural remapping since the inputs to entorhinal cortex are unchanged, our results help elucidate which changes in MEC neurons are sufficient to cause remapping. Remarkably, transgenic depolarization of a subset of MECII neurons resulted in remapping without changing the firing locations of MEC neurons. This is in sharp contrast to the coherent shifts and rotations of grid patterns seen in distinct familiar environments (Fyhn et al., 2007). If one assumes a linear summation model of grid-to-place cell activity (Solstad et al., 2006), then this movement of firing fields could change which grid cells are coactive, thus leading to different place fields in the hippocampus. However, grid cells within a module (Stensola et al., 2012) shift and rotate coherently between distinct environments (Fyhn et al., 2007) such that their relationships are preserved. Since this presumably does not cause remapping, it has been proposed that distinct grid modules may shift relative to each other (Monaco and Abbott, 2011), but this remains to be observed experimentally. It has also been shown that grid fields temporarily expand in both size and scale and that the grid pattern becomes less regular upon introduction to a novel environment (Barry et al., 2012). While we did observe an increase in the size of spatial receptive fields in MEC, we found no significant changes in grid scale or

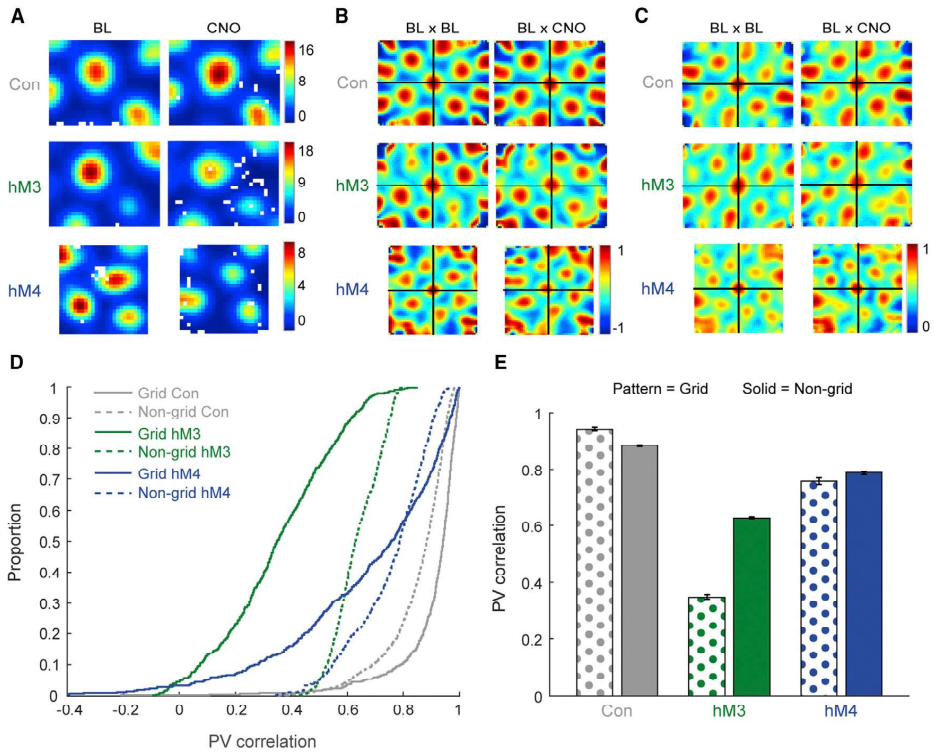

Figure 7. Rate Remapping in Grid Cells following Depolarization of MECII Conveys Spatial Change without a Shift in Grid Field Location

(A) Rate maps before and after CNO injection from Con (top), hM3 (middle), and hM4 (bottom) mice. Same convention used for Figure 2.

(B) Autocorrelograms (BL × BL) and cross-correlograms (BL × CNO) showing stable grid field locations after CNO injection for all example neurons in (A). Red represents maximum correlation and blue represents anti-correlation.

(C) Autocorrelograms (BL × BL) and cross-correlograms (BL × CNO) showing stable grid field locations after CNO injection for an ensemble of grid cells in Con (top, 3 cells), hM3 (middle, 7 cells), and hM4 (bottom, 6 cells) mice. (Note: hM4 grid cells were not simultaneously recorded.) Red represents maximum correlation and blue represents no correlation.

(D) Cumulative distribution functions for population vector (PV) correlations between baseline and CNO sessions in grid and non-grid cells in Con, hM3, and hM4 mice. Solid gray, grid Con; dashed gray, non-grid Con; solid green, grid hM3; dashed green, non-grid hM3; solid blue, grid hM4; dashed blue, non-grid hM4.

(E) Median PV correlations ± SEM between baseline and CNO sessions in grid and non-grid cells in Con, hM3, and hM4 mice. Note that grid cells strongly rate remap compared to non-grid cells in hM3, but not in Con or hM4 mice. Patterned bars, grid cells; solid bars, non-grid cells.

regularity, and it is unclear how an increase in field size alone could lead to remapping in the hippocampus. Transgenic depolarization of MECII also did not produce any significant changes in the firing patterns of border or head direction cells, which maintained their representation of environmental boundaries and directional tuning, respectively. Thus, it is unclear which, if any, of the previously observed changes in MEC are responsible for producing not only artificial remapping, but also natural remapping.

Our most puzzling finding is that both hyperpolarization and depolarization altered the average firing rates of MEC neurons to a similar degree, but only depolarization caused hippocampal remapping. An important difference between these manipulations is that only depolarization led to both increases and decreases in the firing rate of MEC neurons, resulting in greater variability in rate changes relative to the hyperpolarization-induced rate decreases. This paradoxical response to depolarization of MECII stellate cells strongly suggests a shift in the local interneuron network. Several studies have shown that layer II stellate cells are primarily connected via inhibitory interneurons (Dhillon and Jones, 2000; Couey et al., 2013; Pastoll et al., 2013) and that coordinated activity of multiple stellate cells engages this inhibitory network to inhibit other stellate cells (Couey et al., 2013), as we observed here. In contrast, since the basal activity of interneurons is likely not solely sustained by stellate cell activity, hyperpolarizing stellate cells may not be sufficient to disinhibit downstream excitatory neurons. Approximately half of the inhibitory neurons in MEC are parvalbumin-positive (PV+) interneurons (Wouterlood et al., 1995; Miettinen et al., 1996), which are perfectly suited to act as a network switch

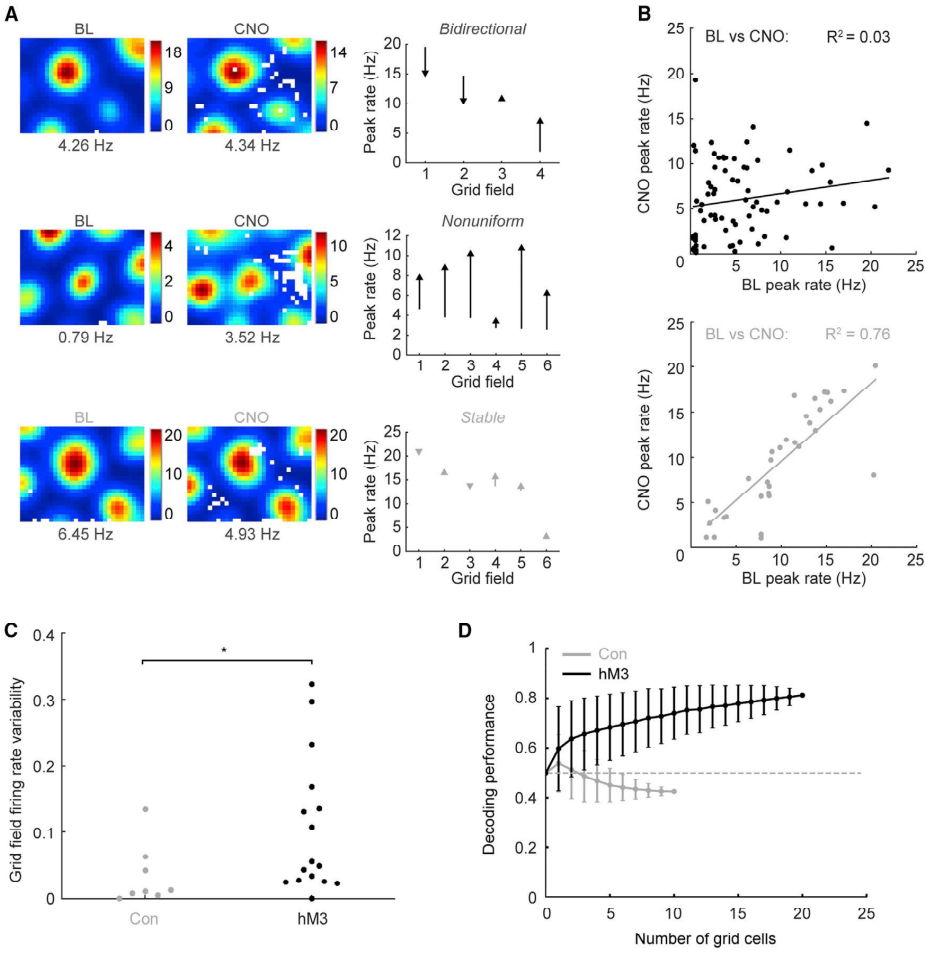

Figure 8. Altered Firing Rate Relationships between Individual Grid Fields Are Observed Only during Artificial Remapping, Potentially Providing a Contextual Signal to the Hippocampus

(A) Rate maps of three representative grid cells before (left) and after (middle) CNO injection. Each row is a cell. Same convention used for Figure 2. Rightmost column shows magnitude and direction of peak firing rate change for each grid field. Each arrow starts at BL rate and ends at CNO rate. Bidirectional (5/17 grid cells, right, top) and nonuniform changes (12/17 grid cells, right, middle) in individual grid field peak firing rates following CNO injection in an hM3 mouse. Stable firing rates (right, bottom) in individual grid fields following CNO injection in a Con mouse.

(B) Peak firing rates of individual grid fields change unpredictably following CNO injection in hM3 mice (top), but remain stable in Con mice (bottom).

(C) CNO-induced rate changes in individual grid fields are significantly more variable within a single grid cell in hM3 (black) versus Con (gray) mice. *$p < 0.05$.

(D) Decoding performance as a function of the number of sampled grid cells for hM3 (black) and Con (gray) mice. Gray dashed line indicates chance decoding performance. Data represented as mean ± standard deviation.

due to their connectivity and intrinsic electrical properties (Ferrante et al., 2016). Compared to other interneurons in MEC, PV+ cells are the most hyperpolarized at rest, but are capable of entering a sustained spiking regime. Furthermore, they inhibit all of the known functional cell types in MEC (Buetfering et al., 2014). Describing stellate cells as communicating via interneurons that act as rectifiers (i.e., they respond more readily to increases in input than to decreases) is therefore a useful simplification in an attempt to understand how MEC may create unique representations for distinct environments by triggering distinct network states. Moreover, computational modeling of cortical neurons as rectifiers has the advantage of easily creating sparse representations in a neural network (Glorot et al., 2011). The question nevertheless remains how this shift in the local network

state translates to changes in spatial firing downstream in the hippocampus.

There is still a large gap in the literature concerning how MEC neurons represent environmental context and how this information influences location selectivity in the hippocampus. One possibility is that the contextual signal in MEC may simply be encoded via population firing rate. In support of this idea, a recent imaging study reported the presence of "context cells" (reelin-positive stellate cells) in MECII, which exhibited significantly different firing rates in distinct environments (Kitamura et al., 2015). We observed cells with significant CNO-induced rate changes compared to controls, but we found a much lower proportion than previously reported (7% versus ~36% by Kitamura et al., 2015). Of course, this could be because we only targeted a subset of stellate cells and thus did not elicit remapping in all place cells. It is unknown whether these proposed context cells are of a particular functional class; however, a more recent electrophysiological study reported that all known functional types in MEC can alter their firing rate in response to changes in visual information (Pérez-Escobar et al., 2016). Indeed, it could be that other functional cell types such as boundary vector cells contribute to remapping (Barry et al., 2006). However, it is difficult to see how the changes that we observed in non-grid cells could result in hippocampal remapping.

Given their prominence in the network and their high spatial selectivity, grid cells are an attractive candidate to signal the need for a distinct place cell code. As mentioned above, it is possible that the contextual signal lies in the changes in the relationships between different grid cell modules (Monaco and Abbott, 2011). From a decoding perspective, grid cells provide highly accurate spatial information, while place cells provide contextual information (Wilson and McNaughton, 1993; Fiete et al., 2008; Sreenivasan and Fiete, 2011; Mathis et al., 2012; Stemmler et al., 2015). Therefore, place cell activity strongly indicates which environment the animal is in, while grid cell activity precisely indicates the animal's location within an environment. Unfortunately, computational models of grid cells are limited by the use of idealistic grid cells with uniform grid fields (Rolls et al., 2006; Solstad et al., 2006; de Almeida et al., 2009; Savelli and Knierim, 2010), even though dominant firing fields are commonly observed experimentally (Ismakov et al., 2015, Soc. Neurosci., abstract). Here, we show that the firing rates of individual grid fields were stable during repeated exposures to a familiar environment but that CNO drastically altered the rates of individual fields in an imbalanced manner *only* in hM3 mice. This observation thus provides a possible mechanism underlying artificial remapping. In fact, this inter-field variability was sufficient to decode whether the network was in a depolarized state with only a few cells, which is analogous to decoding which room the animal is in during natural remapping experiments. It is entirely conceivable that rate changes in grid fields lead to locational changes of hippocampal place fields during natural remapping as well, but it is currently impossible to track the identity of grid fields between environments as they shift and rotate. We propose that this novel mechanism maximizes the contextual information conveyed by grid cells. If it is found that different modules do not shift relative to each other in distinct environments, this would in fact be the only mechanism supported by empirical evidence to explain remapping.

If the spatial changes in MEC underlying remapping are a result of changes in the firing rates of individual grid fields, it raises the question of how this interfield variability arises. Environmental changes have been shown to locally affect properties of the grid pattern (Krupic et al., 2012, 2013, 2015; Stensola et al., 2012). In addition, interneurons have spatially nonuniform firing patterns (Buetfering et al., 2014), suggesting that changes in their activity would differentially affect individual grid fields, consistent with the results presented here. This makes examining the changes in MEC interneuron firing patterns during conditions that elicit hippocampal remapping of particular interest. Taken together, our results mechanistically link changes in grid cell activity to remapping in place cells. Grid cells are in fact able to convey distinct sets of spatial input to the hippocampus without changing their relative position, but only if individual grid fields are considered discrete spatial inputs.

STAR★METHODS

Detailed methods are provided in the online version of this paper and include the following:

- KEY RESOURCES TABLE
- CONTACT FOR REAGENT AND RESOURCE SHARING
- EXPERIMENTAL MODEL AND SUBJECT DETAILS
- METHOD DETAILS
  - Histological Procedures
  - Cell Counting
  - Water Maze
  - Surgical Procedures
  - Electrophysiology Behavioral Protocol
  - Single Unit Recording
  - Unit Isolation and Recording Stability
  - General Electrophysiological Analysis
  - Functional Classification of CA1 Cells
  - Functional Classification of MEC Cells
  - Population Vector Analysis
  - Model of Grid-to-Place Cell Transformation
  - Individual Grid Cell Firing Fields
  - Contextual Discrimination
  - Context-Specific Cells
- QUANTIFICATION AND STATISTICAL ANALYSIS
- DATA AND SOFTWARE AVAILABILITY

SUPPLEMENTAL INFORMATION

Supplemental Information includes five figures and two tables and can be found with this article online at http://dx.doi.org/10.1016/j.neuron.2017.03.001.

AUTHOR CONTRIBUTIONS

Conceptualization, C.G.K.; Methodology, C.G.K.; Software, B.R.K. and B.D.; Formal analysis, B.R.K., C.M.L., and B.D.; Investigation, A.W., D.A., J.D., C.M.L., B.R.K., and N.Z.B.; Writing – Original Draft, B.R.K., C.G.K., and C.M.L.; Writing – Review & Editing, B.R.K., C.M.L., C.G.K., N.Z.B., B.D., D.A., and J.D.; Visualization, B.R.K., C.M.L., B.D., and A.W.; Funding Acquisition, C.G.K.; Resources, C.G.K.; Supervision, C.G.K. and Y.R. (of B.D.).

ACKNOWLEDGMENTS

We thank Y. Yanovich and K. Asumbisa for help with experiments, H. Wu for in situ hybridization, and D.C. Rowland for comments on the manuscript. Supported by NIH Grant R01MH097130-05, Kavli Foundation, the Centre of Excellence scheme of the Research Council of Norway – Centre for Biology of Memory and Centre for Neural Computation, The Egil and Pauline Braathen and Fred Kavli Centre for Cortical Microcircuits, and the National Infrastructure scheme of the Research Council of Norway – NORBRAIN.

Received: September 5, 2016
Revised: December 30, 2016
Accepted: February 28, 2017
Published: March 22, 2017

REFERENCES

Alexander, G.M., Rogan, S.C., Abbas, A.I., Armbruster, B.N., Pei, Y., Allen, J.A., Nonneman, R.J., Hartmann, J., Moy, S.S., Nicolelis, M.A., et al. (2009). Remote control of neuronal activity in transgenic mice expressing evolved G protein-coupled receptors. Neuron *63*, 27–39.

Barry, C., Lever, C., Hayman, R., Hartley, T., Burton, S., O'Keefe, J., Jeffery, K., and Burgess, N. (2006). The boundary vector cell model of place cell firing and spatial memory. Rev. Neurosci. *17*, 71–97.

Barry, C., Ginzberg, L.L., O'Keefe, J., and Burgess, N. (2012). Grid cell firing patterns signal environmental novelty by expansion. Proc. Natl. Acad. Sci. USA *109*, 17687–17692.

Bjerknes, T.L., Moser, E.I., and Moser, M.B. (2014). Representation of geometric borders in the developing rat. Neuron *82*, 71–78.

Brandon, M.P., Bogaard, A.R., Libby, C.P., Connerney, M.A., Gupta, K., and Hasselmo, M.E. (2011). Reduction of theta rhythm dissociates grid cell spatial periodicity from directional tuning. Science *332*, 595–599.

Brandon, M.P., Koenig, J., Leutgeb, J.K., and Leutgeb, S. (2014). New and distinct hippocampal place codes are generated in a new environment during septal inactivation. Neuron *82*, 789–796.

Brun, V.H., Leutgeb, S., Wu, H.Q., Schwarcz, R., Witter, M.P., Moser, E.I., and Moser, M.B. (2008). Impaired spatial representation in CA1 after lesion of direct input from entorhinal cortex. Neuron *57*, 290–302.

Buetfering, C., Allen, K., and Monyer, H. (2014). Parvalbumin interneurons provide grid cell-driven recurrent inhibition in the medial entorhinal cortex. Nat. Neurosci. *17*, 710–718.

Couey, J.J., Witoelar, A., Zhang, S.J., Zheng, K., Ye, J., Dunn, B., Czajkowski, R., Moser, M.B., Moser, E.I., Roudi, Y., and Witter, M.P. (2013). Recurrent inhibitory circuitry as a mechanism for grid formation. Nat. Neurosci. *16*, 318–324.

de Almeida, L., Idiart, M., and Lisman, J.E. (2009). The input-output transformation of the hippocampal granule cells: from grid cells to place fields. J. Neurosci. *29*, 7504–7512.

Dhillon, A., and Jones, R.S. (2000). Laminar differences in recurrent excitatory transmission in the rat entorhinal cortex in vitro. Neuroscience *99*, 413–422.

Ferrante, M., Tahvildari, B., Duque, A., Hadzipasic, M., Salkoff, D., Zagha, E.W., Hasselmo, M.E., and McCormick, D.A. (2016). Distinct functional groups emerge from the intrinsic properties of molecularly identified entorhinal interneurons and principal cells. Cereb. Cortex. Published online June 6, 2016. http://dx.doi.org/10.1093/cercor/bhw143.

Fiete, I.R., Burak, Y., and Brookings, T. (2008). What grid cells convey about rat location. J. Neurosci. *28*, 6858–6871.

Fyhn, M., Molden, S., Witter, M.P., Moser, E.I., and Moser, M.B. (2004). Spatial representation in the entorhinal cortex. Science *305*, 1258–1264.

Fyhn, M., Hafting, T., Treves, A., Moser, M.B., and Moser, E.I. (2007). Hippocampal remapping and grid realignment in entorhinal cortex. Nature *446*, 190–194.

Gatome, C.W., Slomianka, L., Lipp, H.P., and Amrein, I. (2010). Number estimates of neuronal phenotypes in layer II of the medial entorhinal cortex of rat and mouse. Neuroscience *170*, 156–165.

Glorot, X., Bordes, A., and Bengio, Y. (2011). Deep sparse rectifier neural networks. J. Mach. Learn. Res. *15*, 315–323.

Gray, C.M., Maldonado, P.E., Wilson, M., and McNaughton, B. (1995). Tetrodes markedly improve the reliability and yield of multiple single-unit isolation from multi-unit recordings in cat striate cortex. J. Neurosci. Methods *63*, 43–54.

Hafting, T., Fyhn, M., Molden, S., Moser, M.B., and Moser, E.I. (2005). Microstructure of a spatial map in the entorhinal cortex. Nature *436*, 801–806.

Hales, J.B., Schlesiger, M.I., Leutgeb, J.K., Squire, L.R., Leutgeb, S., and Clark, R.E. (2014). Medial entorhinal cortex lesions only partially disrupt hippocampal place cells and hippocampus-dependent place memory. Cell Rep. *9*, 893–901.

Kentros, C.G., Agnihotri, N.T., Streater, S., Hawkins, R.D., and Kandel, E.R. (2004). Increased attention to spatial context increases both place field stability and spatial memory. Neuron *42*, 283–295.

Kitamura, T., Sun, C., Martin, J., Kitch, L.J., Schnitzer, M.J., and Tonegawa, S. (2015). Entorhinal cortical ocean cells encode specific contexts and drive context-specific fear memory. Neuron *87*, 1317–1331.

Koenig, J., Linder, A.N., Leutgeb, J.K., and Leutgeb, S. (2011). The spatial periodicity of grid cells is not sustained during reduced theta oscillations. Science *332*, 592–595.

Köhler, C. (1985). Intrinsic projections of the retrohippocampal region in the rat brain. I. The subicular complex. J. Comp. Neurol. *236*, 504–522.

Kropff, E., Carmichael, J.E., Moser, M.B., and Moser, E.I. (2015). Speed cells in the medial entorhinal cortex. Nature *523*, 419–424.

Krupic, J., Burgess, N., and O'Keefe, J. (2012). Neural representations of location composed of spatially periodic bands. Science *337*, 853–857.

Krupic, J., Bauza, M., Burton, S., Lever, C., and O'Keefe, J. (2013). How environment geometry affects grid cell symmetry and what we can learn from it. Philos. Trans. R. Soc. Lond. B Biol. Sci. *369*, 20130188.

Krupic, J., Bauza, M., Burton, S., Barry, C., and O'Keefe, J. (2015). Grid cell symmetry is shaped by environmental geometry. Nature *518*, 232–235.

Langston, R.F., Ainge, J.A., Couey, J.J., Canto, C.B., Bjerknes, T.L., Witter, M.P., Moser, E.I., and Moser, M.B. (2010). Development of the spatial representation system in the rat. Science *328*, 1576–1580.

Leutgeb, S., Leutgeb, J.K., Barnes, C.A., Moser, E.I., McNaughton, B.L., and Moser, M.B. (2005). Independent codes for spatial and episodic memory in hippocampal neuronal ensembles. Science *309*, 619–623.

Lykken, C., and Kentros, C.G. (2014). Beyond the bolus: transgenic tools for investigating the neurophysiology of learning and memory. Learn. Mem. *21*, 506–518.

Mathis, A., Herz, A.V., and Stemmler, M. (2012). Optimal population codes for space: grid cells outperform place cells. Neural Comput. *24*, 2280–2317.

Miao, C., Cao, Q., Ito, H.T., Yamahachi, H., Witter, M.P., Moser, M.B., and Moser, E.I. (2015). Hippocampal remapping after partial inactivation of the medial entorhinal cortex. Neuron *88*, 590–603.

Miettinen, M., Koivisto, E., Riekkinen, P., and Miettinen, R. (1996). Coexistence of parvalbumin and GABA in nonpyramidal neurons of the rat entorhinal cortex. Brain Res. *706*, 113–122.

Miller, V.M., and Best, P.J. (1980). Spatial correlates of hippocampal unit activity are altered by lesions of the fornix and endorhinal cortex. Brain Res. *194*, 311–323.

Monaco, J.D., and Abbott, L.F. (2011). Modular realignment of entorhinal grid cell activity as a basis for hippocampal remapping. J. Neurosci. *31*, 9414–9425.

Muller, R.U., and Kubie, J.L. (1987). The effects of changes in the environment on the spatial firing of hippocampal complex-spike cells. J. Neurosci. *7*, 1951–1968.

Muller, R.U., and Kubie, J.L. (1989). The firing of hippocampal place cells predicts the future position of freely moving rats. J. Neurosci. *9*, 4101–4110.

O'Keefe, J., and Dostrovsky, J. (1971). The hippocampus as a spatial map. Preliminary evidence from unit activity in the freely-moving rat. Brain Res. *34*, 171–175.

Ormond, J., and McNaughton, B.L. (2015). Place field expansion after focal MEC inactivations is consistent with loss of Fourier components and path integrator gain reduction. Proc. Natl. Acad. Sci. USA *112*, 4116–4121.

Parron, C., Poucet, B., and Save, E. (2004). Entorhinal cortex lesions impair the use of distal but not proximal landmarks during place navigation in the rat. Behav. Brain Res. *154*, 345–352.

Pastoll, H., Solanka, L., van Rossum, M.C., and Nolan, M.F. (2013). Feedback inhibition enables θ-nested γ oscillations and grid firing fields. Neuron *77*, 141–154.

Pérez-Escobar, J.A., Kornienko, O., Latuske, P., Kohler, L., and Allen, K. (2016). Visual landmarks sharpen grid cell metric and confer context specificity to neurons of the medial entorhinal cortex. eLife *5*, 5.

Rolls, E.T., Stringer, S.M., and Elliot, T. (2006). Entorhinal cortex grid cells can map to hippocampal place cells by competitive learning. Network *17*, 447–465.

Rowland, D.C., Weible, A.P., Wickersham, I.R., Wu, H., Mayford, M., Witter, M.P., and Kentros, C.G. (2013). Transgenically targeted rabies virus demonstrates a major monosynaptic projection from hippocampal area CA2 to medial entorhinal layer II neurons. J. Neurosci. *33*, 14889–14898.

Rueckemann, J.W., DiMauro, A.J., Rangel, L.M., Han, X., Boyden, E.S., and Eichenbaum, H. (2016). Transient optogenetic inactivation of the medial entorhinal cortex biases the active population of hippocampal neurons. Hippocampus *26*, 246–260.

Sargolini, F., Fyhn, M., Hafting, T., McNaughton, B.L., Witter, M.P., Moser, M.B., and Moser, E.I. (2006). Conjunctive representation of position, direction, and velocity in entorhinal cortex. Science *312*, 758–762.

Savelli, F., and Knierim, J.J. (2010). Hebbian analysis of the transformation of medial entorhinal grid-cell inputs to hippocampal place fields. J. Neurophysiol. *103*, 3167–3183.

Schlesiger, M.I., Cannova, C.C., Boublil, B.L., Hales, J.B., Mankin, E.A., Brandon, M.P., Leutgeb, J.K., Leibold, C., and Leutgeb, S. (2015). The medial entorhinal cortex is necessary for temporal organization of hippocampal neuronal activity. Nat. Neurosci. *18*, 1123–1132.

Skaggs, W.E., McNaughton, B.L., Wilson, M.A., and Barnes, C.A. (1996). Theta phase precession in hippocampal neuronal populations and the compression of temporal sequences. Hippocampus *6*, 149–172.

Solstad, T., Moser, E.I., and Einevoll, G.T. (2006). From grid cells to place cells: a mathematical model. Hippocampus *16*, 1026–1031.

Sreenivasan, S., and Fiete, I. (2011). Grid cells generate an analog error-correcting code for singularly precise neural computation. Nat. Neurosci. *14*, 1330–1337.

Steffenach, H.A., Witter, M., Moser, M.B., and Moser, E.I. (2005). Spatial memory in the rat requires the dorsolateral band of the entorhinal cortex. Neuron *45*, 301–313.

Stemmler, M., Mathis, A., and Herz, A.V. (2015). Connecting multiple spatial scales to decode the population activity of grid cells. Sci. Adv. *1*, e1500816.

Stensola, H., Stensola, T., Solstad, T., Frøland, K., Moser, M.B., and Moser, E.I. (2012). The entorhinal grid map is discretized. Nature *492*, 72–78.

Taube, J.S., Muller, R.U., and Ranck, J.B., Jr. (1990). Head-direction cells recorded from the postsubiculum in freely moving rats. II. Effects of environmental manipulations. J. Neurosci. *10*, 436–447.

Van Cauter, T., Poucet, B., and Save, E. (2008). Unstable CA1 place cell representation in rats with entorhinal cortex lesions. Eur. J. Neurosci. *27*, 1933–1946.

Vorhees, C.V., and Williams, M.T. (2006). Morris water maze: procedures for assessing spatial and related forms of learning and memory. Nat. Protoc. *1*, 848–858.

Wills, T.J., Cacucci, F., Burgess, N., and O'Keefe, J. (2010). Development of the hippocampal cognitive map in preweanling rats. Science *328*, 1573–1576.

Wilson, M.A., and McNaughton, B.L. (1993). Dynamics of the hippocampal ensemble code for space. Science *261*, 1055–1058.

Wouterlood, F.G., Härtig, W., Brückner, G., and Witter, M.P. (1995). Parvalbumin-immunoreactive neurons in the entorhinal cortex of the rat: localization, morphology, connectivity and ultrastructure. J. Neurocytol. *24*, 135–153.

Yasuda, M., and Mayford, M.R. (2006). CaMKII activation in the entorhinal cortex disrupts previously encoded spatial memory. Neuron *50*, 309–318.

Yetman, M.J., Lillehaug, S., Bjaalie, J.G., Leergaard, T.B., and Jankowsky, J.L. (2016). Transgene expression in the Nop-tTA driver line is not inherently restricted to the entorhinal cortex. Brain Struct. Funct. *221*, 2231–2249.

Zhang, S.J., Ye, J., Miao, C., Tsao, A., Cerniauskas, I., Ledergerber, D., Moser, M.B., and Moser, E.I. (2013). Optogenetic dissection of entorhinal-hippocampal functional connectivity. Science *340*, 1232627.

Zhao, R., Grunke, S.D., Keralapurath, M.M., Yetman, M.J., Lam, A., Lee, T.C., Sousounis, K., Jiang, Y., Swing, D.A., Tessarollo, L., et al. (2016). Impaired recall of positional memory following chemogenetic disruption of place field stability. Cell Rep. *16*, 793–804.

STAR★METHODS

KEY RESOURCES TABLE

REAGENT or RESOURCE	SOURCE	IDENTIFIER
Antibodies		
Rabbit anti-HA	Rockland	Code: 600-401-384; RRID: AB_217929
Fluor 488 Goat anti-rabbit IgG	Thermo Fisher Scientific	SKU: A-11008; RRID: AB_143165
Chemicals, Peptides, and Recombinant Proteins		
Clozapine N-oxide	Sigma-Aldrich	SKU: C0832; CAS Number: 34233-97-7; MDL Number: MFCD00210190; PubChem Substance ID: 24892276
Experimental Models: Organisms/Strains		
Mouse: C57BL/6J	The Jackson Laboratory	Stock: 000644; RRID: IMSR_JAX:000664
Mouse: B6.Cg-Tg(Klk8-tTA)SMmay/MullMmmh	Mutant Mouse Resource & Research Centers	Stock: 031779-MU; RRID: MMRRC_031779-MU
Mouse: Tg(tetO-CHRM3*)1Blr/J	The Jackson Laboratory	Stock: 014093; RRID: IMSR_JAX:014093
Mouse: Tg(tetO-CHRM4*)2Blr/J	The Jackson Laboratory	Stock: 024114; RRID: IMSR_JAX:024114
Software and Algorithms		
MetaMorph Premier	Molecular Devices	https://www.moleculardevices.com/systems/metamorph-research-imaging/metamorph-microscopy-automation-and-image-analysis-software
Photoshop CS4	Adobe Systems	http://www.adobe.com/products/photoshop.html
Image Pro Plus	Media Cybernetics	http://www.mediacy.com/imageproplus
AnyMaze	Stoelting	http://www.stoeltingco.com/anymaze.html
Cheetah	Neuralynx	http://neuralynx.com/research_software/cheetah
MATLAB	MathWorks	https://se.mathworks.com/products/matlab.html
MClust	Redish et al.	http://redishlab.neuroscience.umn.edu/MClust/MClust.html
Python	Python	https://www.python.org/

CONTACT FOR REAGENT AND RESOURCE SHARING

Further information and requests for resources and reagents should be directed to and will be fulfilled by the Lead Contact Dr. Clifford Kentros (clifford.kentros@ntnu.no).

EXPERIMENTAL MODEL AND SUBJECT DETAILS

Our subjects were adult (2 - 6 months, 17 – 37 g) male and female mice. We crossed the EC-tTA line (Mutant Mouse Resource & Research Centers, Stock: 031779-MU; RRID: MMRRC_031779-MU) to hM3Dq- and hM4Di-tetO lines (Jackson Laboratory, Stock: 014093 & 024114; RRID: IMSR_JAX:014093 & RRID: IMSR_JAX:024114) to enable control of neurons in the superficial layers of medial entorhinal cortex. Pups were evaluated for transgenic expression via PCR of genomic DNA isolated from tail biopsies. We also used C57BL/6J (Jackson Laboratory, Stock: 000644; RRID: IMSR_JAX:000664) mice as an additional control group. Mice were kept on a 12-hr light/dark schedule and were fed ad libitum. They were housed in environmentally-enriched transparent Plexiglas cages in a humidity- and temperature-controlled environment. Mice were group-housed prior to surgery or water maze testing and then housed separately. Mice were experimentally-naive before surgery or water maze testing, and were randomly assigned to experimental groups when applicable. All procedures were approved by the Institutional Animal Care and Use Committee at the University of Oregon and the National Animal Research Authorities of Norway. They were performed according to the Norwegian Animal Welfare Act and the European Convention for the Protection of Vertebrate Animals used for Experimental and Other Scientific Purposes.

METHOD DETAILS

Histological Procedures

For HA-antibody labeling, air-dried slides were first washed in 1X phosphate-buffered saline (PBS) (3 × 10 min). Sections were then blocked with 5% NDS (normal donkey serum) in PBT (0.3% Triton in 1X PBS). Slides were placed on a flat staining rack and covered with 0.3 mL blocking solution for 20 min at room temperature. We prepared the primary antibody (rabbit anti-HA; Rockland, Code: 600-401-384; RRID: AB_217929; 1:500 dilution) in a solution of 5% NDS in PBT supplemented with 0.1% NaN3 for extended stabilization. Each section was bathed with 250 μl of the antibody solution, and the slide covered with Parafilm^{TM} and stored overnight at 4°C. We prepared the secondary antibody (Fluor 488 Goat anti-rabbit IgG; Thermo Fisher Scientific, SKU: A-11008; RRID: AB_143165) in PBT. The day following primary antibody processing, sections were washed in PBT (4 × 10 min). Each section was bathed with 250 μl of the secondary solution, covered in Parafilm, wrapped in foil and stored overnight at 4°C. A final wash was then performed with PBT (4 × 10 min) and then 1X PBS (5 min). Slides were then coverslipped and stored at 4°C.

When electrophysiological recordings were complete, mice were anaesthetized with isoflurane and each tetrode was electrolytically lesioned (5 V, 500 ms) for identification. After 24-48 hr, mice were administered a lethal dose of pentobarbital sodium (Euthasol, 50mg/kg) and perfused transcardially with 4% paraformaldehyde in phosphate-buffered saline (PBS). Brains were removed and post-fixed in paraformaldehyde overnight, then transferred to a 30% sucrose solution. Brains were sectioned (30 μm) in the sagittal plane and mounted on glass microscope slides. Slides were air-dried overnight and then processed or stored at −80°C. For identification of recording sites, the tissue was stained with either Cresyl violet or VECTASHIELD Antifade Mounting Medium with DAPI (Vector Laboratories, Inc., Burlingame, CA). The slides were then coverslipped and examined under the microscope. Recording sites were marked on copies of the Paxinos and Franklin atlas (2008) and slides were stored at room temperature.

Cell Counting

Tissue was analyzed from nine mice, counting cells from each region in as many different sections as possible, which ranged from one to three sections. Scans of histochemical RNA in situ and fluorescent Nissls were acquired at 10X magnification and stitched together in MetaMorph Premier (Molecular Devices, CA) using the following equipment: Olympus BX61 microscope, DP72 camera, BX-UCB control box, Prior ProScanIII motorized stage, and Lumen200Pro light source. The scanned files were then saved as jpegs. In situ and Nissl images were analyzed separately to obtain the number of transgenic neurons in each structure and the total number of cells in each structure, respectively. Anatomical regions were delineated using the Paxinos and Franklin sagittal atlas (2008) as a reference, with known anatomical landmarks such as lamina dissecans used to determine the local extent and layers of MEC. The total number of cells in each structure was estimated in Photoshop CS4 (Adobe Systems, CA) using a hole punch technique. A circular outline of fixed area was placed in a region of each structure that was most representative of its overall cell density. All nuclei within this hole punch region were counted. To obtain the total number of cells in each structure, the area of the hole punch was determined by calculating the number of pixels inside the hole punch. The same strategy was used to determine the area of each structure. The area of each structure was then divided by the area of the hole punch and the resulting number was multiplied by the number of cells in that structure. These estimates were then used to obtain the percent of total cells (i.e., nuclei) in each structure that were transgenic.

Water Maze

51 experimentally-naive, unimplanted mice (13 hM3+, 9 hM3-, 13 hM4+, 16 hM4-) were housed in littermate pairs for the duration of water maze training. The control group included single and double negative littermates. All training and tests were performed during the light cycle in a 104 cm diameter pool maintained at 28°C. The water was made opaque with white Tempera paint (Beaverton, OR). We employed a behavioral protocol adapted from Voorhees and colleagues (Vorhees and Williams, 2006). Mice were given one training session consisting of four trials per day for a total of eight days, followed by two days of single probe tests. Each trial was 60 s in duration, or until the mouse remained on the platform for 15 s. Mice that climbed onto the platform but jumped off before 15 s elapsed were guided back to the platform. The inter-trial interval was approximately 120 s. For each trial, the mouse started from a pseudorandom start location, selected from the eight cardinal and intercardinal positions relative to the platform, excluding the location of the platform and those immediately adjacent (i.e., if the platform was at location N, the mouse could start from W, SW, S, SE, or E, but not NW, N, or NE). No start position was used more than once during a single session. During the first two days of training (Days 1 & 2), a wire mesh cup was set atop the 10 × 10 cm platform submerged 1 cm beneath the surface. These visually cued trials were performed to test the mouse's ability to swim to a visible goal. Day 3 was the first of six daily submerged platform spatial acquisition sessions (Days 3-8). Acquisition of the task relied on the use of distal cues beyond the walls of the pool. On Days 9 and 10, mice were given a single probe test during which the platform was absent. On each day, each mouse was placed in the pool at the same pseudorandomly selected start position for that day (following the same rules above), allowed to swim for 60 s, and was then removed. Start positions were not the same on Days 9 and 10. 30 min prior to the first probe trial (Day 9), all mice were injected with CNO as described below. 30 min prior to the second probe trial (Day 10), all mice were injected with saline. All sessions were recorded with a Sony Handycam DCR-HC42 extended on a boom directly over the pool. Swimming behavior was tracked automatically using either Image Pro Plus (Bethesda, MD) or AnyMaze (Stoelting Co, Kiel, WI). The target location was defined as a region with a radius 6 cm from the center of the platform location. Test results were exported to MATLAB for statistical testing and visualization.

Surgical Procedures

All surgeries were performed using aseptic techniques on experimentally-naive mice. Prior to surgical implantation of the microdrives, ketamine (100 mg/kg) was administered as a preanesthetic. Dexamethasone (0.1 mg/kg) and atropine (0.03 mg/kg) were also administered presurgically to ameliorate possible inflammation and respiratory irregularities, respectively. Surgical anesthesia was maintained with isoflurane (1.25%–2.0%, adjusted as necessary for appropriate depth of anesthesia). Eyes were moistened with antibacterial ophthalmic ointment. Mice were placed in a stereotaxic frame and held in position with atraumatic ear bars. The skull was exposed and lambda and bregma were zeroed in the vertical plane. The surface of the skull was cleaned with hydrogen peroxide, lightly scored with a dental pick, and coated with a thin layer of cyanoacrylate glue that was allowed to dry completely before proceeding. For recordings from CA1, one craniotomy was drilled in the left hemisphere overlying the dorsal hippocampus (centered at AP: −1.8 mm; ML: 1.2 mm relative to bregma). For recordings from medial entorhinal cortex (MEC), one craniotomy was drilled in the left hemisphere, exposing the transverse sinus 3.2 mm lateral to the midline. Four additional holes were drilled around the perimeter of the skull for stainless steel anchor screws (00–90 × 1/8") and ground wires from the recording array. The tetrodes of the array were lowered into the cortex overlying the hippocampus or MEC to a depth of approximately 0.8 mm. In MEC, the tetrode array was implanted 300-500 μm anterior of the transverse sinus at a 3 - 6 degree angle aimed posteriorly. Grip Cement (Dentsply, Milford, DE) was applied to secure the array to the skull. After the implant was in place, sterile Vaseline was applied to isolate the tetrodes from the cement, preserving the ability to adjust tetrode depth. Mice were subcutaneously administered buprenorphine (0.06 mg/kg) postoperatively for analgesia to minimize discomfort.

Electrophysiology Behavioral Protocol

All implanted mice were allowed to recover from surgery for seven days, after which screening for units began. A tethered HS-16 or HS-18MM operational amplifier (Neuralynx, Bozeman, MT) was plugged into the tetrode recording array to monitor/record behavior and neuronal activity. Recording sessions occurred based on the presence of neural activity, regardless of the light/dark cycle. All MEC screening and recording sessions were performed in a cue-rich room in either a 90 × 120 cm rectangular environment or a 100 × 100 cm square environment. Each mouse experienced only one environment. All hippocampal screening and recording sessions were performed in a 60 cm diameter cylinder with dominant visual cues. During initial screening sessions, the array was moved down 45-90 μm per day, and an audio channel was monitored for evidence of theta rhythmicity and/or the occurrence of sharp waves. Recordings of MEC activity were initiated when cells with clear spatial or head direction correlates were first observed. Recordings of hippocampal activity were initiated when spiking activity with clear spatial correlates was first observed. Baseline activity was recorded for 30 min. Mice were then removed from the cylinder and given an intraperitoneal injection of either clozapine N-oxide (CNO, Sigma-Aldrich, St. Louis, Missouri, USA) (hM3: 1 mg/kg, 0.1 mg/ml in 10% DMSO/saline solution; hM4: 10 mg/kg, 1.0 mg/ml in 10% DMSO/saline solution) or saline. Immediately following the injection, mice were placed back into the environment and data were recorded for an additional 120 min. Mice were then removed from the environment, placed in their home cages, and returned to the colony room. When recording from the hippocampus, mice were returned to the cylinder for a second 30 min baseline session after a 12-24 hr delay. Experiments were repeated for each mouse as long as activity was present. The hippocampal and MEC control groups include hM3 and hM4 mice injected with saline, and littermate controls injected with either CNO or saline. The MEC control group also includes C57BL/6J mice injected with CNO when the data from this group was indistinguishable from that of the controls (two-sample Kolmorogov-Smirnov test, $p > 0.05$).

Single Unit Recording

Tetrodes were made by spinning together four lengths of 18-micron-diameter 10% iridium/platinum wire (California Fine Wire, Grover Beach, CA) and applying heat to fuse the polyamide coating at one end. The majority of experiments used custom-made four-tetrode recording arrays adapted from methods described by Gray et al. (1995). The coating on the free ends of each wire was removed and each uncoated wire segment was inserted into a channel of an EIB-16 electrode interface board (Neuralynx) and fixed in place with a gold-coated pin. Each EIB-16 loaded with four tetrodes was fixed to a Teflon stage mounted on three drive screws. The drive screws (0–80 × 3/8") allowed depth adjustments of the entire array and served as a structural link to the skull. The remaining experiments used VersaDrive-4 microdrives (Neuralynx), where the tetrodes could each be lowered independently. Neuronal data were acquired using the Cheetah-16 system (Neuralynx). Recorded signals were amplified automatically for each tetrode when the experimenter selected an appropriate input range (typically ± 250-800 μV). The signals were band-pass filtered (spikes: 600 – 6000 Hz; local field potential: 0.1 – 475 Hz) and stored using Neuralynx data-acquisition software. Thresholds were set such that only waveforms of a specified minimum voltage (e.g., 50 μV) were stored. A digital camera mounted above the recording environment and linked to the Cheetah-16 system recorded the position of the mouse by tracking two light-emitting diodes fixed to the headstage and aligned with the body axis of the mouse.

Unit Isolation and Recording Stability

Unit isolation and assessment of recording stability was performed on a total of five distinct 30 min epochs for MEC recordings, including the baseline session (BL) and the 2 hr post-injection session, which was divided into four 30 min epochs for analysis purposes. For CA1 recordings, a final 30 min session a minimum of 12 hr after injection (12+ hr) was included as well. Units were manually separated offline with MClust spike-sorting software (courtesy of David Redish, University of Minnesota) for MATLAB (MathWorks,

Natick, MA) using the strict standards for unit isolation described previously by Kentros et al. (2004), and cluster boundaries were applied across successive sessions to track clusters over time. Isolated clusters corresponding to putative pyramidal neurons formed clear Gaussian ellipses generally based upon peak-to-peak projections of different tetrode wires with minimal overlap with neighboring clusters or noise. These clusters were divided into one of three groups according to a subjective judgment of quality (Q). Q-1 clusters had virtually no overlap on at least one projection and no events within a 2 ms refractory period; Q-2 clusters included clear Gaussians with a small degree of overlap with other clusters or noise; Q-3 cells met neither criteria; Q-off cells did not have enough spikes to judge the quality. Neurons categorized as Q-3 were not included for any analyses. Putative interneurons with generally spherical clusters were assigned Q-values exclusively by cluster boundary criteria. Cluster boundaries were then applied across successive epochs and minor adjustments were made when necessary to optimally separate clusters from each other and from noise. Inspection of spike waveforms, inter-spike intervals, autocorrelations, and cross-correlations were used as additional methods to ensure each cluster was correctly tracked over time. In two-session comparisons (i.e., spatial correlations), it was required that clusters in both sessions passed criteria to be included. In CA1, we recorded 810 cells from 23 mice (7 hM3+, 4 hM3-, 11 hM4+, 1 hM4-). 672 of those cells (83%) met our standards of cluster quality. In MEC, we recorded 383 cells from 17 mice (7 hM3+, 1 hM3-, 5 hM4+, 4 C57BL/6J). 297 of those cells (76%) met our standards of cluster quality.

General Electrophysiological Analysis

Unless otherwise indicated, only the 30-60 min epoch of the 2 hr post-injection recording session was included in the analysis. This epoch was chosen because it captures the peak activity of CNO. The first 30 min included considerable time when CNO was not active, and the last hour was redundant as firing properties did not continue to significantly change after 60 min (Figure S4). Furthermore, it allowed for the comparison of sessions that are equal in length which is more statistically appropriate.

In order to exclude spiking activity occurring during periods of immobility, a walk filter ($\geq$2 cm/s) was applied. Rate maps were then generated by binning the location of each spike (CA1: 2 × 2 cm bins; MEC: 4 × 4 cm bins) for each 30 min epoch, dividing the number of spikes in each bin by the time spent in that bin, and smoothing with a Gaussian. Mean firing rate was defined as the total number of spikes divided by the duration of the recording session. Peak firing rate was defined as the maximal firing rate of all spatial bins. To assess spatial correlation, pairs of rate maps were each reshaped into a single vector and the correlation coefficient (Pearson's linear correlation) between these vectors was calculated. Pixels of incongruity between the two vectors, resulting from unvisited pixels in either epoch, were excluded from the calculation. Example rate maps from hM4 mice in Figures 5F and 7A–7C are displayed using 30-120 min post-CNO injection due to partial coverage during the 30-60 min epoch.

Difference scores were calculated as: (session 2 value – session 1 value) / (session 2 value + session 1 value), i.e., normalized change. These scores are reported in Figures 3A, 3B, 6A, 6B, 6D, 8C, and S5D, as well as in Tables S1 and S2.

Functional Classification of CA1 Cells

For the functional classification of cells, chance levels were estimated using a shuffling procedure. For each cell, its spikes were circularly shifted in time relative to the mouse's position by a random amount between 20 s and 20 s less than the total length of the recording session. The measure of interest was calculated using these shuffled spike times, and this procedure was repeated 500 times for that cell. A distribution of values was generated including the 500 shuffled results from all cells, and the 95th percentile was calculated. Cells were required to meet all defined criteria in either the baseline or the CNO session to be included.

Place cells were defined as putative excitatory neurons (mean firing rate $\leq$ 7 Hz) with good spatial stability in the baseline session (spatial correlation between first and second halves > 0.5), a mean rate $\geq$ 0.1 Hz, and at least one identified place field. Place fields were defined as areas with at least 20 contiguous pixels (80 cm^2) where the firing rate exceeded 20% of the peak rate. Place fields with peak rates lower than 1 Hz were ignored. In-field firing rate was defined as the mean firing rate within the largest place field. Coherence was calculated as the correlation between firing rate in a given spatial bin with the firing rate in its 8 neighboring spatial bins (Muller and Kubie, 1989). Spatial information content was calculated as:

$$\text{information content} = \sum_i p_i \frac{\lambda_i}{\lambda} \log_2 \frac{\lambda_i}{\lambda}$$

where p_i is the probability of the mouse being in the i-th bin (occupancy / total time), λ is the overall mean firing rate, and λ_i is the mean firing rate in the i-th bin (Skaggs et al., 1996).

A place cell was classified as turning on if mean rate > 0.1 Hz and a place field was detected in the CNO session, but mean rate < 0.1 Hz in the baseline session. The converse criteria were used to classify a place cell as turning off. For all other classifications, place cells were required to meet all criteria described in the preceding paragraph in both the baseline and CNO sessions. We evaluated changes in spatial correlation using a shuffling procedure where each cell's baseline rate map was compared to the CNO rate map of a different cell. This procedure was repeated 500 times per place cell to create a shuffled distribution of correlation scores. Place cells with spatial correlation scores less than one standard deviation above the mean of this shuffled distribution were said to have significant shifts in location. Cells that did not exhibit significant shifts in place field location and had absolute mean firing rate difference scores or mean field size difference scores greater than 0.33 were said to have significant changes in firing rate and/or field size.

Functional Classification of MEC Cells

In MEC, chance levels were estimated using a shuffling procedure in the exact manner described above for CA1 cells. Cells with a mean firing rate $\geq$ 10 Hz were classified as putative interneurons (Fyhn et al., 2004). Firing fields for putative excitatory cells were defined as areas with at least 5 contiguous pixels (80 cm^2) where the firing rate exceeded 20% of the peak rate. Firing fields with peak rates lower than 1 Hz were ignored. For analysis of individual grid fields, the firing rate threshold was increased to 35% of the peak firing rate and firing fields with peak rates lower than 0.1 Hz were ignored to optimize grid field detection.

Grid cells were identified by calculating a spatial autocorrelation map for each unsmoothed rate map (Sargolini et al., 2006). A cell's spatial periodicity was determined by comparing a central circular region of the autocorrelogram, excluding the central peak, with versions of this region rotated at 30 degree increments (Sargolini et al., 2006; Langston et al., 2010). Pearson correlations were calculated by comparing the circular region to all rotated versions. 60 and 120 degree rotations should have high correlation scores due to the triangular pattern of the grid, whereas 30, 90, and 150 degree rotations should result in low correlations. Therefore, a cell's grid score was defined as the minimum difference between correlation scores for either rotation from the first group and any rotation in the second group (range: −2 to 2). Cells with scores exceeding the 95th percentile of the shuffled distribution were classified as grid cells. Grid scale was defined as the mean center-center distance from the central grid field in the autocorrelogram to the neighboring fields. Grid rotation was defined as the change in orientation (measured in degrees) between the central grid field in the autocorrelogram and the neighboring fields. Grid shift (or translation) was defined as the distance from the center of the cross-correlogram to the center of the nearest field. Grid rotation and shift in Table S2 are defined as the minimum change between the baseline session and any 30 min CNO epoch.

Border cells were identified by calculating the difference between the maximal length of a wall touching any defined firing field and the average distance of that field from the nearest wall (Bjerknes et al., 2014). This value was normalized by dividing by the sum of the same two values such that border scores ranged from –1 to 1; a score of 1 indicates firing exclusively along the entire length of a wall. Cells with scores exceeding the 95th percentile of the shuffled distribution were classified as border cells.

Head direction cells were identified by plotting firing rate as a function of the mouse's directional heading. Tuning maps were then divided into 6 degree directional bins and the mean vector length of the circular distribution was calculated. Cells with mean vector lengths exceeding the 95th percentile of the shuffled distribution were classified as head direction cells.

Speed scores were defined as the pairwise correlation between firing rate and the mouse's speed (Kropff et al., 2015). Cells with scores exceeding the 95th percentile of the shuffled distribution were classified as speed cells.

Population Vector Analysis

Population vectors (Leutgeb et al., 2005) were calculated in the same manner for CA1 and MEC cells. Every rate map for each recording session was stacked into a three-dimensional matrix such that each *x-y* location contains firing rate information for the entire population. Population vector correlations are then simply Pearson correlations for each *x-y* location between two different recording sessions, yielding a two-dimensional matrix of correlation scores. The baseline session was used for the functional classification of cells.

Model of Grid-to-Place Cell Transformation

A rate difference score was calculated for each recorded grid cell to create a range of scores. These empirically-determined firing rate changes were then applied to a linear summation model of the grid-to-place cell transformation (Solstad et al., 2006). Briefly, the model is a two-layer network where place fields are created by linear summation of weighted inputs from grid cells. The simulation was run with the following parameters: arena size = 100 × 100 cm, bin size = 1 cm, field rate threshold = 20%, minimum field size = 12 cm, grid spacing sampled logarithmically from 28 to 73 cm, number of grid cells = 50, phase jitter = 30%. The simulation was then repeated with the exact same grid cells, but the firing rates of 20% (matched to percentage of transgene expression) of the grid cells were altered to reflect our experimental data. Each cell was multiplied by a random number drawn from the range of rate difference scores mentioned above. We then calculated the spatial correlation between each place cell from the first simulation to the second simulation with altered firing rates.

Individual Grid Cell Firing Fields

Individual grid field firing rates were defined as the peak rate of each firing field, and fields were numbered in Figure 8A according to their peak rate in the baseline session. Grid field rate correlations in Figure 8B were obtained by fitting a line between points representing the peak field rates in two epochs (BL versus CNO, or BL 1st versus 2nd half). The R^2 value (coefficient of determination) is reported for each fit. (Note: One point not shown in the bottom panel for better visualization, but included for all calculations. BL versus CNO: 34 Hz versus 29 Hz.) In Figure 8C, grid field firing rate variability is defined as the variance between the rate difference scores computed for each identified grid field of a given grid cell. Thus, a grid cell with four firing fields would have four rate difference scores, and the variability between them would be plotted as a single point in Figure 8C. The baseline session was used for the functional classification of grid cells for field analyses.

Contextual Discrimination

Rate maps for each grid cell were exported from MATLAB to Python (Python Software Foundation, https://www.python.org/) and normalized to have firing rates between 0 and 1 for the following analysis. Population vectors were then constructed for three recording epochs: baseline (BL), 30-60 min post-CNO injection (CNO1), and 60-90 min post-CNO injection (CNO2). CNO1 was compared to BL and CNO2 by computing the Euclidean distance between the firing rates for each spatial bin. The decoding performance was defined as the fraction of bins for which the distance to CNO2 was closer than the distance to BL. That is, a decoding performance value of 1 indicates that the firing rate of every spatial bin was more similar between CNO1 and CNO2 than it was between BL and CNO1. A decoding value of 0.5 is equal to chance level performance and indicates that the firing rates in half of the spatial bins were more similar to BL, and the other half of the spatial bins were more similar to CNO2. Decoding scores were calculated for increasing numbers of grid cells for both hM3 and control groups. For each number of grid cells along the x axis in Figure 8D, grid cells were randomly selected with replacement from the pool of all recorded grid cells. This procedure was repeated 1000 times and the mean and standard deviation are shown.

Context-Specific Cells

Kitamura et al. (2015) used in vivo calcium imaging to monitor the activity of MEC cells as mice explored two distinct environmental contexts. The authors assessed context-specificity of MEC cells by calculating a rate difference index for each cell: $(X - Y) / (X + Y)$, where X and Y represent the number of calcium events detected in contexts X and Y, respectively. Only cells with > 10 events during a 5 min exposure to one context were included. Scores were first calculated for repeated exposures to the same context, and the 99th percentile of these scores (0.6) was used as a threshold for classifying cells as "context-specific."

While data from calcium imaging experiments cannot be directly compared with the electrophysiological data reported here, we nonetheless attempted to create an analogous measure. We computed rate difference scores (defined above) for all cells and included only those cells with a mean firing rate > 0.1 Hz in either the baseline or CNO session. Our threshold for context-specificity was defined by calculating the 99th percentile of scores for littermate control mice before and after CNO injection (0.85).

QUANTIFICATION AND STATISTICAL ANALYSIS

Unless otherwise noted, all analyses were conducted using MATLAB (MathWorks). The experimenter was blind to the mouse's genotype and experimental grouping during analysis. Two-sided statistical tests were used for post hoc analyses and one-sided tests were used when there was a clear a priori prediction. Statistical significance was defined with alpha level = 0.05. Nonparametric tests were used when the assumptions for parametric tests were clearly violated (Lilliefors normality test). Median values are reported/displayed for nonparametric tests and mean values are reported/displayed for parametric tests. Error is always reported as standard error of the mean (SEM) with the exception of Figure 8D where standard deviation is reported. N represents the number of mice for cell counting and water maze behavior. N represents the number of spatial bins for population vectors in Figures 7D–7E, and Tables S1 and S2. N represents the number of grid cell firing fields in Figure 8B. In all other instances, n represents the number of cells. N is reported in the Results section and in Tables S1 and S2 with the exception of the cell counts, where it is reported in the legend for Figure 1C.

DATA AND SOFTWARE AVAILABILITY

All quantification methods used in the custom scripts are described above. Further requests for custom scripts and data used in this study should be directed to the corresponding author (clifford.kentros@ntnu.no).

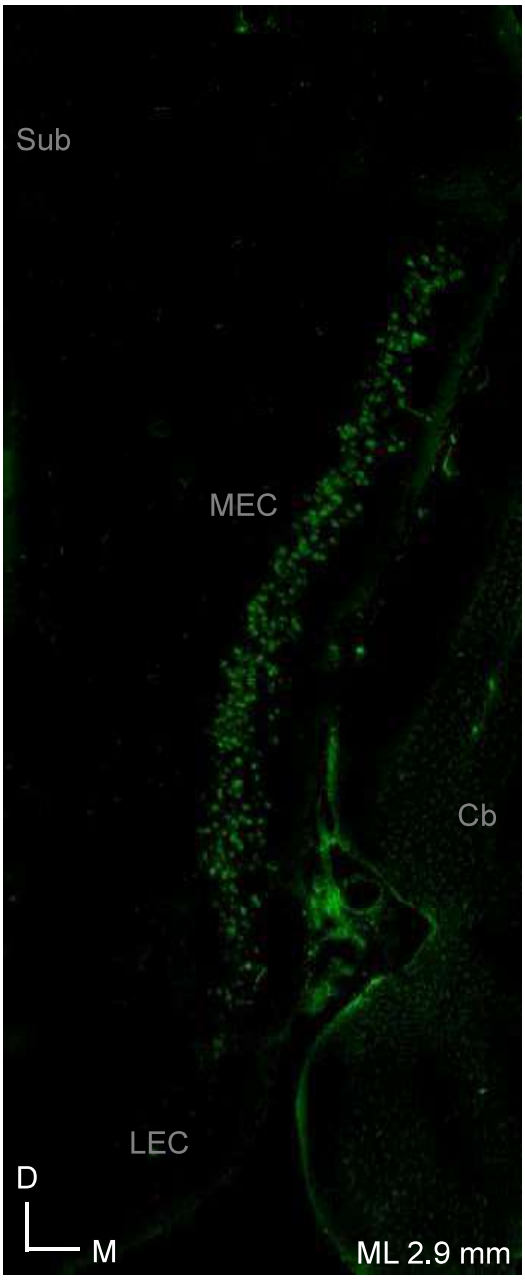

Figure S1

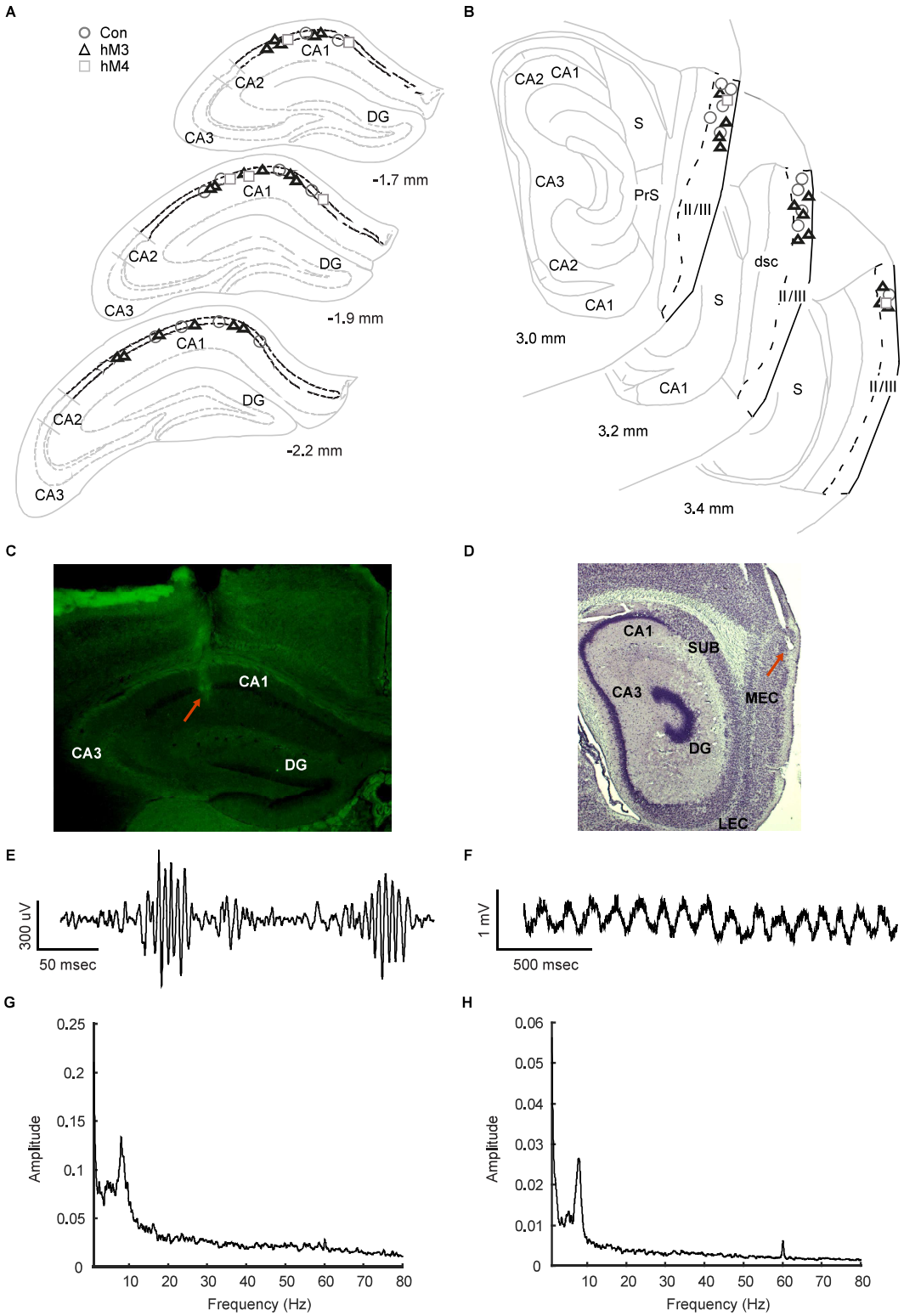
A
Con
hM3
hM4
CA1
CA2
DG
CA3
-1.7 mm
-1.9 mm
-2.2 mm
B
CA2
CA1
S
CA3
PrS
II/III
dsc
3.0 mm
3.2 mm
3.4 mm
C
CA1
CA3
DG
D
CA1
SUB
CA3
MEC
DG
LEC
E
300 uV
50 msec
F
1 mV
500 msec
G
Amplitude
Frequency (Hz)
H
Amplitude
Frequency (Hz)

Figure S2

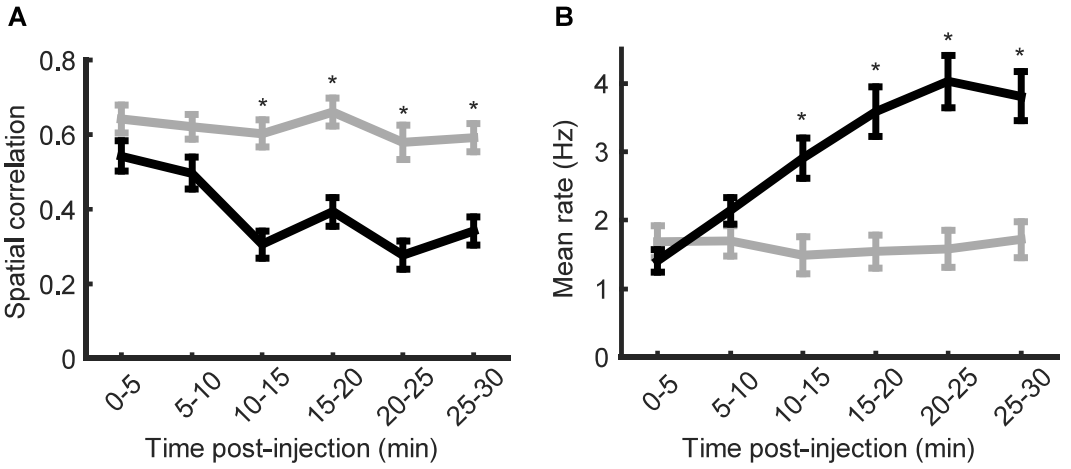
A
Spatial correlation
0.8
0.6
0.4
0.2
0
0-5
5-10
10-15
15-20
20-25
25-30
Time post-injection (min)
B
Mean rate (Hz)
4
3
2
1
0
0-5
5-10
10-15
15-20
20-25
25-30
Time post-injection (min)

Figure S3

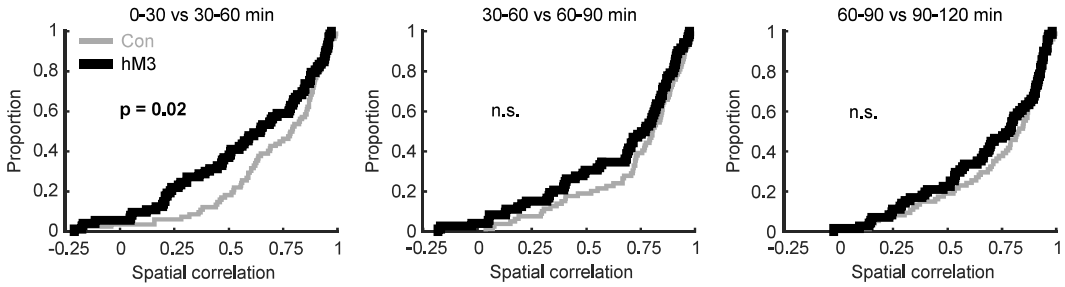
0-30 vs 30-60 min
Con
hM3
p = 0.02
Proportion
Spatial correlation
30-60 vs 60-90 min
n.s.
Proportion
Spatial correlation
60-90 vs 90-120 min
n.s.
Proportion
Spatial correlation

Figure S4

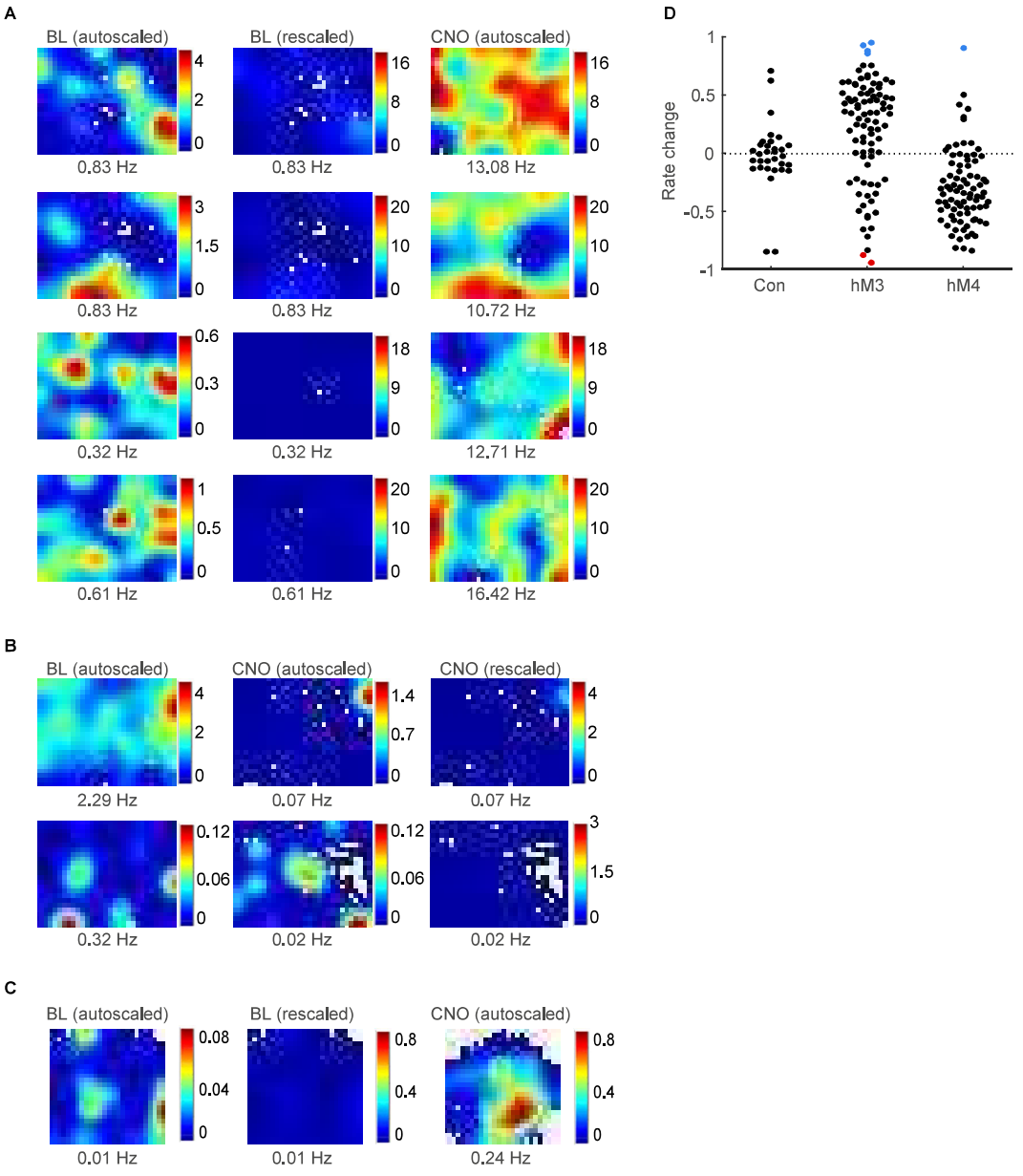
A
BL (autoscaled)
BL (rescaled)
CNO (autoscaled)
0.83 Hz
0.83 Hz
13.08 Hz
0.83 Hz
0.83 Hz
10.72 Hz
0.32 Hz
0.32 Hz
12.71 Hz
0.61 Hz
0.61 Hz
16.42 Hz
B
BL (autoscaled)
CNO (autoscaled)
CNO (rescaled)
2.29 Hz
0.07 Hz
0.07 Hz
0.32 Hz
0.02 Hz
0.02 Hz
C
BL (autoscaled)
BL (rescaled)
CNO (autoscaled)
0.01 Hz
0.01 Hz
0.24 Hz
D
Rate change
Con
hM3
hM4

Figure S5

SUPPLEMENTAL FIGURE LEGENDS

Figure S1, related to Figure 1. Visualization of hM3Dq transgene for cell counting.
Expression of hM3Dq transgene visualized by fluorescent RNA *in situ* and Nissl stain. D = dorsal, M = medial, MEC = medial entorhinal cortex, LEC = lateral entorhinal cortex, Sub = subiculum, Cb = cerebellum, ML = medial/lateral relative to midline.

Figure S2, related to Figures 2, 3, 5-8. Recording sites for electrophysiology experiments.
(A) Tetrode locations in CA1 identified in three coronal sections. Numbers indicate distance from bregma.
(B) Tetrode locations in MEC identified in three sagittal sections. S = subiculum, PrS = presubiculum, dsc = lamina dissecans. Numbers indicate distance from midline.
(C) Representative coronal section used to identify tetrode tracks in CA1.
(D) Representative sagittal section used to identify tetrode tracks in MEC.
(E) Example of awake hippocampal ripple recorded in CA1. Trace is local field potential after band-pass filtering in the ripple band (100 - 400 Hz).
(F) Example of strong theta rhythmicity recorded in MEC. Trace is broadband (0.1 - 475 Hz) local field potential.
Example power spectrum showing high amplitude in the theta band (6-10 Hz) in both CA1 (G) and MEC (H).
Red arrows in (C) and (D) indicate identified recording sites. DG = dentate gyrus, SUB = subiculum, MEC = medial entorhinal cortex, LEC = lateral entorhinal cortex.

Figure S3, related to Figures 2, 3, 5-8. Artificial remapping of place cells and increase in firing rate of excitatory MEC cells occur at the same time following CNO injection.
(A) Spatial correlation for CA1 place cells between baseline and 5-min epochs after CNO injection in Con (gray) and hM3 (black) mice.
(B) Mean firing rate of putative excitatory MEC neurons during 5-min epochs after CNO injection in Con (gray) and hM3 (black) mice.
Data represented as median ± SEM. *$P < 0.05/n$, one-sided Wilcoxon rank sum tests comparing hM3 to Con with Holm-Bonferroni correction for multiple comparisons.

Figure S4, related to Figures 2 and 3. Artificial remapping of place cells is stable 30 mins after CNO injection.
Cumulative distribution functions showing spatial correlation values between consecutive 30-min epochs following CNO injection in Con (gray) and hM3 (black) mice.
0-30 vs 30-60 min: $D^* = 0.2280$, $p = 0.0151$; 30-60 vs 60-90 min: $D^* = 0.1670$, $p = 0.1142$; 60-90 vs 90-120 min: $D^* = 0.1264$, $p = 0.2978$; one-sided Kolmogorov-Smirnov tests.

Figure S5, related to Figures 6 and 8. A small proportion of MEC neurons exhibit large changes in mean firing rate following CNO injection.
Rate maps of cells which exceed the firing rate criterion of Kitamura et al. (2015).
(A) Four cells from hM3 mice significantly increased their firing rate following CNO injection, (B) two cells from hM3 mice significantly decreased their firing rate following CNO injection, and (C) one cell from an hM4 mouse significantly increased its firing rate following CNO injection.

(A-C) Each row is a cell and each column is the baseline or CNO session. Maps from sessions with lower firing rates are scaled both within session (autoscaled) and to the peak firing rate of the other session (rescaled) in order to visualize firing patterns. Red represents maximum firing, blue is silent, and white represents unvisited pixels. Mean rate indicated below rate maps.
(D) Change in mean firing rate for each MEC cell (putative excitatory and inhibitory) following CNO injection in Con, hM3, and hM4 mice. Cells which exceed the firing rate criterion are shown in blue (increases) and red (decreases). Note that the identified neurons do not appear to represent a unique population of MEC neurons, but rather they are likely the tails of a continuous distribution.

Table S1, related to Figures 2 and 3. Further characterization of CA1 neurons.
All statistical tests compare either hM3 or hM4 to Con mice. Statistically significant results ($\alpha = 0.05$) are in bold. Number of cells is indicated parenthetically following each group name. Mean values are reported for t-tests and median values are reported for rank sum tests. *Change* refers to a difference score (i.e. normalized change, see methods).

Measure	Mean/median ± SEM	Test	P value	Test statistic
Change in in-field firing rate (place cells)	Con (73) = -0.06 ± 0.03	Two-sided independent t-test		
	hM3 (67) = 0.05 ± 0.04		p = **0.04**	t(138) = 2.12
	hM4 (99) = -0.01 ± 0.03		p = 0.27	t(170) = 1.11
Change in spatial information (place cells)	Con (91) = -0.08 ± 0.02	Two-sided independent t-test		
	hM3 (80) = -0.24 ± 0.03		p = **1.51×10^{-6}**	t(169) = -4.99
	hM4 (106) = -0.06 ± 0.02		p = 0.44	t(195) = 0.78
Shift in location of peak rate (cm) (place cells) (bin width = 2 cm)	Con (91) = 11.66 ± 1.64	One-sided Wilcoxon rank sum test		
	hM3 (80) = 23.11 ± 1.84		p = **2.89×10^{-4}**	Z = 3.44
	hM4 (106) = 8.89 ± 1.41		p = 0.72	Z = -0.59
Change in number of firing fields (place cells)	Con (91) = 0 ± 0.03	Two-sided Wilcoxon rank sum test		
	hM3 (79) = 0 ± 0.03		p = 0.10	Z = -1.67
	hM4 (106) = 0 ± 0.03		p = 0.47	Z = 0.73
Change in interneuron mean firing rate	Con (33) = -0.07 ± 0.03	Two-sided independent t-test		
	hM3 (29) = -0.00 ± 0.03		p = 0.14	t(60) = 1.49
	hM4 (31) = -0.07 ± 0.03		p = 1.00	t(62) = 1.27×10^{-4}

Table S2, related to Figures 5-8. Further characterization of MEC neurons.
All statistical tests compare either hM3 or hM4 to Con mice. Statistically significant results (α = 0.05) are in bold. Number of cells is indicated parenthetically following each group name. Number of spatial bins is indicated for population vectors. Mean values are reported for t-tests and median values are reported for rank sum tests. *Change* refers to a difference score (i.e. normalized, see methods) while *difference* refers to the raw difference. Grid cells were recorded from approximately three modules per group of mice.

Measure	Mean/median ± SEM	Test	P value	Test statistic
Population vector correlation (putative excitatory cells)	Con (1315) = 0.91 ± 0.00	One-sided Wilcoxon rank sum test		
	hM3 (690) = 0.60 ± 0.00		p = **1.13×10^{-281}**	Z = -35.84
	hM4 (1248) = 0.80 ± 0.00		p = **9.62×10^{-146}**	Z = -25.68
Difference in gridness	Con (9) = -0.09 ± 0.15	One-sided Wilcoxon rank sum test		
	hM3 (19) = -0.36 ± 0.16		p = 0.09	Z = -1.33
	hM4 (9) = -0.33 ± 0.25		p = 0.15	rank sum = 73
Difference in grid scale	Con (12) = 0.11 ± 1.01	Two-sided Wilcoxon rank sum test		
	hM3 (20) = -0.60 ± 0.86		p = 0.60	Z = -0.53
	hM4 (10) = -0.80 ± 2.12		p = 0.87	Z = -0.16
Grid rotation (degrees)	Con (12) = 1.16 ± 3.65	One-sided Wilcoxon rank sum test		
	hM3 (20) = 0.96 ± 2.99		p = 0.52	Z = -0.04
	hM4 (10) = 8.44 ± 4.35		p = **0.02**	Z = 2.15
Grid translation (cm) (bin width = 4 cm)	Con (13) = 1.70 ± 4.31	One-sided Wilcoxon rank sum test		
	hM3 (21) = 3.64 ± 3.32		p = **0.02**	Z = 2.13
	hM4 (11) = 1.79 ± 0.98		p = 0.57	Z = -0.17

Difference in border score	Con (3) = -0.02 ± 0.04	One-sided Wilcoxon rank sum test		
	hM3 (14) = -0.02 ± 0.14		p = 0.48	rank sum = 125
	hM4 (27) = -0.05 ± 0.06		p = 0.24	Z = -0.69
Difference in preferred angle (degrees) (HD cells)	Con (24) = 3.34 ± 10.39	One-sided Wilcoxon rank sum test		
	hM3 (55) = 3.36 ± 6.30		p = 0.31	Z = 0.49
	hM4 (54) = 2.24 ± 6.80		p = 0.37	Z = 0.33
Difference in mean vector length	Con (24) = 0.02 ± 0.05	One-sided Wilcoxon rank sum test		
	hM3 (58) = -0.03 ± 0.02		p = 0.42	Z = -0.20
	hM4 (53) = -0.02 ± 0.03		p = 0.37	Z = -0.34
Difference in speed score	Con (50) = 0.01 ± 0.01	One-sided independent t-test		
	hM3 (94) = -0.01 ± 0.01		p = 0.07	t(142) = -1.51
	hM4 (84) = 0.03 ± 0.01		p = 0.92	t(32) = 1.38
Change in grid cell mean firing rate	Con (9) = -0.06 ± 0.04	Two-sided Wilcoxon rank sum test		
	hM3 (21) = 0.00 ± 0.11		p = 0.86	Z = 0.18
	hM4 (11) = -0.39 ± 0.09		p = **0.02**	Z = -2.36
Change in border cell mean firing rate	Con (3) = -0.19 ± 0.08	Two-sided Wilcoxon rank sum test		
	hM3 (14) = 0.41 ± 0.12		p = 0.20	rank sum = 137
	hM4 (30) = -0.46 ± 0.06		p = 0.25	Z = -1.16
Change in HD cell mean firing rate	Con (10) = 0.01 ± 0.17	Two-sided Wilcoxon rank sum test		
	hM3 (58) = 0.32 ± 0.07		p = 0.46	Z = 0.74
	hM4 (54) = -0.38 ± 0.05		p = **0.03**	Z = -2.15

Change in interneuron mean firing rate	Con (4) = 0.02 ± 0.04	Two-sided Wilcoxon rank sum test		
	hM3 (8) = 0.11 ± 0.04		p = 0.11	rank sum = 62
	hM4 (14) = -0.35 ± 0.07		p = **0.02**	rank sum = 110

Paper 2

Paper 3

ISBN 978-82-326-4690-6 (printed version)
ISBN 978-82-326-4691-3 (electronic version)
ISSN 1503-8181

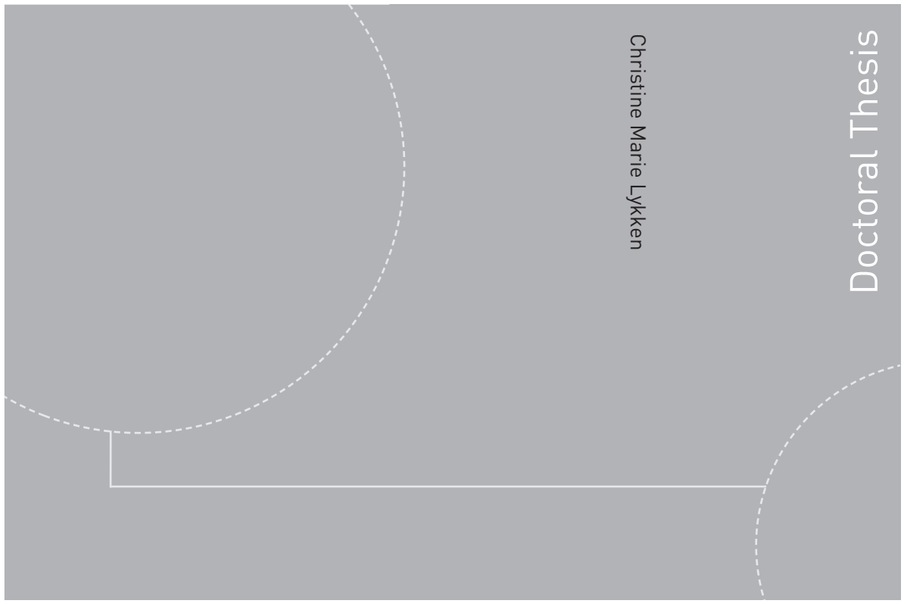

Doctoral theses at NTNU, 2020:171

Christine Marie Lykken

The contribution of grid field firing rates to hippocampal remapping

NTNU
Norwegian University of
Science and Technology
Faculty of Medicine and Health Sciences
Department of Neuromedicine and Movement Sciences

NTNU
Norwegian University of
Science and Technology

Doctoral theses at NTNU, 2020:171

NTNU

NTNU
Norwegian University of
Science and Technology